The microstructure of MX-80 clay with respect to its bulk physical properties under different environmental conditions

Roland Pusch

Geodevelopment AB

March 2001

The microstructure of MX-80 clay with respect to its bulk physical properties under different environmental conditions

Roland Pusch

Geodevelopment AB

March 2001

Abstract

Quantification of clay microstructure can be made by use of digitalized micrographs taken by transmission electron microscopy using suitably impregnated specimens.

Practically useful microstructural parameters refer to the fraction of a thin section that represents dense and soft parts of the clay matrix. The derived microstructural parameters are directly coupled to the most important bulk physical properties, i.e. the hydraulic conductivity, gas penetrability, swelling pressure and cation/anion diffusion capacities. The proposed model for characterizing clay microstructure is termed MMM.

Pre-Quaternary clays that have been investigated and characterized with respect to the microstructure represent two possible stages in long term alteration of the KBS3 buffer clay. One of them has been exposed to repository-like conditions for a few thousand years and has a smectite content of up to 25 %. It is not much more permeable than MX-80 clay. The other is assumed to have been converted from smectite-rich bentonite to illite by being exposed to such conditions for millions of years. The different physical properties in bulk are explained by the different microstructural constitutions.

Summary

A model of microstructural evolution of MX-80 buffer is presented in the report. Quantification of the microstructure is made by use of digitalized micrographs taken by transmission electron microscopy using suitably impregnated specimens with appropriate thickness. The model is termed MMM, a successor of the earlier GMM.

Practically useful microstructural parameters refer to the fraction of a thin section that represents dense and soft parts of the clay matrix. The derived microstructural parameters are directly coupled to the most important bulk physical properties, i.e. the hydraulic conductivity, gas penetrability, swelling pressure and cation/anion diffusion capacities.

The study has shown that even at very high densities, softer and more pervious zones exist in the form of interconnected "external" voids filled with more or less dense clay gels. At bulk densities exceeding 2000 kg/m^3 after water saturation, the gel density is also high but for low bulk densities it may be so much reduced that the gels do not remain stable at high electrolyte content of the porewater. The fact that the density variations are small for high bulk densities means that the separation of matrix components ("fracturing") that is required for letting gas through is on the same order of magnitude as the bulk swelling pressure. For lower bulk densities, displacement or consolidation of the clay gels in "external" voids is concluded to take place in conjunction with gas penetration.

At high densities the limited degree of continuity and constrictions of the channels leading to anion-excluding charge conditions mean that the anion diffusion capacity is very low, while cation diffusion may be extensive because it takes place not only through channels but also through the interlamellar space and along the surfaces of stacks of lamellae, i.e. by surface diffusion.

Two Pre-Quaternary clays that have been investigated and characterized with respect to the microstructure represent two possible stages in long term alteration of the KBS3 buffer clay. One of them has been exposed to repository-like conditions and has a smectite content of up to 25 % and is not much more permeable than MX-80 clay. The other is assumed to have been converted from smectite-rich bentonite to illite by being exposed to such condicitons for millions of years and has a higher conductivity. The different hydraulic properties are explained by the different microstructural constitutions.

Sammanfattning

En modell för uppkomsten av mikrostrukturen hos MX-80 buffert ges i rapporten. Kvantifiering görs med hjälp av digitaliserade mikrofotografier tagna med transmissions-elektronmikroskop med användning av på lämpligt sätt preparerade prov med anpassad tjocklek.

Praktiskt användbara mikrostrukturella parametrar avser andelen av en provsektion som representerar täta respektive lösa partier av lermatrisen. De härledda värdena på de mikrostrukturella parametrarna är direkt kopplade till de viktigaste fysikaliska egenskaperna i bulk, dvs hydrauliska konduktiviteten, svällningstrycket och diffusionskapaciteten hos katjoner och anjoner.

Undersökningen har visat att det till och med vid mycket hög densitet finns lösare och mer genomsläppliga partier i form av förbundna "externa" porer fyllda med mer eller mindre täta lergeler. Då bulkdensiteten överskrider 2000 kg/m^3 efter vattenmättnad är geldensiteten också hög men vid lägre bulkdensitet kan den reduceras så mycket att gelen inte är stabil om porvattnets elektrolytinnehåll är högt. Det faktum att densitetsvariationerna är små vid hög bulkdensitet betyder att det åtskiljande av matriskomponenterna ("spjälkning") som erfordras för att få gas att tränga igenom är av samma storleksordning som svälltrycket. För lägre bulkdensitet är slutsatsen att förskjutning eller konsoldering av lergelen i "externa" porer äger rum i samband med gasgenomträngning.

Vid höga densiteter leder den begränsade konnektiviteten och förträngningarna hos kanalerna till en laddningssituation som utesluter anjoner, vilket betyder att den diffusiva anjontransportkapaciteten är mycket låg, medan katjontransporten kan vara omfattande eftersom den äger rum inte bara i kanalerna utan också genom de interlamellära utrymmena och längs ytorna på stackarna av lameller, dvs. genom ytdiffusion.

Två prekvartära leror som undersökts och karakteriserats med avseende på mikrostrukturen representerar två möjliga stadier i förändringen hos KBS3-bufferten över längre tid. En av dem har varit exponerad för en slutförvarlik miljö och har ett smektitinnehåll av upp till 25 % och har inte avsevärt högre genomsläpplighet än MX-80. Den andra antas vara smektitrik lera som ombildats till illit genom exponering för sådan miljö under miljontals år och har högre genomsläpplighet. De olika hydrauliska egenskaperna förklaras av de olika uppbyggnaderna hos mikrostrukturen.

Contents

Symbols and definitions

D_a	=	apparent diffusion coefficient
D_e	=	effective diffusivity
D_p	=	pore diffusivity
e	=	void ratio
F_2, F_3	=	Microstructural parameters
g	=	gravity
K	=	hydraulic conductivity
K_d	=	sorption factor
M^I, M^{II}, M^{III}	=	metal cations
n	=	porosity
p	=	normal stress
p_S	=	swelling pressure
R	=	molar gas constant
S_r	=	degree of water saturation, volume %
t	=	time
T	=	temperature
u	=	water pressure
w	=	water content (ratio)
w_L	=	liquid limit
w_P	=	plastic limit
ε	=	strain
ρ	=	bulk density
ρ_d	=	dry density
ρ_{sat}	=	density of fluid-saturated material
σ	=	pressure
σ^I	=	effective pressure (stress)
τ	=	shear stress

The following terms are used for the various microstructural constituents:

- Flake, lamella: Single sheet of smectite crystal lattice.
- Stack of flakes: Coherent particle consisting of a number of aligned lamellae.
- Aggregate: Coherent group of stacks.
- Clay gel: Coherent network of aggregates.
- Void, pore: Open or filled space in clay gel or between ballast grains.
- External voids: Open or filled space between stacks of lamellae.
- Internal voids: Interlamellar space.
- External water: Free water.
- Interlamellar (internal) water: Adsorbed water.

1   Scope

Soil mechanical investigators dealing with classical geotechnical problems like slope stability and settlement of buildings have always been trying to understand the various mechanisms for basing their mathematical models on a sound physico/chemical basis. This led to the fruitful co-operation between mineralogists and soil engineers exemplified by Ivan Th. Rosenqvist and Laurits Bjerrum in Norway, and by James K. Mitchell and various soil physicists like Philip Low in the US a few decades ago. Their work deepened our understanding of the relationship between the microstructure and bulk physical properties of illitic and kaolinitic clays, especially respecting the importance of the physical state of the porewater. For smectitic clays the corresponding knowledge has been very limited until recently but the present report, which compiles international and particularly Swedish R&D, is believed to shed some light on the issue.

The need for understanding the detailed behavior of buffers and backfills intended for isolating radioactive waste is very significant because of the seriousness of the issue and because temperature, chemistry and microbiology are major factors. Also, time is a much more important parameter than in ordinary soil mechanics. This has been manifested by the EC-study "Microstructural and chemical parameters of bentonite as determinants of waste isolation efficiency" (Contract F14W-CT95-0012), which showed that the microstructural constitution largely determines the isolation potential of bentonite-based buffers and backfills.

Since the formal report of the EC-study by necessity had to be rather compact a number of important issues were given limited space and the primary aim of the present document is to give a more comprehensive description of the matter.

2   The MX-80 bentonite clay material

2.1   Geological background

Contemporary with a marine episode in Cretaceous time there was extensive volcanic activity in the Western Cordillera of North America by which large quantities of ash were formed and blown by the prevailing winds. The result was a series of ash deposits on the brackish inland sea. They settled and became buried by marine or land-derived materials and with time the sediments were deeply buried and consolidated by more recent sediments. Many of these ancient ash layers later altered to bentonite.

In the Black Hills area in Wyoming the bentonite beds have a thickness of a few centimeters to a few meters and appear in a series of marine shales, marls and sandstones [1]. The Wyoming bentonites have been exploited by the American Colloid Co for decades for production of various commercial clay materials like the MX-80 clay, which is a smectite-rich clay with a special grading. It has a particularly good reputation among the large number of commercial smectitic clays because it has Na as major adsorbed cation and therefore extraordinarily good colloidal, plastic and bonding properties. However, in recent years extensive exploitation of the rather thin bentonite beds has tended to yield changes in the composition of the clay products and checking of the smectite and organic contents as well as the amount and type of accessory minerals, is needed for quality assurance.

2.2   Granulometry

2.2.1   Grains, granules

The raw bentonite material used for preparation of MX-80 is dried in rotating kilns and ground to yield a granulated clay powder with the size distribution shown in Figure 2-1.
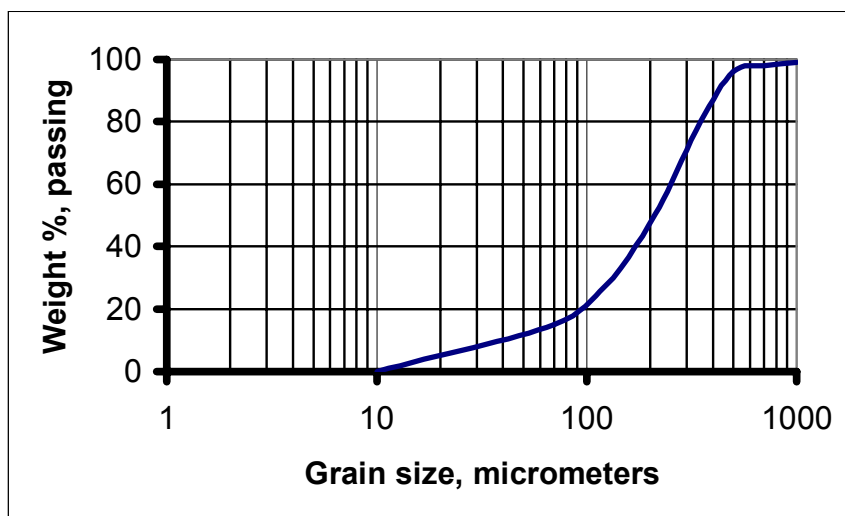

Figure 2-1. *Typical grain size distribution of MX-80.*

2.2.2 Constitution of grains

The grains are composed of numerous montmorillonite lamellae, which form stacks as basic units. These stacks are typically 30 to 100 Å thick with a diameter of about 0.05 to 0.25 μm Dispersion of smectite clays like MX-80 can not break up the clay into such small units as illustrated by measurements compiled in Figure 2-2.
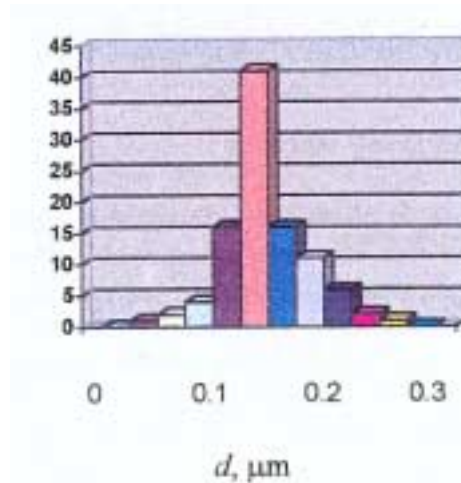

Figure 2-2. *Frequency in percent (vertical axis) of maximum diameter of particles of effectively dispersed Na montmorillonite as evaluated by transmission electron microscopy.*

The stacks are estimated to consist of 3–5 lamellae with equally oriented crystal axes in Li^+ or Na^+ saturated smectite and of about 10 lamellae if Ca^+ or polyvalent cations occupy the interlamellar space. The difference is assumed to be due to the stronger particle association caused by the latter types of cations.

2.3 Composition

2.3.1 Chemical constitution

Bulk MX-80 contains 65–75 % montmorillonite, 10–14 % quartz, 5–9 % feldspars, 2–4 % mica and chlorite, 3–5 % carbonates and chlorite, and 1–3 % heavy minerals.

The chemical composition is as follows:

SiO_2 61–65 %, Al_2O_3 22–25 %, Fe_2O_3 1–7 %, MgO 1–2 %, CaO 0–0.6 %, Na_2O 0–1 %, K_2O 0–3 %

The dominant adsorbed cation is Na (60 %), while Ca represents about 25 % and Mg around 10 %. Fe, Cu, and K are adsorbed to a small extent. In microstructural modelling it is assumed that montmorillonite makes up 100 % of the minerals and that Na is the only adsorbed cation. The derived models will therefore deviate somewhat from the true microstructural constitution but since accessory minerals are dispersed in the montmorillonite mass this simplification should be acceptable.

2.3.2   Crystal structure of montmorillonite

Definition of the crystal structure of montmorillonite requires that a stack consisting of at least two lamellae of the type shown in Figure 2-3 is considered. Both models in the figure are possible, the traditional Hofmann/Endell/Wilm version may be valid for temperatures exceeding 130–150°C or adsorption of other cations than Li and Na, while the Edelman/ Favejee version may apply to lower temperatures than about 100°C with Li and Na in exchange positions. The latter model implies that more OH-radicals are available than in the firstmentioned model in which OH is exposed only at the particle edges.
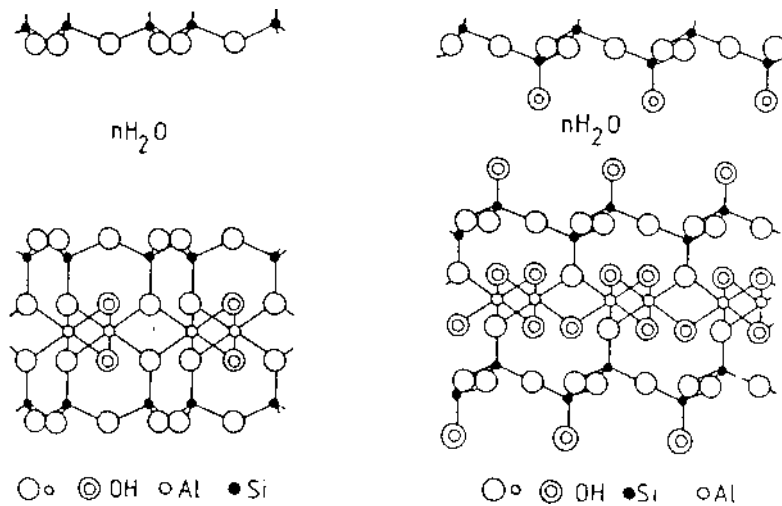
Figure 2-3. *Crystal constitution models for montmorillonite. Left: Hofmann/Endell/Wilm. Right: Edelman/Favejee [2].*

2.3.3   Inorganic amorphous components

Dissolved mineral particles yield free silica, aluminum and magnesium in the porewater, which is commonly nearly saturated with respect to Si, and some of these elements spontaneously rearrange to form inorganic colloids like Fe and Al compounds (sesquioxides), such as iron oxyhydroxides. Many reactions are very redox-sensitive and as in the case of combination of iron and sulphur, which may have the form of polysulphides and not simple species, the products are large precipitating complexes. Many of the compounds of colloidal or nearly colloidal size [3] are believed to be amorphous as illustrated by electron diffractograms obtained by applying transmission electron microscopy. They can be considered as solid microstructural components in most cases.

2.3.4 Organic components

The various types of organic species in smectitic clay range from millimeter-sized tissues emanating from plants, fungal and animal activities, to organic molecules representing ultimate degradation products of organic life [4, 5]. They can form organic colloids and should be considered since simple estimates show that the pore space that they occupy is not negligible. In the present report inorganic and organic colloids are treated as a common group of microstructural constituents.

2.4 Hydration properties

2.4.1 Influence of chemical potential of water

Water with few dissolved ions has a higher chemical potential than water with solutes. The drop in potential for increasing the ion concentration can be expressed as in Eq. 2.1 [6]:

$$\mu_o = -kTCv \tag{2.1}$$

where: k = Boltzmann's constant
T = Temperature
C = Cation concentration in hydrates formed at
    mineral surfaces
v = Partial volume of water

The cations cause polarization of neighboring water molecules by which their mobility drops and the chemical potential is reduced. Further reduction is due to van der Waals attraction between the hydrates and adjacent mineral lattice and to hydrogen bonds established between the hydrates and lattice hydroxyls. Interlamellar hydrates are pressed together by the attraction between the lamellae, which increases the chemical potential. It is hence highest for low water contents and higher for interlamellar hydrates than for hydrates on basal surfaces of clay particles. Nakano et al [6] found that the chemical potential of the first hydrate adsorbed on basal surfaces is on the order of E7 J/kg, and about E2 J/kg for hydrates at around 60 Å from the surfaces.

This theory can be used for calculating water retention curves in the form of relationships between the water content and the chemical potential. The values naturally depend on the number of lamellae as illustrated by the much higher chemical potential (3E4 J/kg) for the volumetric water content 20 % when the number of lamellae is 8 than when this number is 4 (5E3 J/kg). The water retention of dense clay is hence higher than of soft clays. Similarly, the chemical potential of the porewater is much higher of dense than of soft clay.

2.4.2 Interlamellar hydration

The interlamellar space offers large amounts of hydration sites due to the crystal lattice constitution, which determines the charge and coordination of adsorbed cations and water molecules. The hydration properties control the swelling potential, plasticity and rheological behavior and are hence of fundamental importance.

The coordination of interlamellar cations, the crystal lattice and the water molecules depends strongly on the size and charge of the cations and of the charge distribution in the lattice. 3 hydrate layers in montmorillonite can only be formed when sodium, lithium or magnesium are in interlamellar positions according to Table 2-1, from which one finds that montmorillonite is the only smectite mineral that can expand by forming 3 interlamellar hydrates. This means that montmorillonite clay can swell more than other smectite minerals, which gives it better sealing properties. However, this is the case only when Li^+, Na^+ and Mg^{2+} are in interlamellar positions. With K^+ or Ca^{2+} in these positions a third hydrate does not form in this or any other smectite mineral because of the charge and size of these ions.

When submerged in free water, the hydration of an initially dry montmorillonite crystallite proceeds until the maximum number of hydrates is formed, provided that there is no geometrical restraint. In humid air, the number of hydrates depends on the relative humidity.

Table 2-1. Number and thickness of interlamellar hydrate layers in Å [7].

Smectite	**M[1)]**	**1st hydrate**	**2nd hydrate**	**3rd hydrate**
Montmorillonite	Mg	3.00	3.03	3.05
	Ca	3.89	2.75	–
	Na[2)]	3.03	3.23	3.48
	K	2.42	3.73	–
Beidellite	Mg	2.69	2.69	–
	Ca	2.30	2.30	–
	Na	2.15	2.15	–
	K	2.54	–	–
Nontronite	Mg	2.92	3.00	–
	Ca	3.05	3.37	–
	Na	2.70	2.79	–
	K	2.60	–	–

[1)] M adsorbed cation [2)] Lithium resembles Na in this respect

Figure 2-4 shows a suggested model of the organization of the first interlamellar hydrate when Na^+ and Ca^{2+} are in interlamellar positions. The water molecules are located just over and partly in the hexagonal openings depending on the pressure and type and hydration state of the interlamellar cations.

Other models have been proposed for the low-temperature Edelman/Favejee crystal constitution (Figures 2-3 and 2-5). Here, up to three hydrate layers are hosted in the interlamellar space when Li^+ or Na^+ are present, while the strong hydration potential of Ca^{2+} does not allow for this sort of structuring and instead implies the Hofmann/Endell/Wilm crystal constitution.

The physical consitution and properties of the interlamellar water is not known with certainty. The opinion ranges from the assumption that motion of interlamellar water is not highly restricted at room temperature, as concluded from the finding that the specific heat capacity is

equal to that of ice for 100 K<T<150 K then rising to that of liquid water at 273 K, to the belief that interlamellar water has an energy state and rigidity similar to that of ice as concluded from studies based on NMR, RM and IR techniques [9].
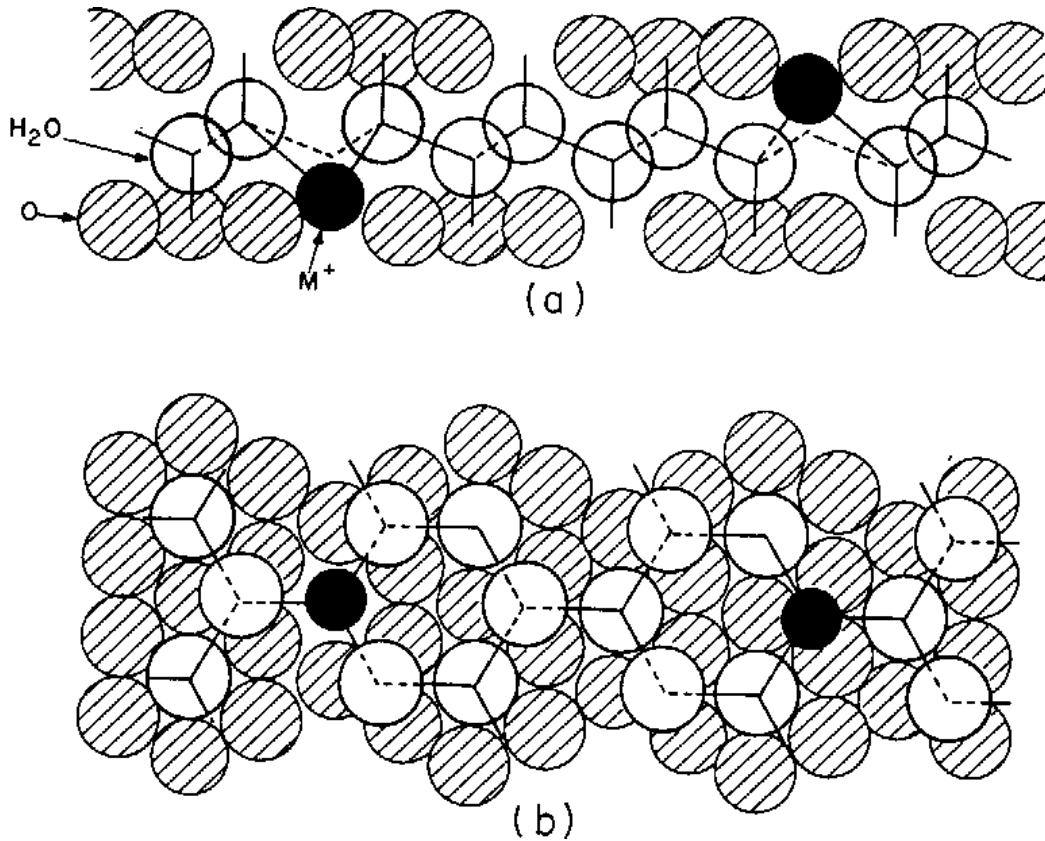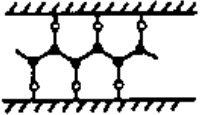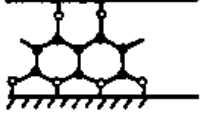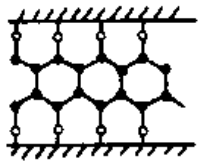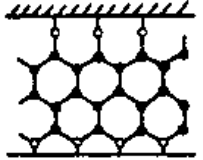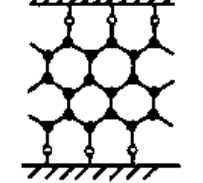

Figure 2-4. Organization of 1-hydrate interlamellar water molecules in montmorillonite. M is metal cation. Shaded circles are basal plane oxygens [8]. Upper picture a) is cross section, lower planar view b).

Spin-echo proton measurements interpreted such that one can distinguish between intra- and extralamellar water suggest that the relaxation time T_2 is around 20–40 μs for protons in interlamellar water in montmorillonite as compared to 2.3 s in free water [10]. This obvious difference indicates strong structuring and very limited mobility of interlamellar water.

A recent study by use of vapor pressure measurements and X-ray diffraction technique supports the conclusion that three distinct hydrate layers are established in the interlamellar space and that they are as strongly held to the clay lattice as ice although the interlamellar water is layered rather than 3D-structured [11]. This study led to the conclusion that the number of hydrates is related to the water content as shown in Table 2-2 for Na montmorillonite with a dry density of 1200 kg/m^3 (1750 kg/m^3 at complete water saturation).

	Schematic interlayer structure	H_2O molecules per unit cell	Basal spacing, Å	g H_2O/g clay	mM H_2O/g clay	Remarks
0		0	12.30	0; 0.084[a]	0; 4.667[a]	Unstable; no hydration; four OH groups per unit cell
1		2.66	15.05	0.059	3.278	Unstable
2		5.33	17.81	0.119	6.661	Stable monolayer
3		8.0	18.73	0.179	9.944	Unstable
4		10.67	21.49	0.238	13.222	Stable; two layers
5		13.32	22.41	0.297	16.5	Unstable
6		16.0	25.17	0.357	19.833	Stable; three layers

[a] At complete dehydroxylation.

Figure 2-5. *Water lattice configuration in interlamellar positions of Li- and Na montmorillonite* [2].

Table 2-2. Number of hydrate layers in compacted Na montmorillonite with a dry density of 1200 kg/m^3 as a function of the water content [11]. The clay was mixed with distilled water.

Water content, % (by weight)	Number of hydrates
<7	0
7–10	1
10–20	1–2
20–25	2
25–35	2–3
>35	3

2.4.3   Extralamellar hydration

External surfaces are basal planes and edges of the stacks of lamellae. The firstmentioned consist of hexagonal arrangements of oxygens or hydroxyls and can attach water molecules by establishing hydrogen bonds. However, diffuse electrical double-layers are formed here with a relatively high concentration of cations near the surface, which affects the organization and physical state of the hydrates. There are reasons to believe that the viscosity of the adsorbed water is higher than that of free water but that the mobility of the molecules is higher than that of interlamellar water. It is assumed that no more than 3 hydrate layers are adsorbed at the free surfaces and that only the first of them has physical properties that deviate significantly from those of free water.

At low bulk densities the fraction of interlamellar, immobile water is naturally higher than at high bulk densities as illustrated by Figure 2-6. The impact of the type of adsorbed cation in the diagram is explained by the difference in numbers of interlamellar hydrates as described earlier in this chapter.
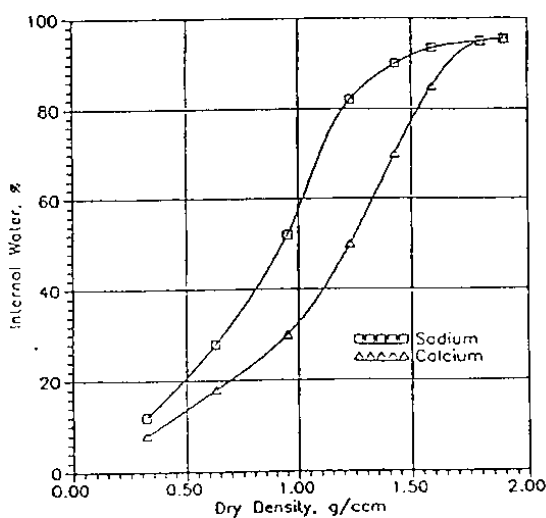

Figure 2-6. Theoretical relationship between bulk dry density in g/cm3 and the content of interlamellar ("internal") water expressed in percent of the total porewater content [12].

2.5   Hydration at elevated temperature

The influence of temperature and water pressure on water sorption and particle thickness of montmorillonite clay confined in autoclaves under controlled water pressure conditions has been examined by several investigators [13, 14]. A typical, carefully conducted test comprised a series of experiments on montmorillonite slurry with a fluid content of 800 % (density 1050 kg/m^3) that was placed in a cell exposed to temperatures up to 200°C and to hydraulic pressures of up to 40 MPa. The molality of the NaCl solution that was used for saturation was 1 to 5. This study showed that the interlamellar spacing was hardly changed at all in the different tests, which is explained by the fact there was no effective pressure in the clay or on its boundaries.

Another series of experiments was made on MX-80 clay saturated with distilled water and enclosed in autoclave cells giving high porewater overpressures by the heating. The overpressure is estimated to have been 40–70 MPa for temperatures up to 200°C and the swelling pressure of the clay samples, which had a density of 1300 kg/m^3, is believed to have been about 70 kPa. XRD analysis after extraction of the clay and preparing it by sedimentation in the usual fashion demonstrated very small changes in interlamellar spacing, i.e. from 16.7 Å for room temperature reference samples to 16.7 to 17.3 Å spacings (001) for samples heated for 0.5 years at 150 and 200°C, respectively.

The latter study hence confirmed that no permanent contraction or compression takes place under very low effective pressure in the course of the heat treatment but the peak heights were increased by 5 and 50 %, respectively, indicating that alignment of stacks of lamellae had in fact taken place. This process was probably caused by compression and reorientation of the stacks under the effective pressure that actually existed. It is believed that compression of the stacks of lamellae was triggered by heat-induced reduction of the strength of the interlamellar hydrate layers [15]. Permanent reduction in interlamellar spacing can result from cementation of precipitated compounds but the initial spacing will otherwise be restored as discussed in Chapter 6.

2.6   Tentative conclusions from examining MX-80 clay

The following aspects and conclusions are significant:

- Changes in the degree of interlamellar hydration at complete water saturation of the clay requires changes in effective pressure.

- Hydration/dehydration is perfectly reversible if the clay is completely water saturated but associated microstructural changes may cause hysteresis effects.

2.7 References

1. Grim R E, Gueven N, 1978. Bentonites. Developments in Sedimentology 24. Elsevier Publ. Co.

2. Forslind E, Jacobsson A, 1972. Clay-water systems. Water, a Cemprehensive Treatise (Ed. Franks), Plenum, New York.

3. Gast R G, 1977. Surface and colloid chemistry. Minerals in Soil Environment (Ed. Dinauer), Soil Science Society of America, Madison, Wisconsin.

4. Pusch R, 1973. Influence of organic matter on the geotechnical properties of clays. Document D11:1973, Nat. Swed. Build. Res. Council, Stockholm.

5. Pusch R, 1999. Mobility and survival of sulphate-reducing bacteria in compacted and fully water saturated bentonite – microstructural aspects. Technical Report TR-99-30, SKB, Stockholm.

6. Nakano M, Fuji K, Hara K, Hasegawa H, Fujita T, 1998. Changes of the stacked structure of montmorillonite in unsaturated bentonite with compression: Estimation based on calculated chemical potential of water. Preprints Workshop on Microstructural Modelling of Natural and Artificially prepared Clay Soils with Special Emphasis on the Use of Clays for Waste Isolation (Ed Roland Pusch). Clay Technology AB, Geodevelopment AB, SKB, POSIVA, EC.

7. Kehres A, 1983. Isothermes de deshydration des argiles, energies d'hydration – Diagrammes de pores surface internes et externes. Doct. Thesis Universite Paul Sabatier de Toulouse.

8. Mamy J, 1968. Recherches sur la position des cation echangeables et de l'eau dans les montmorillonite: Proprietes dielectriques et structure du film d'eau. Ann. Agron., Vol.19 (p.175).

9. Carlsson T, 1986. NMR-studies of pore water in bentonite/water/electrolyte. Mate. Res. Soc., Ed. Werme, Vol 50 (p.609).

10. Pusch R, 1993. Evolution of models for conversion of smectite to non-expandable minerals. SKB Technical Report TR 93-33.

11. Torikai Y, Sato S, Ohashi H, 1995. Thermodynamic properties of water in compacted sodium montmorillonite. Nuclear Technology, Vol 115 (pp. 73–79).

12. Pusch R, Karnland O, Hökmark H, 1990. GMM – A general microstructural model for qualitative and quantitative studies of smectite clays. SKB Technical Report TR 90-43, SKB, Stockholm.

13. Colten V A, 1986. Hydration states of smectite in NaCl brines at elevated pressures and temperatures. Clays and Clay Minerals, Vol 34 (pp. 385–389).

14. Pusch R, Karnland O, 1988. Hydrothermal effects on montmorillonite. A preliminary study. SKB Technical Report TR 88-15, SKB, Stockholm.

15. Pusch R, 1987. Permanent crystal lattice contraction – a primary mechanism in thermally induced alteration of Na bentonite. Scientific Basis for Nuclear Waste Management. In Bates & Seefeldt (Ed), Materials Research Society Symposium, Proc. Boston (pp. 791–802).

3 Maturation of MX-80 buffer

3.1 General

Maturation is the term for water saturation and homogenization. For the basic case of an incompletely water saturated element of clay confined between stiff boundaries that provide water, the rate of saturation is a complex process, involving both hydration and microstructural reorganization in the form of local expansion and consolidation in conjunction with breakage, deformation, displacement and rotation of stacks and aggregates of stacks.

3.2 Primary structure of compacted MX-80 powder

3.2.1 General

According to a procedure considered by SKB, POSIVA and ENRESA, air-dry clay powder is poured in a form and compacted uniaxially or triaxially under high pressure to form highly compacted blocks.

The powder grains have an internal structure inherited from the natural bentonite beds where the clay material was mined. They consist of a relatively homogeneous matrix of more ore less aligned stacks of lamellae between which there are very small, isolated voids. Commonly exploited bentonites have a dry density of 1900 to 2200 kg/m^3 with 1 or 2 hydrate layers in the interlamellar space. The charge conditions within the stacks, which contain 3–5 lamellae in Na montmorillonite and about 10 lamellae in Ca montmorillonite, are different from those at the external surfaces of the stacks in the sense that only cations are present in the interlamellar space while complete electrical double-layers are formed at the outer surfaces. At such high bulk densities the charge conditions and the energy state of the hydrates in the interlamellar space control the expandability and swelling pressure, while at low densities, the interaction of stacks through their electrical double-layers determines these properties.

According to a standard procedure clay blocks are prepared by compacting air-dry clay powder under a pressure of 100 MPa. The dry density of the grains is about 1980 kg/m^3 for 10 % water content by weight, and the dry density of the powder mass poured in the form and slightly compacted is about 1200 kg/m^3 and 1800 kg/m^3 in saturated form. Uniaxial compression causes reduction in void space between the grains and deformation of the grains that has been calculated by applying the boundary element code BEASY [1], assuming the powder grains to behave elastically.

The calculation started by investigating the contact region of the two spheres in the unit cell with respect to their interaction. It was performed stepwise applying constraints to the system matrix that allowed large amounts of sliding. The conclusion was that the sphere contacts should be taken as sticking, while those between the spheres and the boundaries, i.e. the cell walls, can be taken as frictionless and sliding. The compressive strain was calculated in 3D taking the initial powder particles to be spherical and form unit cells consisting of one big grain and 8 small grains, which roughly matches the granular distribution of MX-80 powder. The diameter was assumed to be 0.35 mm for the big grain and 0.10 mm for the small ones. The initial void ratio corresponded to 1.08 and the initial "effective" porosity (i.e. excepting

the small voids in the granules) 47 %, both being representative of slightly compacted MX-80 powder. A unit cell with 1/8 of a big grain and 1 small grain is shown in Figure 3-1.

The modulus of elasticity of the grains was taken as 500–5000 MPa in different calculations while Poisson's ratio was set at 0.3 in all of them. The resulting uniaxial deformation of the unit cell with 0.175 mm edge length was 0.052 mm, yielding a total uniaxial compressive strain of the system of about 28 %, which is on the same order of magnitude as recorded at practical compression. The reduction in "external" pore volume is from 0.00255 mm^3 to 0.00165 mm^3, i.e. by 34 %. The net dry density of the model clay is 1850 kg/m^3 yielding a density after complete water saturation of 2050 kg/m^3. Buffer with this density is taken as reference clay in this chapter.
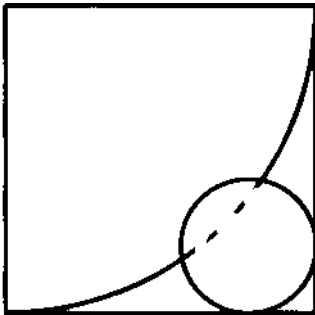

Figure 3-1. *Unit cell with 1/8 of big grain (0.35 mm) contacting one small grain (0.10 mm). The edge length of the cubical cell is 0.175 mm.*

3.2.2 Distribution of stresses and water in the freshly compacted MX-80 clay

Grain stresses and interlamellar water in the freshly compacted clay

The stress state of the grains was found to be very high in the centers of the grains and at their contacts. Thus, the Mises stress exceeds 200 MPa in the interior of the grains while it is zero in the shallow, free parts. Where the stress is higher than 200 MPa water will be totally expelled from the interlamellar space to the shallow parts of the grains where the stress is much lower. These stress-free parts absorb water that diffuses from the inner parts, and expand to host up to 3 hydrate layers in Na clay and 2 layers in Ca clay. Examination of parallel, consecutive sections of the computer-vizualised unit cell showed that there are open voids in all sections consisting of two to three channels with 10–20 μm diameter in the tightest ones, while in the most open sections there are three channels with up to 80 μm width.

Grain expansion and hydration

Subsequent uptake of water from the boundaries of the unit cell will cause expansion of the grains but this process will be different in different parts of the grains; the dense central parts being under high pressure will take up little or no water, while the rest will expand. Taking the expansion of the grains to be exclusively caused by interlamellar uptake of water one can calculate the resulting "external" porosity and pore dimensions and this has been made by use

of BEASY [1, 2]. Figure 3-2 shows the outcome of the calculations in simplified form. The unit cell compressed uniaxially in the compaction phase is shortened and the subsequent hydration yields expansion of the grains such that the remaining voids form channels with varying aperture.
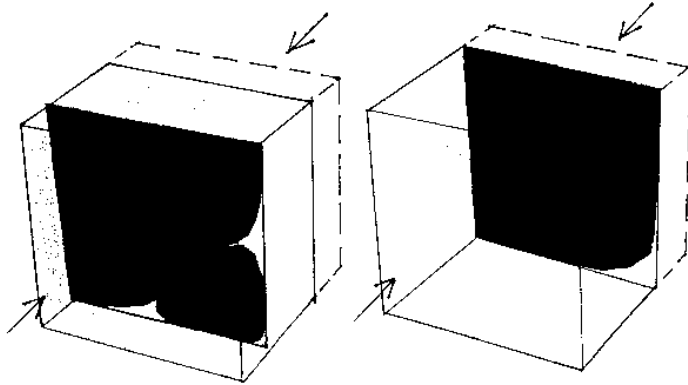

Figure 3-2. *Axial shortening of the unit cell in the compaction phase, and resulting permeable voids forming channels as illustrated by two sections of the hydrated cell.*

While there are no straight open channels between the expanded grains through the clay, tortuous channels are formed by interconnected voids with a diameter of down to10 μm. A 1 mm^2 cross section through this model clay with a density at saturation of 2050 kg/m^3 contains 3 voids with 10 μm diameter. However, because of the statistical distribution of the grain orientation and because the grains do not make up perfect stacks of smectite lamellae but contain small voids between small stacks, it is expected that there are voids ranging from tens of Å to tens of micrometers.

In practice, the very high shear stresses that are associated with the compaction exceed the shear strength of the grains and they hence break and produce fragments that move into the voids where they rearrange and form gels of lower density than the central parts of the grains. This means that there are considerable variations in density on the microstructural scale, which is of great practical importance as we will see in later chapters.

3.3 Secondary, hydration-generated structure of MX-80 clay

3.3.1 Microstructural processes

The dense MX-80 grains become hydrated and expand when exposed to water. A cross section through matured (water saturated and "homogenized") MX-80 clay is illustrated in Figure 3-3, which shows expanded grains between which clay gels are spontaneously formed by linking of aggregates that exfoliate from the grains. The gel density is a function of the size of the voids between the expanded grains. For lower gel densities than about 1600 kg/m^3 and Ca as adsorbed cation and also at higher electrolyte contents than about 2000 ppm with Na as

major cation the gels are not physically stable; they coagulate and form separate aggregates, thereby contributing rather little to the flow resistance at permeation.

Grains with interlamellar voids

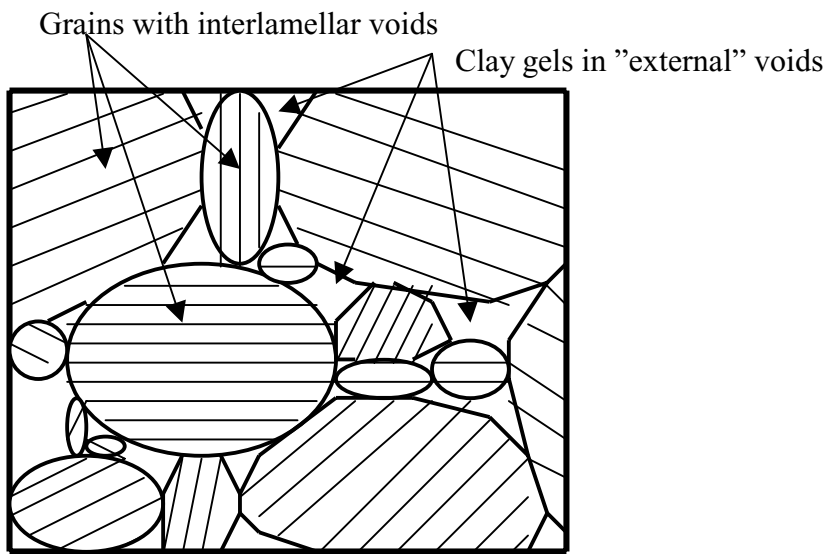Clay gels in "external" voids

Figure 3-3. Generalized microstructure of MX-80 clay formed from compacted powder grains. The gel fillings have different densities, lowest for the largest voids and highest for the smallest voids.

3.3.2   Expansion and deformation of grains

Naturally, the idealized conditions represented by the unit cell are not perfectly valid in practice, primarily because 20 % of the grains are smaller than 0.10 mm, meaning that the largest voids in the tightest sections after compaction are smaller than 5–10 µm. Another factor is that the grains are in fact anisotropic and hence expand significantly more in one direction than in the others, i.e. almost 3 times more than for grains with randomly oriented stacks of flakes. This means that where the big grain of the unit cell expands towards the small grain there will be no open space left in cross sections of the type shown in Figure 3-4, irrespective of the orientation of the small grain. Where the lamination of the small grain is oriented parallel to that of the big grain, the tightness is even stronger and expansion to hold more than 1–2 hydrate layers in the stacks will not be possible. This gives a major contribution to the bulk swelling pressure.

3.3.3   Formation of clay gels by release and rearrangement of clay aggregates from expanding grains

Release of clay particles

Exposure of the grains to water entering the system of open voids in the compacted clay makes them absorb water and since this process is not uniform, mechanical stresses are generated in the grains. Non-uniform expansion and quick migration of water will release particles consisting of stacks of lamellae of which many are assumed to remain bonded to the expanding grains while others are free to move in the voids [2].
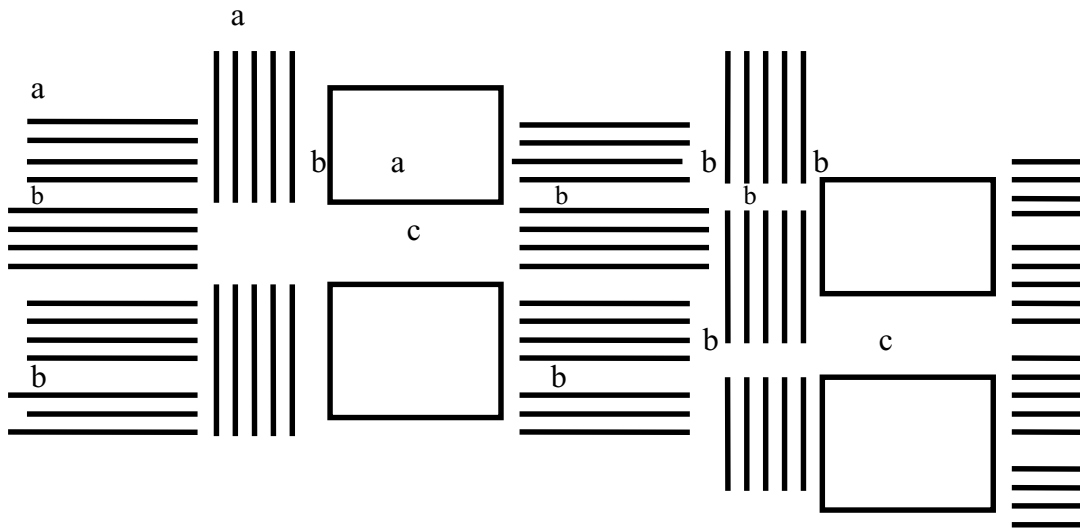
Figure 3-4. *Schematic 2D structure of smectite clay formed from expanded grains.
a)=anisotropic grains taken to be one big stack of lamellae. b) channels with diameters
ranging between a few tens of Å to several micrometers , c) Local, wide void with a diameter
of a few tens of micrometers.*

Impact on aggregation of porewater chemistry

The porewater chemistry is the dominant factor affecting the density and structure of the clay
gels formed in the voids between expanding grains. The impact, which is illustrated in Figure
3-5, explains why e.g. Ca bentonite has a higher hydraulic conductivity than Na bentonite.

Figure 3-5. *Schematic picture of coagulation of clay particles. Left: Structurally
homogeneous clay network. Right: Coagulation by increased electrolyte concentration in the
porewater.*

Gelation process

Dispersed particles move by Brownian molecular motion and easily form gels if the charge is favorable. The motion is both rotational and translatory and the highest probability is that particle contact is established edge-to-edge [4]. However, the charge distribution over the particle surfaces an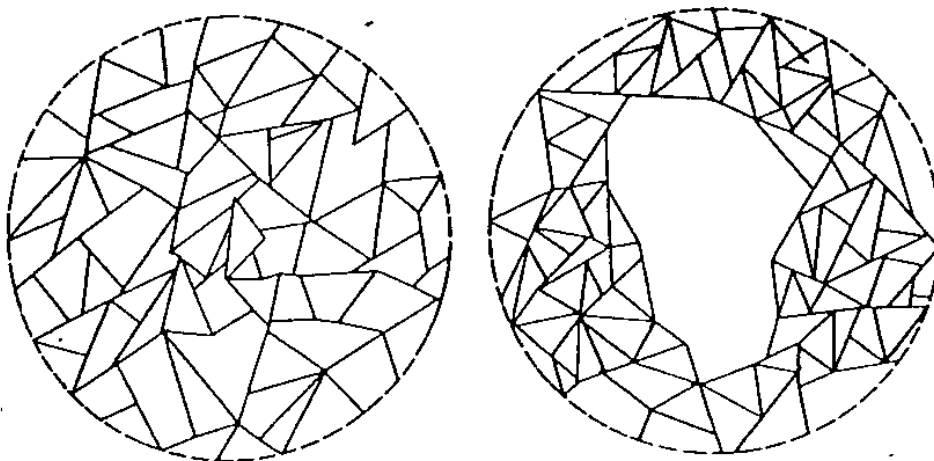d also the conditions for bringing particles in close contact affect the way in which adjacent particles make and remain in contact.

The most simple structure model implies that coagulation of dispersed particles takes place by Coulomb-type attraction of nearby particles, i.e. through bonding of the commonly positively charged part of one particle and negatively charged parts of an adjacent particle. There is strong evidence that the edges of the stacks are positively charged in the neutral and acid pH ranges (pH <7–8), while the basal planes carry a negative charge, hence yielding edge-to-face aggregation.The positive charges are believed to result from processes of the type indicated by Eq.3.1 [5].

$$\text{Al-O-Al} \longrightarrow (\text{Al-O} + \text{Al}) + (\text{H OH}) \longrightarrow \text{Al-(OH)} \qquad\qquad (3.1)$$

Negative edge charge is believed to result from dissociation of structural OH. However, it has been proposed that this is a questionable process since the hydroxyls are bound to lattice aluminum or magnesium and stay in the lattice but in protonated form [5]. Spontaneously approaching particles with negative edge charge and negatively charged basal planes, which conditions prevails at pH>8, can become bonded together by ion-pairing [6].

Equally charged smectite clay particles in suspensions can in fact also associate in a face-to-face fashion by electrical double layer interaction [6] but the coupling is weak except at low and moderate electrolyte contents. Particle association of this sort may take place spontaneously in suspensions but it is typical of compressed ("consolidated") and sheared states. Association of edge-to-edge (reticulate) form results from rotationary motion of dispersed particles with ion-pair bonding being responsible for the interparticle coupling [4]. Even detailed electron microscopy may not give a true picture of the interparticle association. Thus, edge-to-face coupling caused by Coulomb attraction of different edge and basal plane charges may in fact be face-to-face contacts since the edges are often very thin and curved and micrographs may hence give the same impression as a true edge-to-face association. Edge-to-edge contacts may in fact be of edge-to-edge or edge-to face type because of difficulties in interpreting electron micrographs.

At face-to-face coupling, lateral growth of stacks of lamellae may take place leading to large, i.e. micrometer-sized, flat aggregates. Light scattering and viscosity measurements of montmorillonite in the pH range 6–13 have indicated formation of ribbons of edge-to-edge flocs, but cardhouse-type edge-to-face association is probably the dominant structuring process at neutral and acid pH [6].

Nature and size of gel-forming aggregates

Particles in suspensions are affected by Brownian motion that provides opportunities for interparticle coupling of both equally and differently charged crystallites if the concentration of solids is sufficiently high. Thus, in principle, suspensions are not stable but undergo coagulation through formation of particle aggregates.

Aggregation by coagulation of discrete montmorillonite particles and small aggregates have been investigated by use of transmission and scanning electron microscopy [7]. Figure 3-6 illustrates the arrangement of particles in very soft gels (<1300 kg/m^3) of cardhouse type formed in natural smectite clay. The micrographs show many apparent edge-to-face contacts and edge-to-edge couplings and also face-to-face arrangements but they may in fact all be of the same type. Figure 3-7 serves as documentation of the process of grain expansion and disintegration of smectite grains on hydration.

Figure 3-6. *Transmission electron micrograph of stacks of montmorillonite lamellae forming a very open structure of cardhouse type (Bar is 1 μm). Sample from the Pacific floor with 81 % clay content, mostly smectite, and a void ratio of 3.5 (bulk density about 1300 kg/m^3). A zeolite aggregate is seen at the base. Micrograph by R H Bennett.*
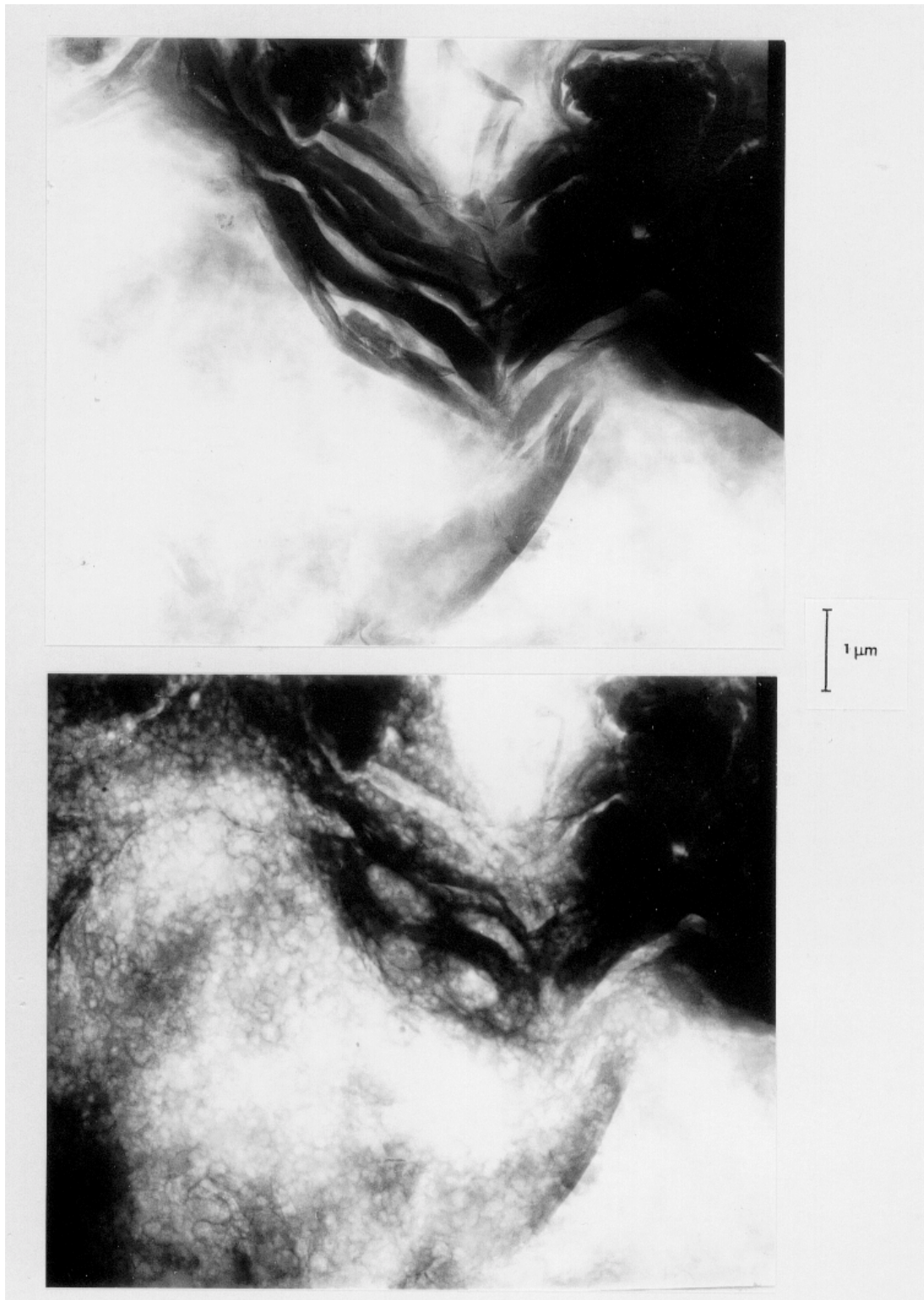
Figure 3-7. Expansion of vacuum-dried MX-80 clay at hydration in humid cell placed in a 1.5 MV transmisson electron microscope [7]. Upper: Dry state. Lower: Hydrated and expanded state. Bar is 1 μm.

3.4　Rate of water saturation

3.4.1　Hydration potential

The hydration potential of compacted smectite powder is determined by the number of stacks per unit volume, of which the dry density is a measure, and of the number of hydrates in the stacks of lamellae, as well as of the type of adsorbed cation. The hydration potential, which can be calculated using thermodynamics [8] is manifested by the suction exerted by the clay as illustrated by Table 3-1.

The density distribution in the microstructure means that very dense parts have the highest affinity for water and the softest one the lowest hydration potential. Open continuous voids remain dry at low and medium relative humudity (RH) but they become water-filled by capillary forces if contaced with water or air with RH 100.

Table 3-1. Generalized hydration conditions of MX-80. A/B gives data for Na (A), and Ca (B).

Dry density, kg/m³	Density at complete water saturation, kg/m³	Number of interlamellar hydrates	Suction, MPa	Ratio of volume of extralamellar voids and total volume (external porosity)	Ratio of volume of interlamellar voids and total volume (internal porosity)
1800	2130	(1–2)/2	15/20	0.13/0.13	0.10/0.10
1350	1850	2/2	1/1	0.35/0.35	0.30/0.30
900	1570	3/2	0.3/0.02	0.57/0.50	0.50/0.45

The continuous voids are assumed to make up an orthogonal network of channels, which, at water satuaration, will be filled filled with porous clay gels containing capillary voids. This implies a variation in density on the microstructural level.

3.4.2　Processes

Hydration of the non-saturated clay implies that the grains expand and ultimately form the gel-filled channels indicated in Figure 3-3. The dense clay matrix has a high hydration potential and expands at a rate that is determined by the access to water. One can distinguish between three boundary conditions:

1) The clay is contacted with water vapor (RH=100 %).

2) The clay is contacted with liquid water that is not pressurized.

3) The clay is contacted with pressurized water.

The different conditions are believed to cause different hydration rates as described below.

1. Contact with water vapor

Water molecules migrate into the open voids and get sorbed on exposed mineral surfaces from where they migrate into the interlamellar space that has the highest hydration potential. Since the migration takes place along surfaces with differences in water content as driving force, the entire process is one of diffusion. The saturation process is sufficiently slow to let entrapped air be dissolved and diffuse from the clay without delaying the saturation process.

2. Contact with non-pressurized liquid water

Water is sucked up by capillary forces in the open channels from which water molecules migrate into finer voids and further into the interlamellar space. Since the clay matrix thereby expands the channels become closed rather early and the hydration is then controlled by diffusion as in Case 1. The hydration process can be described as one of diffusion. For initially non-saturated smectite-rich clay contacted with free water but prevented from expanding the diffusion coefficient can be taken as 3E-10 m^2/s [9].

Calculation of the rate of wetting of compacted MX-80 blocks considering it to be controlled by diffusion using this value has yielded the results in Table 3-2 and in Figures 3-8 and 3-9. For the calculation, which concerned uniaxial uptake of water from one end of a confined sample, the results were expressed in terms of dimensionless quantities, τ and x/L, where x is the distance from the inlet boundary and L is the length of the sample. The calculations were made by Jarmo Lehikoinen, VTT, Finland using a computer code developed in conjunction with an earlier study [2].

Dimensionless time, $\tau = \dfrac{Dt}{L^2}$,

where $D = 3.0 \times 10^{-10}$ m^2/s, and $L = 20$ mm or $L = 400$ mm.

The calculations were made for two different intial degrees of water saturation, 50 and 85 %, of which the firstmentioned corresponds to the water content of blocks prepared by compacting air-dry MX-80 powder under 50–100 MPa pressure (w=10–12 %), and the other a water content of about 20 %, which requires artificial wetting of the powder before compaction.

Table 3-2. Time required for attaining water saturation profiles shown in Figs. 3-8 and 3-9.

τ (-)	t (days)	
	$L = 20$ mm	$L = 400$ mm
0.1	1.5	617
0.5	7.7	3086
1.0	15.4	6173
1.5	23.1	9259

Initial water saturation 50 %

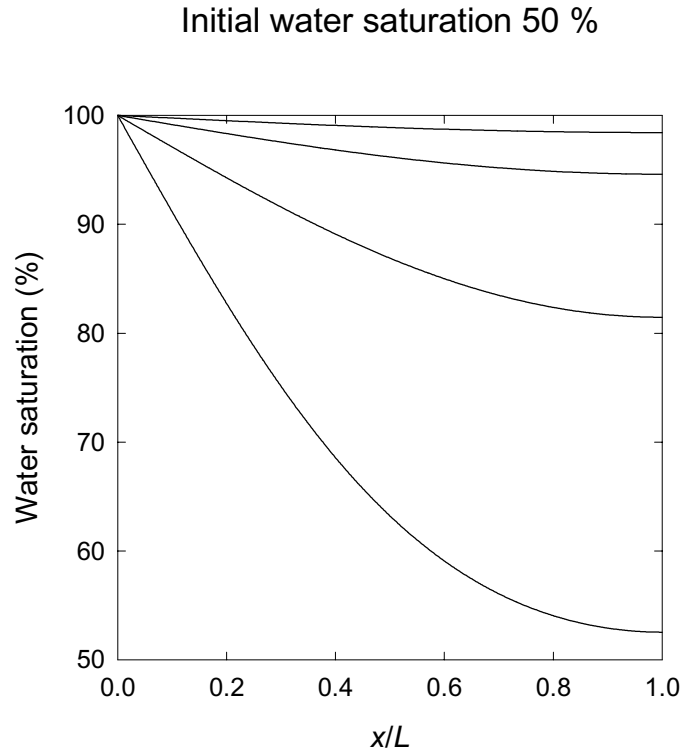**Figure 3-8.** *Evolution of clay water saturation for 50 % initial saturation. Lines from top to bottom, τ = 1.5, 1.0, 0.5 and 0.1.*
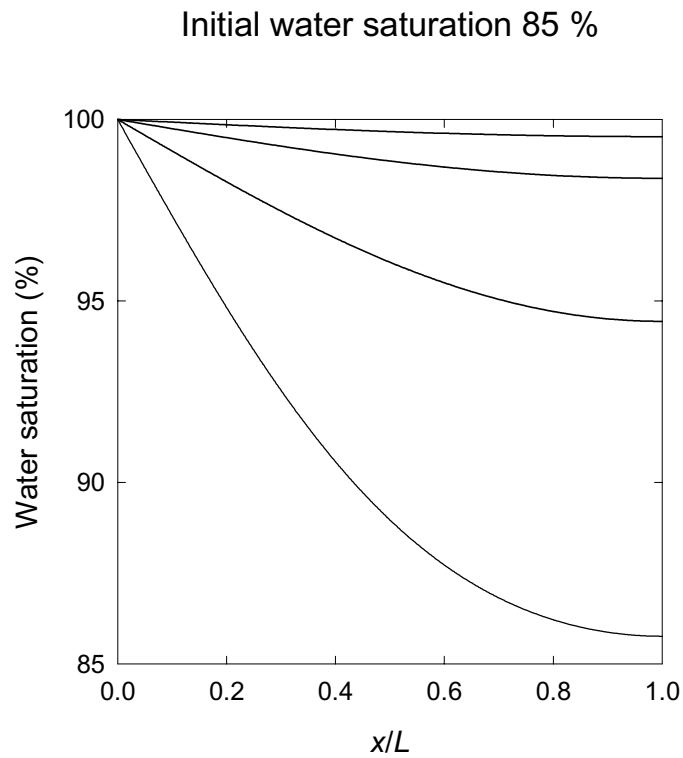
Initial water saturation 85 %

Figure 3-9. *Evolution of clay water saturation for 85 % initial saturation. Lines from top to bottom, τ = 1.5, 1.0, 0.5 and 0.1.*

These calculations demonstrate that it will take about 15 days to reach about 90 % saturation of all parts of the sample with 20 mm length and 50 % initial degree of saturation, and that a 400 mm block will require about 17 years to reach 90 % saturation. For an initial degree of water saturation of 85 % an increase to 90 % will require about 4 years. One hence finds that the saturation of buffer blocks in KBS3 deposition holes will be very slow if the water pressure is low.

3. Contact with pressurized water

Water is pressed into the largest open channels and moves quickly and deeply into the clay matrix, particularly when the pressure and electrolyte contents are high. The penetrating water displaces air and compresses the unsaturated matrix. Since a considerable fraction of the voids become water-filled quickly, the average degree of saturation is expected to be raised very early and the dominating process hence being redistribution of water from the larger channels into the clay matrix and associated redistribution of minerals. No systematic tests of this sort have been performed yet and the hypothethis can therefore not be validated. However, preliminary experiments with MX-80 clay with a dry density of 1800 kg/m^3 (2130 kg/m^3) have shown that saturation of 50 mm long cylindrical samples exposed to a temperature gradient of 70°C (30°C at one end and 100°C at the opposite) with water entering from the cold end was much quicker at a water pressure of 500 kPa than of 50 kPa (Table 3-3).

Table 3-3. Water saturation of 50 mm long samples with an average dry density of 1800 kg/m^3 and initial water content of 10 % exposed to a temperature gradient and a water pressure at the cold end for 45 days [Karnland SKB Arb. Rapp. 95-31]. 3.5 % NaCl solution.

Distance from cold end, mm	Water content after 45 days at 50 kPa pressure	Water content after 45 days at 500 kPa pressure
10	47	45
20	45	40
30	32	38
40	12	37
50	8	40

3.4.3 Influence of porewater chemistry

Saturation with saline water is expected to speed up the wetting rate because the gels formed in the voids between the grains will coagulate and let water in through wider passages (cf. Figure 3-5). This would be particularly obvious for a Ca-rich solution, the hypothesis being supported by the earlier mentioned hydrothermal tests referred to in Table 3-3, which also comprised tests with different salt solutions. Table 3-4 shows that an increase in water content of the inner, hot parts of a sample exposed to a solution with 3.5 % CaCl$_2$ solution took place in contrast to the case with 3.5 % NaCl solution.

Table 3-4. Water saturation of 50 mm long samples with an average dry density of 1800 kg/m³ and initial water content of 10 % exposed to a temperature gradient and a water pressure at the cold end for 45 days [Karnland SKB Arb. Rapp. 95-31]. 50 kPa water pressure.

Distance from cold end, mm	Water content after 45 days for 3.5 % NaCl solution	Water content after 45 days for 3.5 % CaCl₂ solution
10	47	45
20	45	41
30	32	38
40	12	33
50	8	28

3.4.4 Influence of water pressure

Ongoing additional tests indicate that a water injection pressure on the order of 0.5 to 1 MPa has a significant impact on the wetting rate of dense MX-80 clay. Such a pressure can be applied in boreholes in compacted blocks for speeding up the hydration and if it develops at the rock/buffer contact in a deposition hole it is expected that cause significantly quicker water uptake than provided by pure diffusion as described in earlier in this chapter. Water will also penetrate the joints between the buffer blocks and enter the initially empty slot between the canister and the blocks where it will be vaporized. This process will be stopped rather quickly because of the saturation of the outer parts of the blocks, which makes the joints self-seal, but the amount of water that has passed through will cause some wetting of the blocks adjacent to the canisters. The vapor formed may cause some chemical changes of the clay as discussed in a later chapter.

3.5 Water retention

3.5.1 General

Dehydration of the buffer will take place close to the hot canisters early after application of the latter in the deposition holes. Water will be vaporized and migrate in gaseous form from the hot part to the colder outer part of the buffer as illustrated by Figure 3-10. The drying means that extralamellar water will be lost first followed by surface-diffusive migration of interlamellar water to the outer surfaces of the stacks of lamellae and further to the wider passages where it evaporates etc. There will a balance between the amount of extralamellar and interlamellar water.

If the blocks have been prepared by using wetted powder the process will be somewhat different. Thus, softer parts of the clay matrix, i.e. the gel fillings will dehydrate most easily, which means that a system of interconnected larger voids may be formed and that further dehydration involves loss of water from the interlamellar space. The process of dehydration is hence an inversed hydration scenario with some hysteresis due to homogenization with respect to water content and density of the clay matrix.

Under the foreseen temperature conditions in KBS3 deposition holes macrostructural changes will take place in the drying part of the buffer in the form of radial and horizontal fractures with an aperture of several millimeters. It is not known if they self-seal completely at the end of the hydration process or if chemical processes take place at their surfaces.
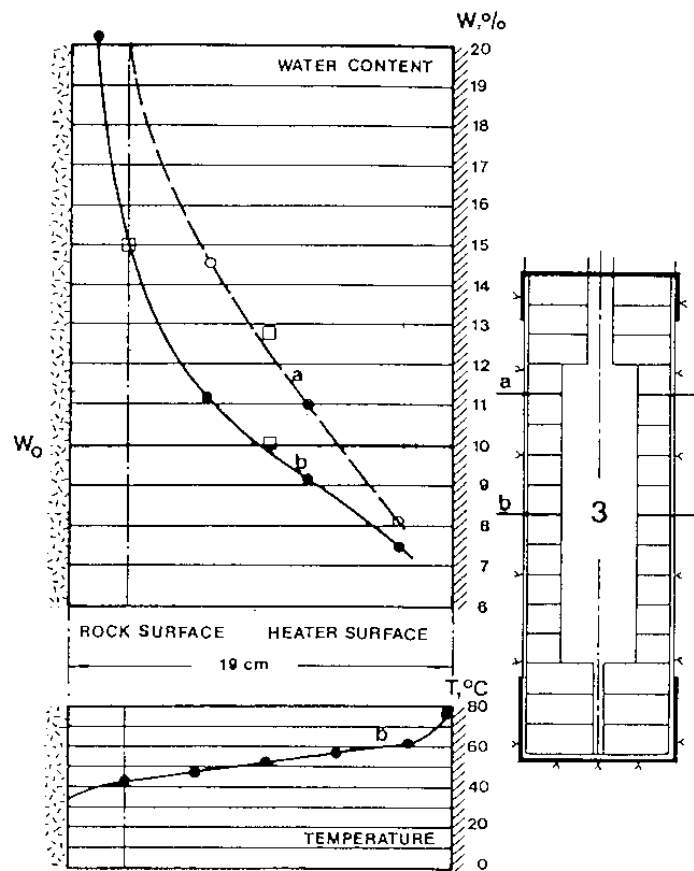

Figure 3-10. *Moisture distribution at two levels in MX-80 buffer embedding a 600 W heater in a "deposition hole" with 0.76 m diameter and 3 m depth in Stripa granite. The profiles represent the conditions after 4 months. At the rock contact the clay was fully saturated (20 % water content), while the water content had been reduced from the initial water content 10 % to about half the buffer thickness [10]. Fractures were observed at the excavation of the clay for determination of the water content distribution.*

3.5.2   Salt accumulation

The earlier mentioned study (O. Karnland, SKB Report 95-31, Tables 3.3 and 3.4) of the effect of thermal gradients, water pressure and porewater composition, gave some information on salt accumulation and precipitation in the hydrating clay and indicated that this phenomenon must have an impact on the microstructure and thereby on the bulk properties of the clay. Hence, it showed that enrichment of electrolytes and certain accessory minerals can be significant at 100°C under the investigated temperature gradient, i.e. 14°C per centimeter. Thus, it was found that sodium chloride and sulphate peaks appeared at the wetting front, a possible mechanism being cyclic evaporation/condensation of the solution driven in from the cold end of the samples. The recorded sulphate peak was assumed to originate from sulphur-bearing minerals that dissolved and appeared as gypsum and anhydrite at the wetting front. These minerals have a reversed solubility, i.e. they precipitate at increased temperature.

The influence of salt accumulation on the microstructure is believed to be a more extensive coagulation than would be caused by the average electrolyte content of the fluid with which the clay is being saturated.

3.6   Tentative conclusions from examining the maturation of MX-80 clay

The following findings are significant:

- The bentonite powder that is used for preparing clay buffer blocks can be relatively coarse-grained since the compaction pressure, which is commonly about 100 MPa, causes crushing by which a size distribution is obtained that is suitable for reaching a high degree of homogeneity of the compacted blocks. Both isostatic and uniaxial compaction yield blocks that are free of visible fissures and fractures if the size is rather small, while special techniques must be applied for preparing large, fracture-free blocks [11, 12]. After hydration under confined conditions, which causes expansion of the powder grains and formation of soft clay gels by exfoliation of aggregates from the expanding and disintegrating grains, the clay matrix has a varying density on the microscopic scale, which controls a number of bulk properties, particularly the hydraulic and gas conductivities.

- The rate of water saturation can be described as one of diffusion at low water pressure. At high pressure water moves in quickly through wider void systems and is distributed in the clay matrix by secondary diffusion. A high electrolyte content speeds up the saturation even more.

- When the initial degree of water saturation is low, i.e. about 50 %, water flow through film transport takes place from cold towards hotter and drier parts of the clay, where it is evaporized and flows back in vapor form in a cyclic manner. This appears to bring in salt that accumulates at the wetting front. The effect of this process can be minimized by hydrating the clay powder used for block compaction, or by injecting water under high pressure in the clay blocks.

3.7   References

1. BEASY, 1995. User Guide, Computational Mechanics BEASY Ltd, Southampton, UK.

2. Pusch R, Muurinen A, Lehikoinen J, Bors J, Eriksen T, 1999. Microstructural and chemical parameters of bentonite as determinants of waste isolation efficiency. Final Report, European Commission Contract No F14W-CT95-0012.

3. Pusch R, 1983. Stability of bentonite gels in crystalline rock – Physical aspects. SKB Technical Report TR 83-04.

4. Pusch R, 1970. Clay Microstructure. Nat. Swed. Build. Counc., Document D:8. Nat. Swed. Build. Council, Stockholm.

5. Lagaly G, 1989. Characterization of flow of kaolin and bentonite dispersions. Applied Clay Science, Vol.4 (pp.105–123).

6. Swartzen-Allen S L, Matijevic E, 1974. Surface and colloid chemistry of clays. Chemical Reviews, Vol.74, No.3 (pp.385–391).

7. Pusch, R, 1987. Identification of Na-smectite hydration by use of ”humid cell”. High Voltage Microscopy. Applied Clay Science, Vol.2 (pp.343–352).

8. Ichikawa Y, Kawamura K, Nakano M, Kitamaya K, Kawamura H, 1998. Unified molecular dynamics/homogenization analysis for water flow in bentonite. Int. High-level Radioactive Waste Management Conference (ANS), Las Vegas.

9. Börgesson L, 1985. Water flow and swelling pressure in non-saturated bentonite-based clay barriers. Engineering Geology, Vol.21 (pp.229–237).

10. Pusch R, 1994. Waste Disposal in Rock. Developments in Geotechnical Engineering, 76. Elsevier Publ. Co, ISBN:0-444-89449-7.

11. Johannesson L-E, Börgesson L, Sanden T, 1995. Compaction of bentonite blocks. Development of technique for industrial production of blocks which are manageable by man. SKB Tecnical Report TR-95-19.

12. Johannesson L-E, Nord S, Pusch R, Sjöblom R, 2000. Isostatic compaction of beaker shaped bentonite blocks on the scale 1:4. SKB Technical Report TR-00-14, SKB, Stockholm.

4 Microstructural constitution at complete water saturation – the MMM model

4.1 Influence of porewater chemistry

4.1.1 Electrolyte concentration

As in the evolution of the microstructure the porewater chemistry plays an important role since it determines the interlamellar spacing and the interaction between stacks of lamellae through electrical double layers that are formed at their external basal planes. It appears that although most of the surface area and cation exchange capacity – which are of great importance for the physico/chemical stability of the microstructure of smectite clay – are related to the interlamellar space, it may still be that the sites on external surfaces are very important [1]. This is related to the electrical double-layers in Figure 4-1, which illustrates the constitution and extension of the double-layers at the basal planes of stacks of lamellae under marine and fresh-water conditions, respectively. Figure 4-2 describes the charge distribution in the narrow space between two adjacent parallel montorillonite particles with a spacing that allows development of complete electrical double-layers. This matter is basic to the understanding of ion diffusion, which is discussed later in Chapter 5 of this report.
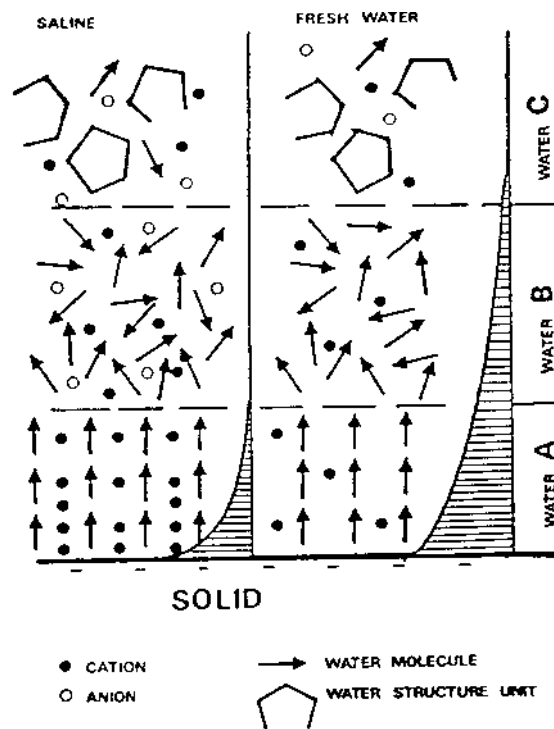

Figure 4-1. *Schematic picture of electrical double-layers at mineral surfaces in saline (marine) and fresh water, respectively. Water A is largely immobile, while Water B is assumed to have a low viscosity. Water C has the same properties as normal, free water.*

As indicated by Figure 4-1 the electrical double-layers extend to a larger distance from the mineral surface at low porewater electrolyte concentrations than at high ones, which means that the clay expands to larger volume in the firstmentioned case.
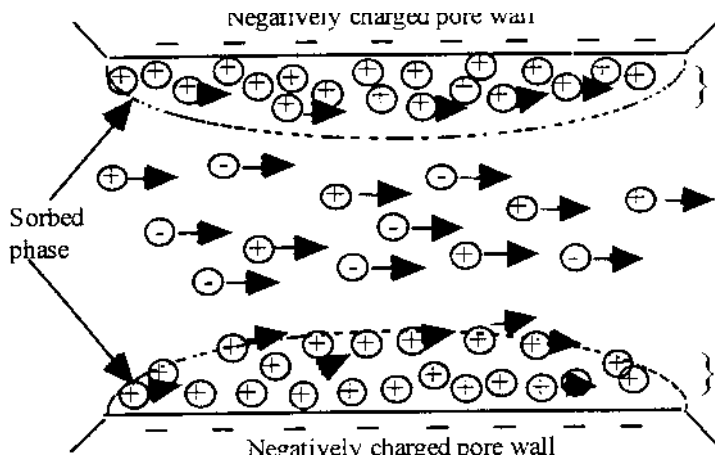

Figure 4-2. Schematic picture of interacting electrical double-layers (After Neretnieks).

The implication of Figure 4-2 is that the space between clay aggregates is smaller at higher densities and that the equally charged units repell each other and hence contribute to the swelling pressure.

4.1.2   Type of adsorbed cation

Since the number of smectite lamellae forming a stack is 3–5 for Na^+ in exchange positions, while it is around 10 for Ca^{2+}, the Ca-state implies that the stacks are thicker and that the softer clay parts consist of bigger particle aggregates yielding larger open voids with a higher degree of continuity than in the Na-state. At high electrolyte concentration with Na as dominant cation coagulation of the softer parts takes place but the voids will not be as large as when Ca is the dominant cation in electrolyte-rich porewater.

The effect of changes in porewater composition on the microstructural constitution is obvious: If the clay initially has Na^+ in the exchange positions and the porewater becomes rich in Ca^{2+}, partial interlamellar dehydration takes place because the stacks of lamellae contract and the voids between them become larger and more continuous, which leads to a drop in shear strength and swelling pressure under constant bulk volume conditions, and to an increased hydraulic conductivity.

4.1.3   Combined influence of density and porewater chemistry

The resulting impact of porewater salinity and bulk density on the microstructure is illustrated by Figure 4-3, in which reference to the swelling pressure is also made. For Ca smectite the much fewer contacts between stacks, i.e. the lower frequency of interacting external double-layers, means that the influence of the salt content on the swelling pressure is appreciably smaller than for the Na case at low and intermediate bulk densities. Hence, there is a difference between Na and Ca smectites concerning their swelling behavior, which is explained by microstructural differences.
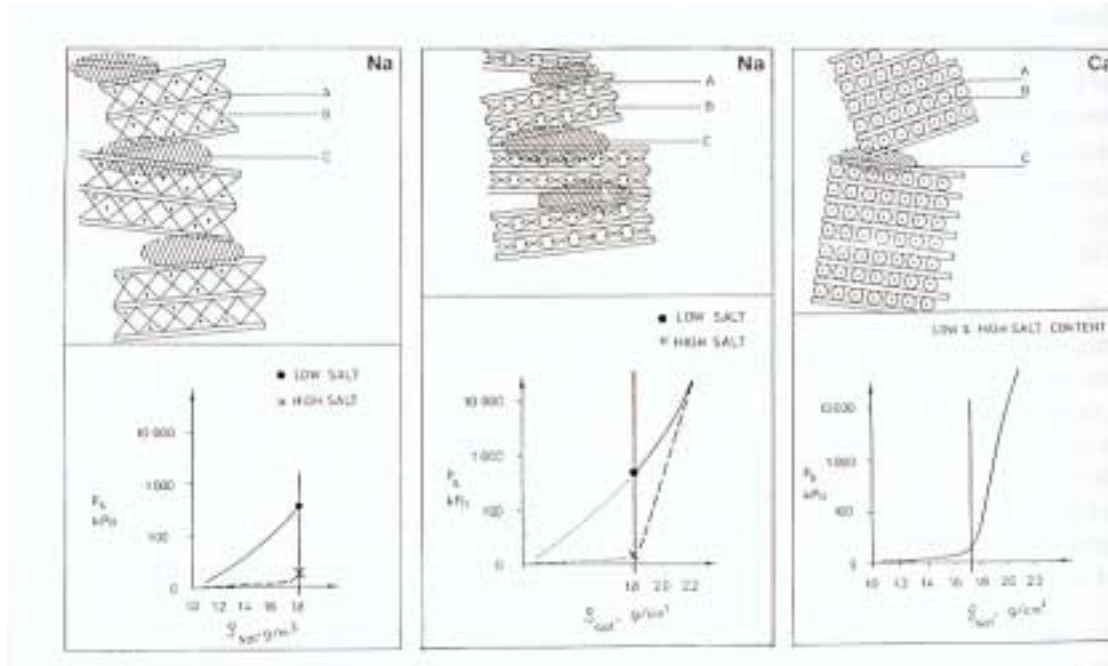

Figure 4-3. *Schematic pictures of stack assemblages and influence of density (at water saturation, expressed in g/cm³ (1 g/cm³ equals 1000 kg/m³) and salinity for Na and Ca montmorillonite clay. A) Lamella, B) Interlamellar space, C) Stack contact region with interacting electrical double-layers [2].*

Naturally, there is a corresponding effect on the hydraulic conductivity in the sense that a high density and a low electrolyte content in the porewater represent a very low conductivity of Na-smectite while that of dense smectite clay in Ca-state is somewhat higher. For low densities the difference between the two states becomes more obvious and for densities lower than 1600–1800 kg/m³ Ca-smectite becomes very conductive because of the above-mentioned lack of microstructural continuity and coherence.

4.2 Microstructural modelling

4.2.1 Quantification of microstructure

The clay matrix is defined here to consist of two major components [3]:

1. Stacks, stack aggregates and non-smectite grains *(a)*
2. Gel-filled voids and unfilled voids *(b)*

This distinction is made on the ground that the firstmentioned component is completely or largely impermeable while the latter offer no or little flow resistance. A further reason is that component *a* is largely responsible for the swelling pressure and that ion migration in it takes place by both pore and surface diffusion but almost entirely by pore diffusion in the *b*-space. The two microstructural components are related through the coefficients F_2 for 2D and F_3 for 3D conditions and their ratio depends on the average and individual bulk densitites as specified in Figure 4-4. The basis for determining these parameters is micrographs of very thin sections of the clay, which must be prepared in a fashion that preserves the microstructural features as well as possible.
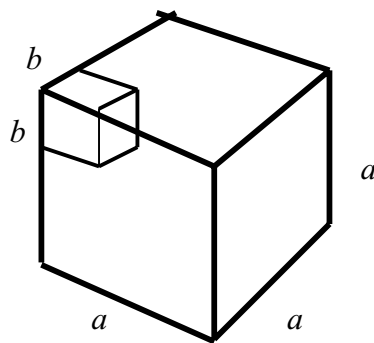
$$2D: \quad F_2=b^2/a^2 \qquad b=a(F_2)^{1/2}$$

$$3D: \quad F_3=b^3/a^3 \qquad F_3=F_2\,(F_2)^{1/2}=(F_2)^{3/2}$$

$$\rho_{av}=\rho_b F_3 + \rho_a(1-F_3)$$
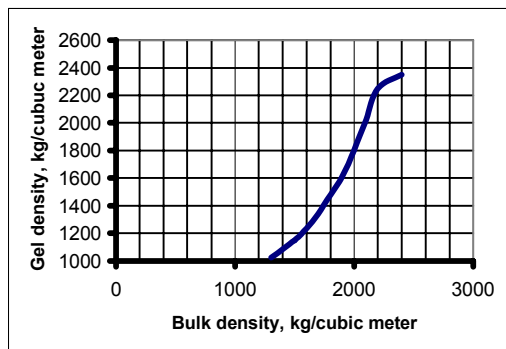

Figure 4-4. *Microstructural parameters. ρ_{av} is the average "bulk" density of the clay and ρ_a and ρ_b the average density of components a (stacks, stack aggregates and non-smectite minerals) and b (soft gel fillings and open space). The diagram shows average gel density (ρ_b) versus average bulk density (ρ_{av}).*

4.2.2   Preparation of micrographs for microstructural quantification

General aspects

Microstructural quantification requires preparation of representative two-dimensional pictures for evaluation of void size and density, which excludes application of scanning microscopy. Electron transmission microscopy (TEM) of clays based on the experience from biology was introduced from early 1960 and its applicability has been assessed in several contexts by different investigators [4, 5, 6, 7]. Impregnation of the clay must be made for preparing hard specimens from which thin sections can be obtained using ultramicrotomy, atom milling or conventional grinding. The required thickness depends on the purpose of the microstructural investigation.

It is essential that the preparation does not alter the clay microstructure significantly. Minor changes related to a change in basal spacing of stacks of smectite lamellae may not be avoidable but the overall pattern of varying void size and clay density must not be appreciably changed. It is hence needed that the porewater is replaced by an impregnation liquid that can enter and fill the voids in approximately the same fashion as water. A second requirement is that the hardened impregnation material must give the clay a strength that permits sectioning without causing mechanical disturbance. Cutting has to be made by use of very sharp glass or diamond knives. Still, where the edge hits quartz, feldspar or heavy minerals these may not be intersected or truncated but moved by the propagating knife causing much disturbance, like folding and disruption of the clay matrix. Such defects will not be caused by alternative preparation techniques like abrasion by neutron bombardment or atomic milling but they may cause other problems.

While the traditional acrylate method works well for clays with illite and chlorite as dominant clay minerals, special measures have to be taken when treating expanding clays. Thus, very significant expansion and disintegration take place if the specimens are not effectively confined.

The" traditional" acrylate method

For acrylate preparation the procedure is as follows. A prismatic specimen with a base area of a few square millimeters and a length of about 10 mm is cut from the water-saturated sample such that its orientation in situ can be defined. It is placed in a solution consisting of 50 % by weight of ethyl alcohol and 50 % distilled water for 30 minutes followed by emplacement in 90/10 ethyl alcohol/water and 99.5 % ethyl alcohol for 5 min. each. It is then transferred to a solution consisting of 85 % by weight of butyl methacrylate and 15 % methyl methacrylate for 45 minutes, the process being repeated twice. Finally, the specimen is transferred to a solution of 98 % monomer and 2 % 2.4-dichlorbenzoylperoxide (EMW) catalyst for 90 minutes. Polymerization is obtained by heating to 60°C for 15 hours.

The "direct" acrylate method

The absence of pressure gradients when applying the "traditional" acrylate method means that stepwise replacement of the respective porewater solutions takes place by diffusion, which is a rather slow process. The whole preparation sequence is therefore very time-consuming and attempts have been made to speed it up by drying the clay and then saturating it with the aforementioned solution consisting of butyl/methyl methacrylate and 2.4-dichlorbenzoylperoxide catalyst in one step only [8].

The disturbance caused by saturating the clay with monomer according to this simpler method may be less severe than that caused by the repeated exposure to different solutions of the traditional technique. However, the influence of drying prior to saturation may cause significant disturbance and needs to be considered. Dehydration by heating clay specimens at $105^{o}C$ or by freeze-drying causes shrinkage of the stacks of flakes by complete loss of interlamellar water, but freeze-drying produces less overall shrinkage and partial preservation of the continuity of the particle network. The difference is small for dense smectites but can be considerable for low densities. Slow drying at RH 40–50 % followed by quick vacuum treatment is estimated to give give slightly less or the same disturbance as freeze-drying at least for high densities (Figure 4-5), and this method is promising for preparation of clays with a density at saturation of at least 1600–1700 kg/m^{3}.
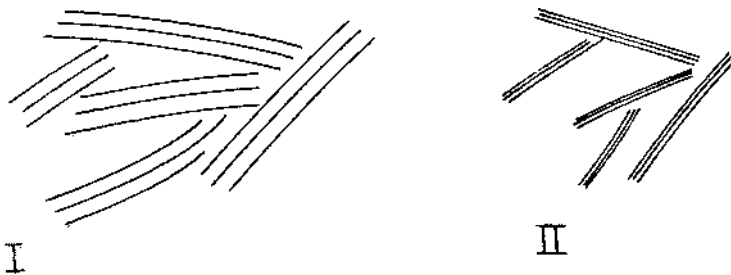

Figure 4-5. Structural effect on smectite clay by drying [9]. Left: Expanded hydrated stacks. Right: Collapsed, dry stacks.

Relevance

The degree to which the microstructural features are preserved by acrylate embedment has been determined by comparing micrographs of acrylate-treated specimens and specimens examined under humic conditions in high voltage electron microscopes (HVEM), and by measuring the swelling pressure in the course of saturating air-dry samples with acrylate solution representing the above-mentioned final solution with catalyst. The HVEM study showed the typical aggregated form of smectite clays (cf. Chapter 2) and the development and magnitude of the swelling pressure was found to be very similar to what is commonly observed when saturating air-dry clay with water (Figure 4-6). Hence, the simpler method is judged to be useful.
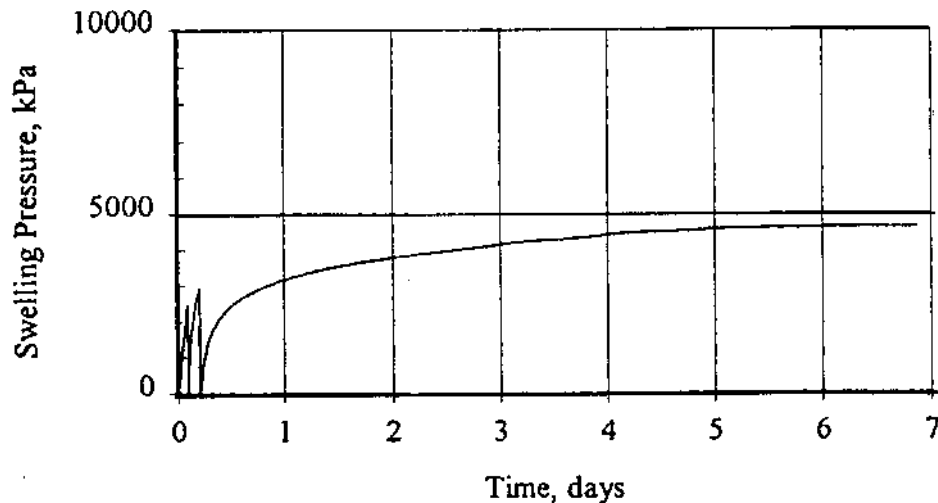
Figure 4-6. *Swelling pressure built up during saturation of an air-dry MX-80 sample with butyl/methyl methacrylate. Dry density about 1700 kg/m³.*

4.2.3   Evaluation of microstructural parameters

The parameters F_2 and F_3 can be evaluated from digitalized TEM micrographs with different degrees of greyness representing different densities. They can be converted into different colors for easy interpretation and representation of the variation of density. In the current R&D work this is made by transforming scanned micrographs to digitalized form using the OFOTO 2 code with subsequent coloring using the GRAPHIC CONVERTER 2.9.1 code on a MacIntosh Power PC6100/66. An example of a processed TEM picture is shown in Figure 4-7. Using only four colors, clear distinction can be made of parts representing different densities: black parts, i.e. the most electron-absorbing components being the densest parts of component *a*, and red parts relatively dense parts of the same component. Green areas represent soft, porous parts of component *b* while white represents open parts of this component. For correlation with experimental hydraulic conductivity data the fraction of a section represented by the black (very dense) and relatively dense (red) parts are considered to be impermeable, while the permeable fraction is taken to be the green and white parts [3].

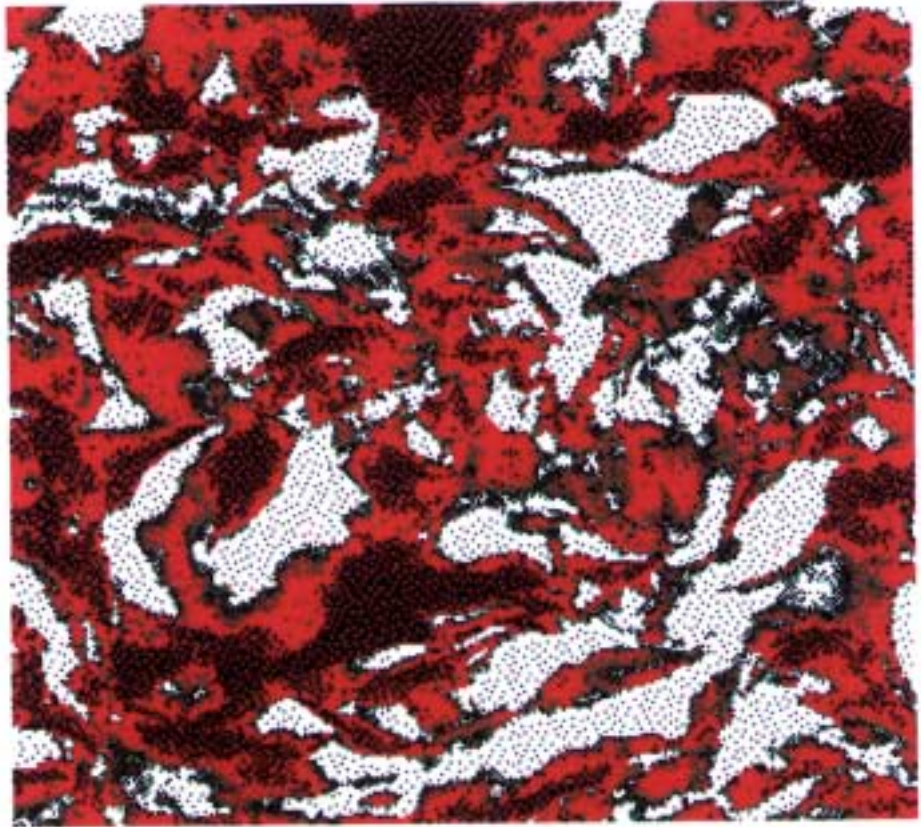| Black | 23.8 % |
Red	43.0 %
Green	14.7 %
White	18.4 %

Figure 4-7. *Example of digitalized micrograph of MX-80 clay with a bulk density at saturation of 1800 kg/m^3. Black=densest parts of clay matrix a. Red=relatively dense parts of the same component. Green=soft, porous parts of component b. White represents open parts of this component. Bar is 1 μm.*

4.2.4   Representativeness

Section thickness

The thickness of the section from which micrographs are taken is of fundamental importance. The ideal thin section is of course a two-dimensional plane since the thicker the section the smaller the possibility to identify voids included in the clay matrix as illustrated by Figure 4-8. However, a reduced thickness makes the section fragile and experience shows that 200–400 Å is a practical limit when using ultramicrotomy for the cutting operation. The question of what thickness one can accept depends on the required resolution and need for discerning microstructural details.
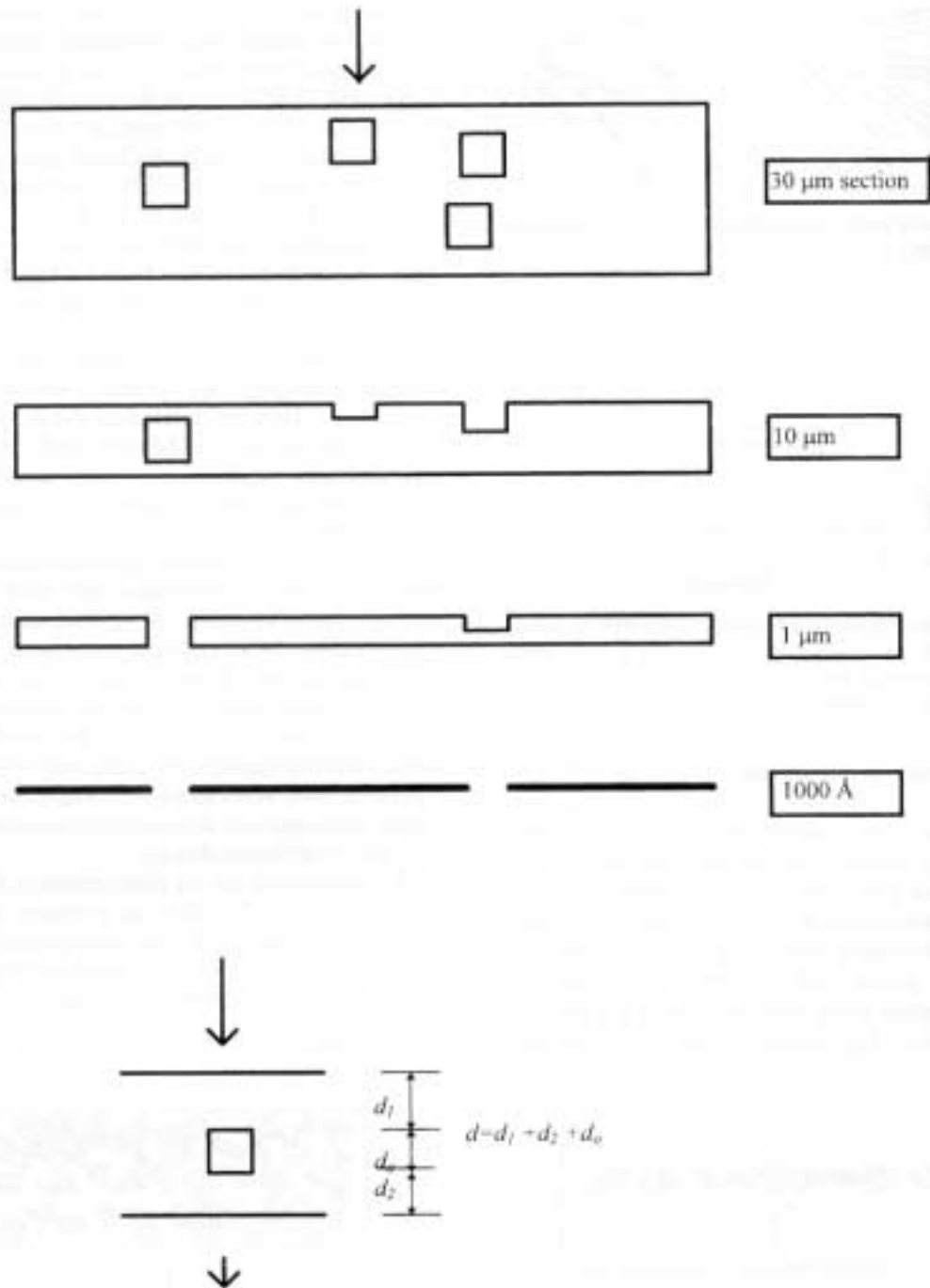
Figure 4-8. *Influence of section thickness on the interpretation of the microstructure. The figure show clay films with different thickness prepared from clay with the same void system. The lowest picture shows an element with defined geometry. Arrows indicate radiation (light or electron beam) [10].*

Labels in figure: 30 μm section, 10 μm, 1 μm, 1000 Å

$d = d_1 + d_2 + d_o$

For quantifying microstructural components like *a* and *b*, which represent density variations, the problem is to find out how the section thickness affects the possibility of making relevant evaluation. The issue is to determine how the "greyness" of the micrograph is related to the density. Very dark parts are strongly energy-adsorbing microstructural components, like solid, non-smectite minerals or very dense smectite aggregates, while very bright parts represent open voids filled with impregnation substance. Intermediate degrees of greyness represent clay gels of different density.

A fundamental law in photography [11] expresses the ratio of greyness *G* of the photographic plate, i.e. the micrograph, and the radiation energy amount *E*, which is the product of the radiation intensity *i* and time of exposure *t*:

$$G = A \, E = \log it \qquad\qquad (4.1)$$

Where: G = greyness
         A = constant
         E = radiation energy
         i = radiation intensity
         t = time

The greyness *G* is inversely proportional to the density ρ and thickness *d* of the film, which, for constant *i* and *t*, gives the expression:

$$G = B(\rho d)^{-1} \qquad\qquad (4.2)$$

Where: B = constant
         ρ = density
         d = film thickness

Disregarding from diffraction and geometry-related optical distortions and from absorption by the void-filling impregnation substance, the greyness of the micrograph intensity on the exit side of the discrete element in Figure 4-8 is:

$$G = B \, [\Sigma \, (\rho \, d)]^{-1} \qquad\qquad (4.3)$$

Comparing a film with 3 μm thickness with one having 30 μm thickness the ratio of the *G*-values is 10. For making direct quantitative comparison of the *G*-values possible the radiation energy must hence be 10 times higher for the 30 μm film thickness. This may have an impact on the crystal lattice stability, especially the location of alkali ions.

While identification of the most detailed features of clay crystallites requires a resolution power that only films thinner than 500–1000 Å can provide, certain quantitative microstructural analyses can be made by using significantly thicker films. Thus, if the objective is to interpret different degrees of greyness in terms of density variations it is possible to do so if calibration has been made by analysing ultrathin sections. For artificially prepared smectite clays using clay powder that hydrates under confined conditions, sufficient information may be obtained by examining 10 μm films. Hence, clays of this sort with a density of 1700 to 2000 kg/m^3 at water saturation are commonly characterized by the presence of one 3–5 μm wide zone of soft gels per 1000 μm^2 cross section area. Such a zone located in the center of the film in the lower sketch in Figure 4-8 would mean that the

thickness of the dense matrix ($d_1 + d_2$) would be about 50 % of that of the surrounding homogeneous clay matrix. The greyness of the micrograph where the channel is located would then be 50 % of that of the rest of the film, which is sufficient to indicate the presence of such a channel or local void. However, no detailed information on the zone can be obtained and one can not distinguish between a case with one void and cases with two or several thinner voids located on top of each other. A 30 μm clay film gives even less information on density variations while films with a thickness of about 5 μm provide considerably more information on density variations than 10 μm sections. Micrographs of sections with 1 μm thickness have provided much valuable information although details of the microstructure are obscured.

Scale and size

Depending on the scale, *a* or *b* may dominate. Thus, focusing on open voids and soft gels at high magnification gives very high F_2 and hence also F_3-values, while focusing on dense aggregates gives very low values of F_2 and F_3. Micrographs with an edge length of at least 30 μm seem to be representative for the larger part of the clay matrix. Figures 4-9 and 4-10 serve as illustrations of this. Hence, while the digitalized micrographs in Figure 4-9, representing a magnification of 3000 x, give lower figures for insected open voids (white) at increasing bulk density, those in Figure 4-10, representing a magnification of 30000 x, are approximately independent of the bulk density because they happen to represent denser or softer parts of the matrix. Comprehensive microstructural analyses have indicated that F_2 and F_3 are related to the average bulk density of saturated MX-80 clay as shown in Figure 4-11. Using data from plottings of bulk density versus F_3 the approximate relationship between gel density (component *b*) and average bulk density shown in Figure 4-12 has been derived.

Analytical form of F_2 and F_3

F_2 and F_3 can be expressed as functions of the bulk density at saturation ρ_{bs}
and the gel density ρ_{gs} as given by Eqs.(4.4) to (4.7).

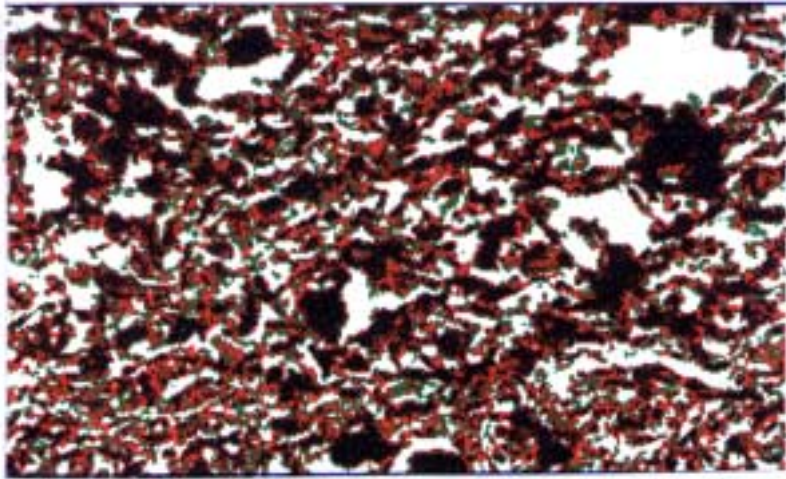$$F_2 = 10^{(-0.0007875\,\rho_{bs} + 0.745)} \tag{4.4}$$

$$F_3 = 10^{(-0.00125\,\rho_{bs} + 1.3)} \tag{4.5}$$

$$F_2 = 10^{(-0.0007142\,\rho_{gs} + 0.7142)} \tag{4.6}$$
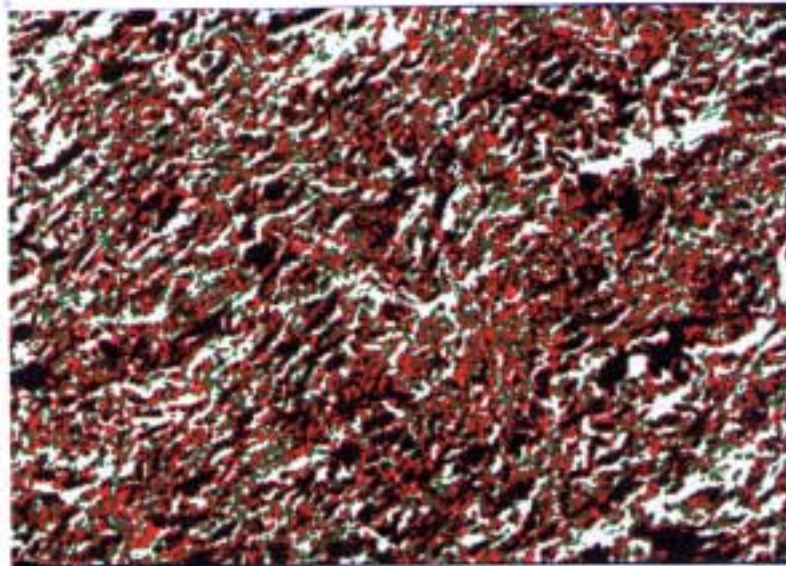
$$F_3 = 10^{(-0.001\,\rho_{gs} + 1)} \tag{4.7}$$

1600 kg/m³

Softest part
(white) is 23.6 %

1800 kg/m³

Softest part
(white) is 18.5 %

2000 kg/m³

Softest part
(white) is 9.6 %

Figure 4-9. Digitalized micrographs of MX-80 clay showing the change in the fraction of sectioned empty voids (white) at increasing bulk density. Magnification 3000 x.

1600 kg/m³

Softest part
(white) is 19.7 %

1800 kg/m³

Softest part
(white) is 22.0 %
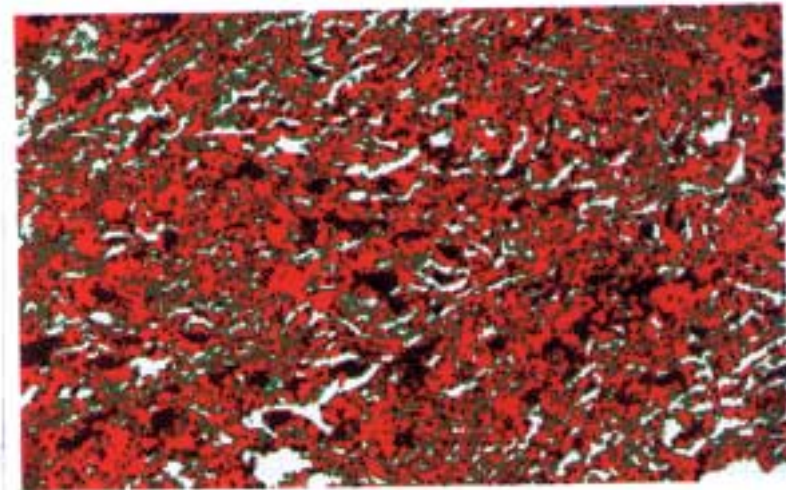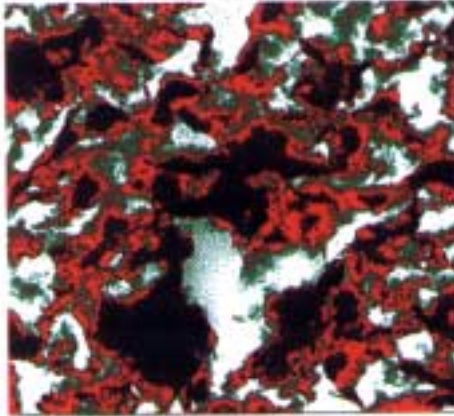
2000 kg/m³

Softest part
(white) is 22.0 %

Figure 4-10. Digitalized micrographs of MX-80 clay showing the change in the fraction of sectioned empty voids (white) at increasing bulk density. Magnification 30000 x.
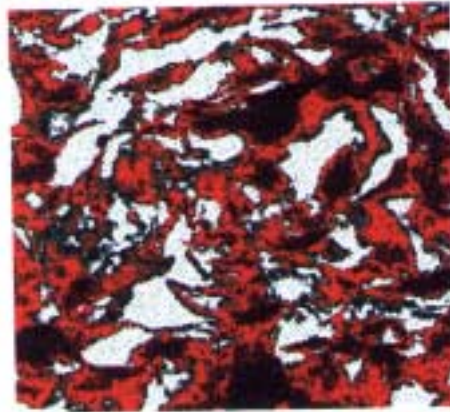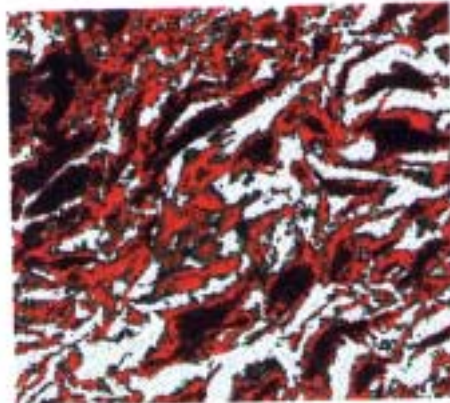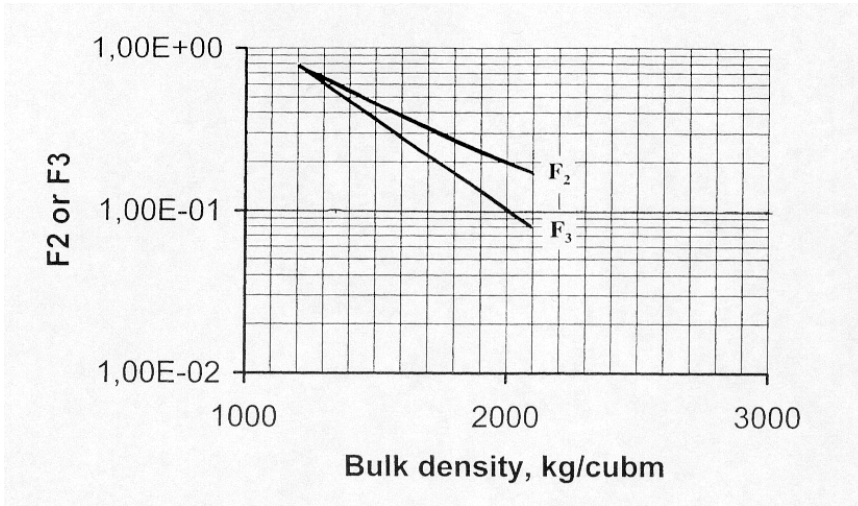
Figure 4-11. *F_2 and F_3 versus bulk density. Data based on microstructural analysis of MX-80 clay.*
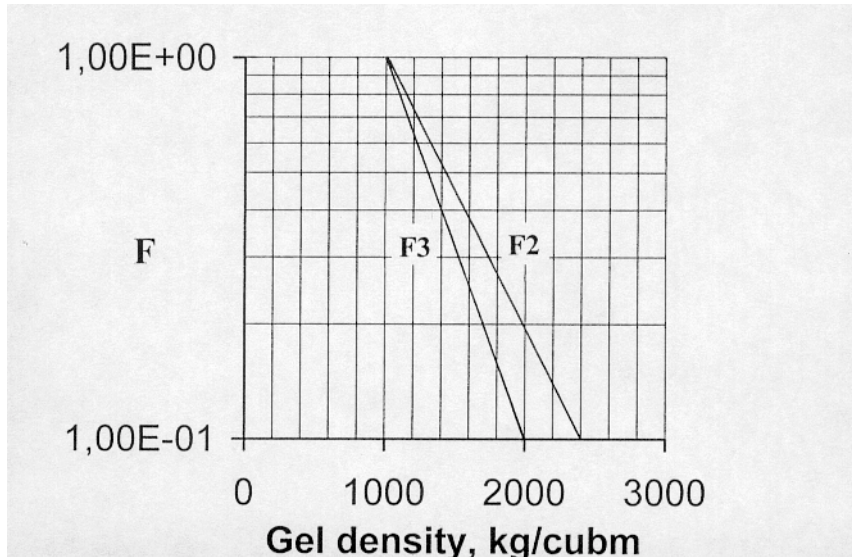
Figure 4-12. *F_2 and F_3 versus gel density. Data based on microstructural analysis of MX-80 clay.*

The difference between Na and Ca clay is that the soft (green) fraction of a section is smaller and the open (white) fraction wider in the Ca-state, but since their sum is assumed to be unchanged the *b* component and the average gel density ρ_{gs} stays constant. Since the hydraulic conductivity of this component is much higher in the Ca-state the bulk conductivity is naturally significantly higher than in the Na-state.

4.3 Examples of evaluated electron micrographs

Figures 4-13 to 4-16 are examples of transmission electron micrographs that have been examined for determining density variations by automatic scanning and for deriving representative relationships between bulk density and the parameters F_2 and F_3. Figure 4-13 represents a soft MX-80 clay with a bulk density of 1300 kg/m^3, the microstructural pattern being of honeycomb type. This sort of microstructural constitution, which easily undergoes coagulation if the porewater is salt, is characteristic of the clay component of mixtures of bentonite and ballast materials like silt, sand and gravel.
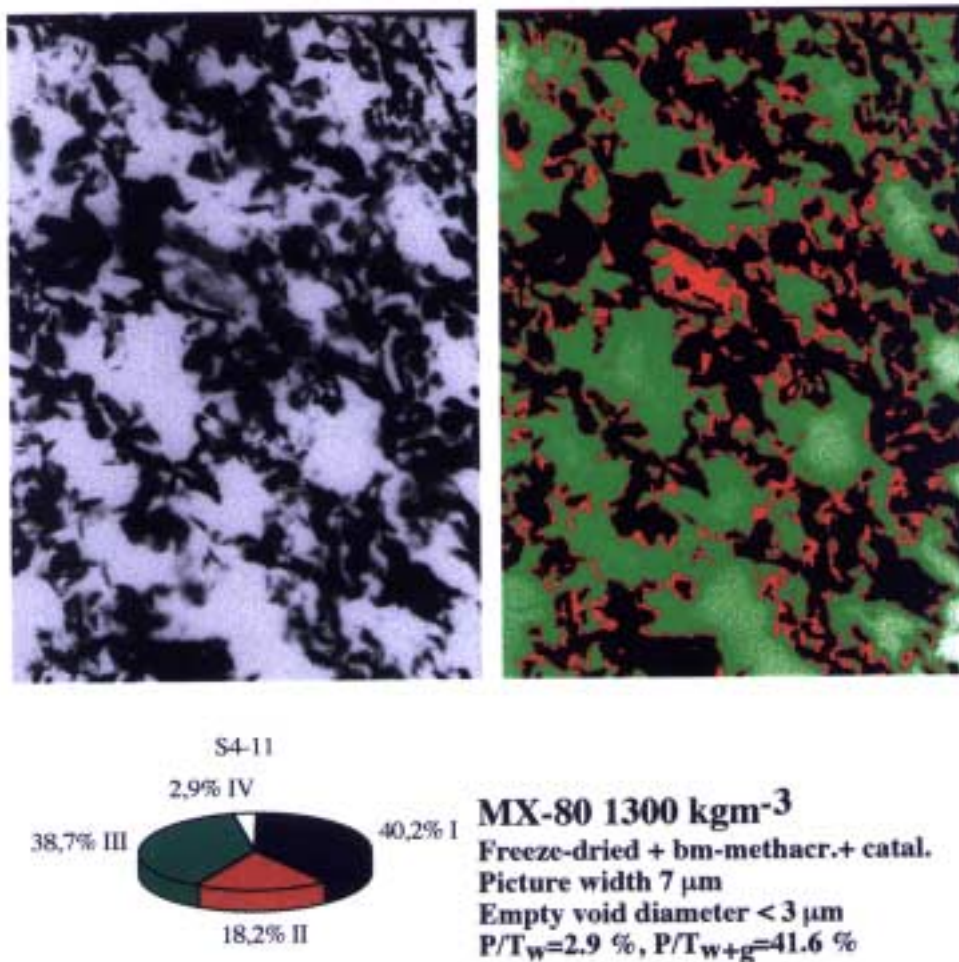
Figure 4-13. Digitalized transmission electron micrographs of 300 Å section of MX-80 with a bulk density of 1300 kg/m³. The relative fractions of very dense (black), relatively dense (red), soft (green) and open (white) parts of the section are given in the picture. P/T$_w$ represents ratio of total area and area of open voids (white). P/T$_{w+g}$ represents ratio of total area and area of open voids (white) and soft gels (green).

S1-11

10,2% IV

24,6% III

33,8% I **MX-80 1600 kgm-3**
Dried + bm-methacrylate + catalyst
Picture width 30 μm
Empty void diameter < 5 μm
P/T_w=10.2 %, P/T_{w+g}=34.6 %

31,3% II

S1-12

12,3% III 1,4% IV

20,6% II

65,8% I **MX-80 1600 kgm-3**
Dried + bm-methacrylate + catalyst
Picture width 7 μm
Empty void diameter < 3 μm
P/T_w=1.4 %, P/T_{w+g}=13.7 %
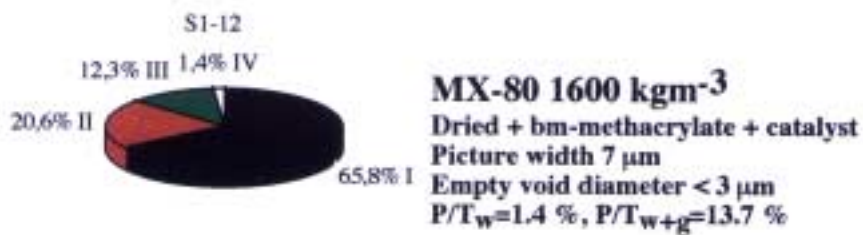
Geodevelopment AB

Figure 4-14. *Digitalized transmission electron micrographs of 300 Å section of MX-80 with a bulk density of 1600 kg/m³. The relative fractions of very dense (black), relatively dense (red), soft (green) and open (white) parts of the section are given in the picture. P/T_w represents ratio of total area and area of open voids (white). P/T_{w+g} represents ratio of total area and area of open voids (white) and soft gels (green).*

54

S1-21

3,9% IV
28,6% III
21,7% I
45,8% II

MX-80 1800 kgm^{-3}
Dried + bm-methacrylate + catalyst
Picture width 30 μm
Empty void diameter < 3 μm
P/T_w=3.9 %, P/T_{w+g}=32.5 %

S1-22

9,1% IV
17,0% III
51,0% I
23,0% II
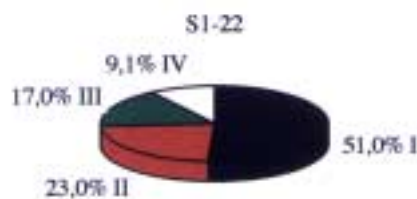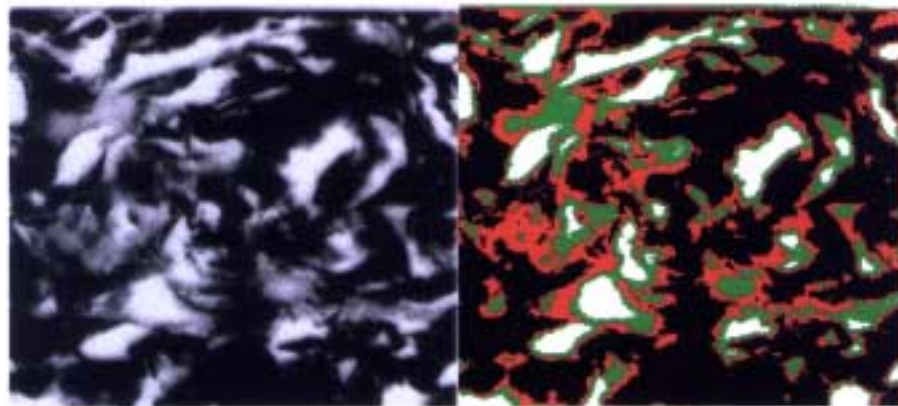
MX-80 1800 kgm^{-3}
Dried + bm-methacrylate + catalyst
Picture width 7 μm
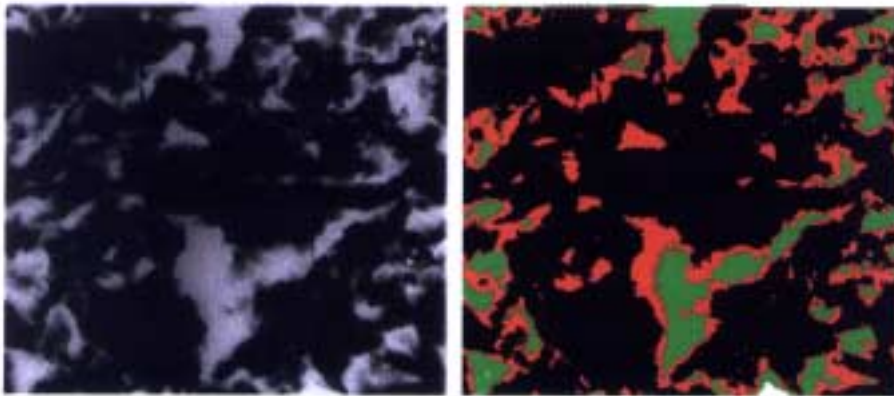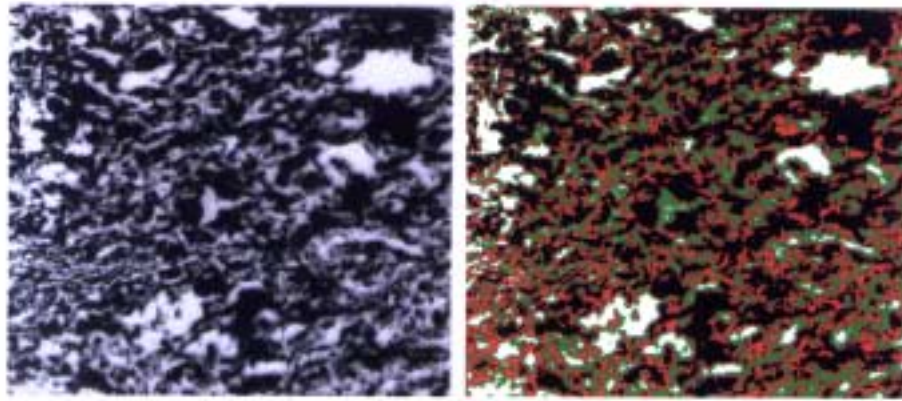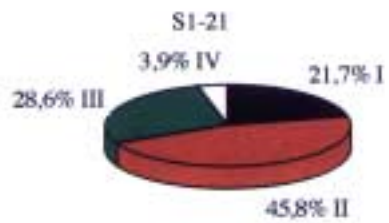Empty void diameter < 1 μm
P/T_w=9.1 %, P/T_{w+g}=26.1 %

Figure 4-15. *Digitalized transmission electron micrographs of 300 Å section of MX-80 with a bulk density of 1800 kg/m^3. The relative fractions of very dense (black), relatively dense (red), soft (green) and open (white) parts of the section are given in the picture.P/T$_w$ represents ratio of total area and area of open voids (white). P/T$_{w+g}$ represents ratio of total area and area of open voids (white) and soft gels (green).*
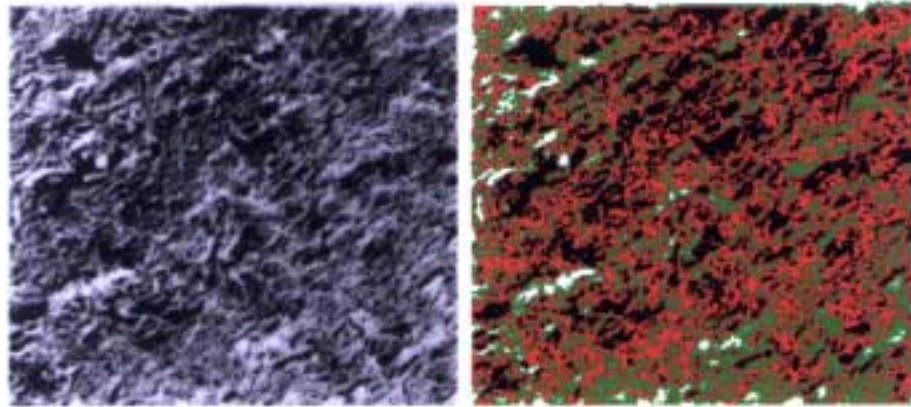
Figure 4-16. *Digitalized transmission electron micrographs of 300 Å section of MX-80 with a bulk density of 2000 kg/m³. The relative fractions of very dense (black), relatively dense (red), soft (green) and open (white) parts of the section are given in the picture.P/T_w represents ratio of total area and area of open voids (white). P/T_{w+g} represents ratio of total area and area of open voids (white) and soft gels (green).*
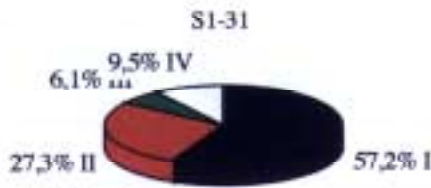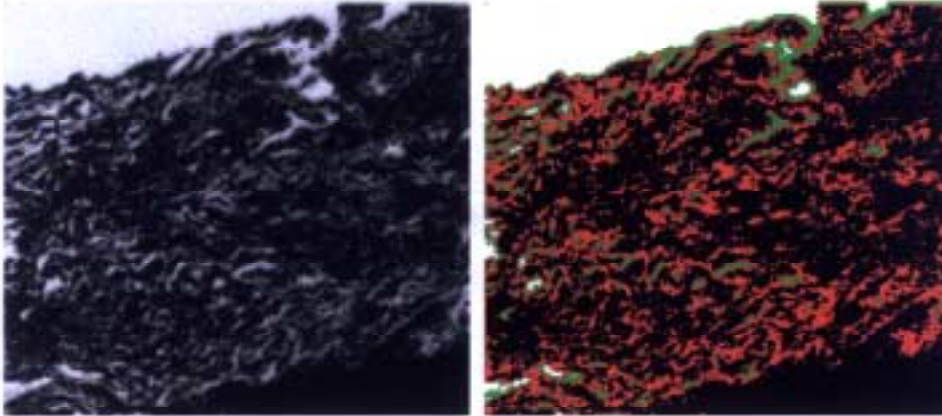
4.4   Correlation with other microstructural models

4.4.1   General

A number of attempts have been made in later years to propose microstructural models for explaining the physical behavior of clays. Most of these refer only to the detailed particle-to particle interaction and pay no attention to the void system and the scale-dependent variation in density of the clay matrix. One exception is the GMM model [12] that was developed for correlating the microstructural constitution of artificially prepared clay buffer materials and their major physical properties. It will be very briefly described here.

4.4.2   The GMM model

Microstructure of compacted clay powder

The model is based on the assumption that the bentonite grains are isotropic and expand to hold 2 or 3 interlamellar hydrates depending on the available space and on the type of adsorbed cation. Spontaneous exfoliation of stacks of lamellae takes place from parts of the grains that are not compressed and this leads to formation of clay gels in the "external" voids between the expanded grains as shown schematically in Figure 3-3. The density of the gels is assumed to depend on the bulk clay density and on the size of the voids according to Table 4-1. For the sake of clarity microstructural data refer to three specific clay densities (*A, B, C*) but interpolation between them can be made. The effective porosity is defined as the ratio of all voids between the powder grains and the total volume [12].

Table 4-1. Density and effective porosity (n) of compacted MX-80 powder grains according to the GMM model.

Clay type	Bulk density of air-dry powder, kg/m^3	Dry density, kg/m^3	Density at compl. Saturation, kg/m^3	*n*
A	2000	1800	2130	0.13
B	1500	1350	1850	0.35
C	1000	900	1570	0.57

Hydration and maturation

Water uptake and expansion of the grains to hold 2 or 3 interlamellar hydrates yields the theoretical effective porosity given in Table 4-2. For the highest initial bulk density (Type *A*) complete uptake to 2 and 3 hydrates is not geometrically possible. It is assumed that 2/3 of the grains expand to host 2 complete hydrates and that no aggregate takes up 3 hydrates. The effective porosity is defined as the ratio of all water-filled "external" exatralamellar voids between the aggregates of stacks and the total volume [12].

Table 4-2. Density and effective porosity (n) of water saturated MX-80 clay according to the GMM model [12].

Clay type	n	
	2 hydrates	3 hydrates
A	0.015[*]	–
B	0.20	0.05[*]
C	0.47	0.37[*]

[*] Matured state. The values used for conductivity calculations

Gel fillings in "external" voids

As for the presently presented model the external void volume of the GMM model that remains after the expansion of the granules will not be free from mineral particles. Soft clay gels, exfoliated from the granules are assumed to be formed in the pore space and they determine the hydraulic conductivity of the bulk clay. The density of these gels is assumed to depend on the size of the external voids. In order to reflect the pore size ranges observed for the three types of clay, means and standard deviations are set to match the following conditions:

1. The minimum diameter of external voids in the three types of clay is 0.1 μm.

2. For clays *A, B* and *C* the maximum diameter of the external voids is 5 μm, 20 μm and 50 μm, respectively.

Assuming further that the diameter of the external voids are normally distributed, and that the density of the clay gels in the external voids are as assumed in Table 4.3, and also that the gel structure is regular orthogonal with the "walls" consisting of 3 lamellae in Na montmorillonite and 10 when the the clay is in Ca form, one finds that the pore size of the gel fillings are those given in Table 4-4.

Table 4-3. Generalized data of gel density as a function of the bulk density and diameter D_e of external voids [12].

Clay type	Bulk density, kg/m^3	Gel density in kg/m^3 for D_e = 1–5μm	Gel density in kg/m^3 for D_e = 5–20 μm	Gel density in kg/m^3 for D_e = 20–50 μm
A	2130	1300	–	–
B	1850	1300	1200	–
C	1570	1300	1200	1100

Table 4-4. Average free space d_1 in gel fillings according to the GMM model [12].

Gel density kg/m³	d_1, Å Na gel	d_1, Å Ca gel
1300	340	700
1200	570	1 100
1100	1 230	10 000

The channels formed by the gel-filled external voids are assumed to have a varying diameter and be "crankshaft"-shaped in applying the model in flow calculations.

4.4.3 Similarities and differences between the GMM and the presently proposed model

The general form of the two models is similar, but a number of basic data and relationships are arbitrary in the GMM model while they are founded on experiments for the presently proposed model, which is named MMM. The major differences and similarities between the two are the following:

- GMM assumes isotropic bentonite grains, which is debatable. The present model MMM allows for stochastic variation in grain isotropy and orientation.

- GMM assumes homogeneously filled ("external") voids between dense aggregates. This gives lower and more questionable average gel densities than the present model MMM.

- GMM prescribes gel capillary dimensions that are not validated. The present model MMM does not describe the detailed particle-to-particle arrangement but averages the constitution, which is simpler and more relevant with respect to its true stochastic nature.

- The ("external") voids between dense aggregates prescribed by GMM agree well with those recorded in the microscopy performed in the development of the MMM model and the cross section area of these voids are in good agreement with the F_2-data of the MMM model.

4.5 MX-80 clay interacting with organics represented by HDPy⁺

4.5.1 General

Organic cations and molecules may replace inorganic ones in the interlamellar space of smectites and occupy external sites on stacks of smectite lamellae. Migration of organic cations or neutral molecules into MX-80 clay is estimated to be effectively hindered at high bulk densities due to their size and low replacement potential while they can diffuse into soft clay, replace interlamellar water and form coatings on particle aggregates. This may cause substantial changes in physical properties, like the shear strength [13, 14].

For certain purposes treatment of smectite clay with certain organic substances may be considered, an example being preparation of MX-80 clay with hexadecylpyridinium (HDP_y^+) for substantial raising of the anion exchange capacity [3]. The organization of the HDP_y^+ cations in interlamellar positions may be of the type shown in Figure 4-17, which is valid in principle for other organic cations and neutral molecules in the interlamellar space as well [14]. Treatment of MX-80 and the resulting microstructure will be reported in this chapter.
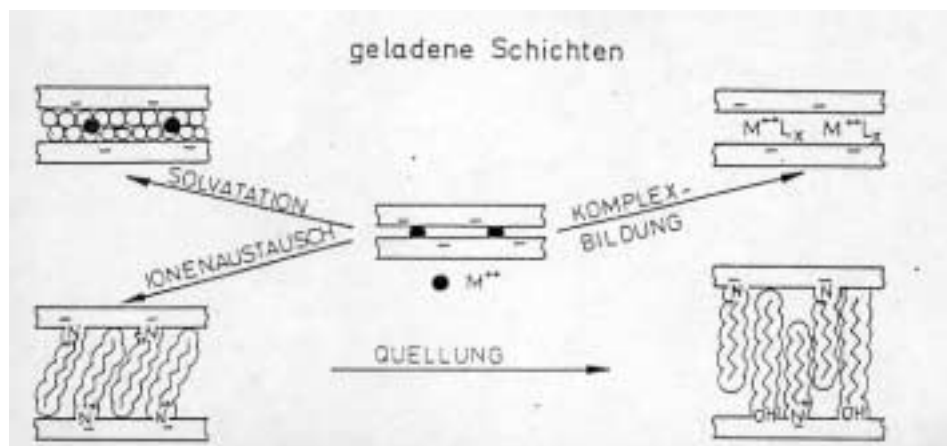
Figur 4-17. Sorption of organic elements in the interlamellar space of smectite [3].

4.5.2   Preparation of MX-80 in HDPy$^+$ form

MX-80 can be prepared with HDP_y^+ by dispersion of clay powder in distilled water and then adding the chloride salt of the quarternary alkylammonium ion of hexadecylpyridinium to yield complete cation exchange from the original Na/Ca/Mg-state. After removal of excess organic ions the clay suspension is dried and powdered by grinding to approximately the same grain size distribution as ordinary MX-80 clay. HDPy$^+$ is adsorbed to about 150 % of the CEC. It is estimated that it takes place in cationic form up to 100 % CEC and that additional uptake is in molecular form.

Much higher pressures are required to reach high densities (>1600 kg/m^3) than for untreated powder; a density corresponding to a density of 1760 kg/m^3 after water saturation requiring 100 MPa. The reason is that interlamellar adsorption of HDPy$^+$ expands the interlamellar space to about 18 Å, which corresponds to about 6 hydrate layers. However, the stacks become much less compressible than in the hydrated form. Samples prepared in the study reported in [3] had a density after saturation with distilled water of 1630 and 1760 kg/m^3.

Specimens for electron and light microscopy were prepared by applying the acrylate technique. Thin sections with about 400 Å thickness for TEM were obtained by use of ultramicrotomy while 10 μm sections were prepared by grinding and polishing according to the common procedure in petrology.

4.5.3 Microstructural constitution

General features

Figure 4-18 shows the microstructural constitution of a HDPy$^+$ –treated clay sample with 1760 kg/m^3 density. The aggregated pattern with voids with a maximum diameter of up to 40 μm between the dense aggregates is particularly obvious when examining the digitalized picture. Micrographs of 10 μm thick sections, which only exhibit voids larger than this measure, validated that a large part of the sectioned clay contains open or very permeable voids.
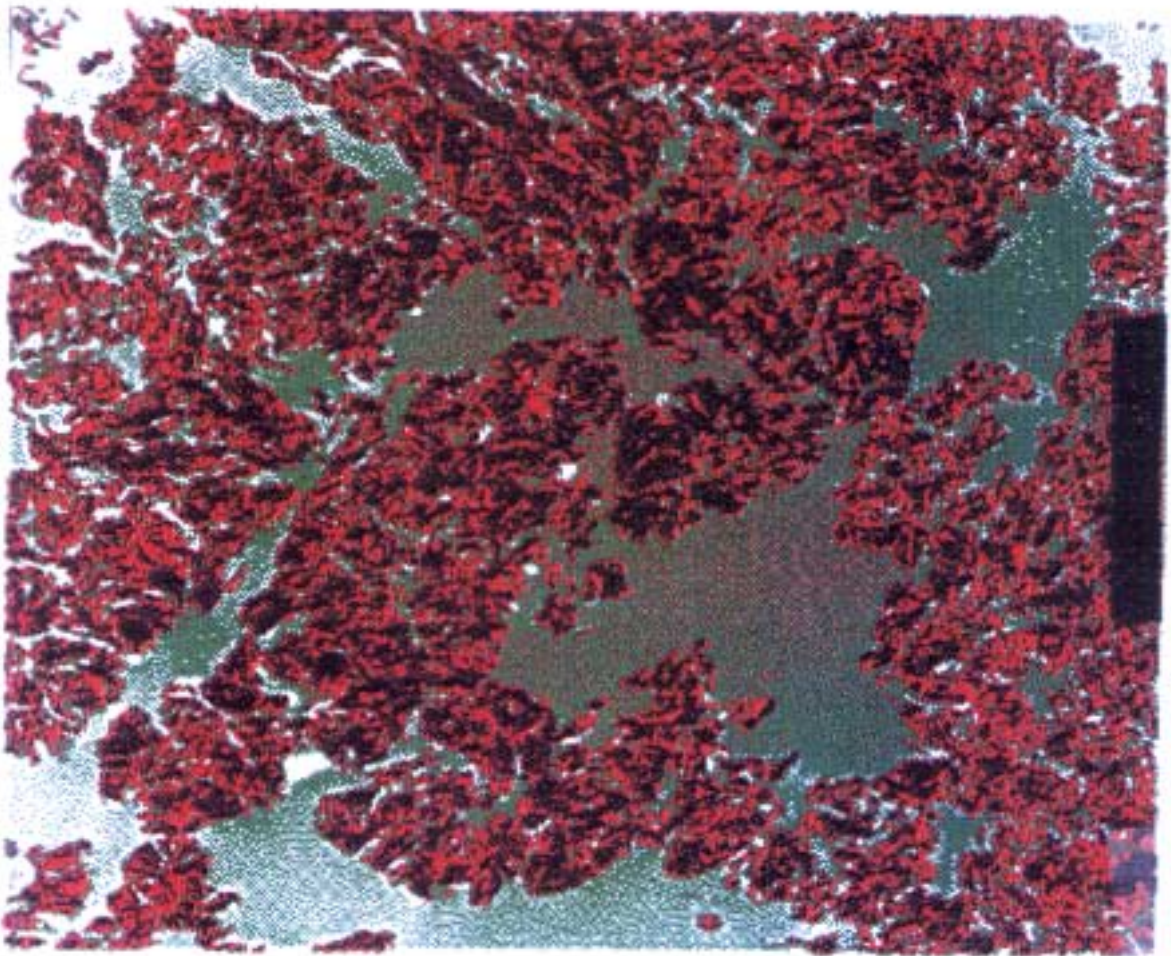
Figure 4-18. *Example of digitalized TEM micrograph of HDPy$^+$-treated MX-80 clay with 1760 kg/m^3 density. Bar is 10 μm.*

The *F*-parameters evaluated from the examination of TEM and ordinary thin sections are as shown in Table 4-5:

Table 4-5. Microstructural parameters of HDPy$^+$-treated MX-80 with a density of 1760 kg/m^3 at saturation with distilled water.

Micrograph type	F_2	F_3
TEM	0.51	0.37
Light microscopy	0.29	0.16

The values in Table 4-5 give two informations:

1. The *F*-values evaluated by TEM are significantly higher than for untreated MX-80 clay, which is caused by larger open voids in the HDPy$^+$-treated material. It is hence more like very fine-grained silt than smectite clay.

2. The lower *F*-values evaluated by light microscopy using about 25 times thicker sections are explained by the presence of unrevealed voids located in the sections as expected.

4.6 Tentative conclusions from microstructural modelling

The following aspects and conclusions are significant:

- Microstructural models for uncompacted, compacted and hydrated MX-80 buffer clay have been derived based on numerical calculations in which the bentonite grains are assumed to be spherical with varying anisotropy and orientation.

- Microstructural parameters have been derived on a theoretical basis for 2D and 3D conditions. They evolve from the basic models and are related to 2D cross sections through MX-80 clay of different densities represented by micrographs of ultrathin sections.

- Digitalization of micrographs of acrylate-treated clay forms a suitable basis for automatic recording of microstructural parameters.

4.7 References

13. Papelis C, Hayes K F, 1996. Distinguishing between interlayer and external absorption sites of clay minerals using X-ray absorption spectroscopy. Colloids and Surfaces, Physicochem. Eng. Aspects, Vol.107, Elsevier Publ. Co (pp.89–96).

14. Pusch R, 1994. Waste Disposal in Rock. Developments in Geotechnical Engineering, 76. Elsevier Publ. Co, ISBN: 0-444-89449-7.

15. Pusch R, Muurinen A, Lehikoinen J, Bors J, Eriksen T, 1999. Microstructural and chemical parameters of bentonite as determinants of waste isolation efficiency. European Commission Final Report Contr. No. F14W-CT95-0012.

16. Pusch R, 1967. A technique for investigation of clay microstructure. J. Microscopie, Vol.6 (pp.963–986).

17. Bennett R H, Bryant W R, Keller G H, 1977. Clay fabric and geotechnical properties of selected submarine sediment cores from the Mississippi Delta. NOAA Professional Paper 9. US Dept. of Commerce, Nat. Oceanic and Atmospheric Adm. Rockville, Md.

18. Bennett R H, Bryant W R, Hulbert M H, 1991. Microstructure of fine-grained sediments. Frontiers in Sedimentary Geology. Springer Verlag, New York.

19. Pusch, R, 1971. Microstructural features of Pre-Quaternary clays. Acta Universitatis Stockholmiensis, Stockholm Contributions in Geology, Vol.XXIV:1, Stockholm.

20. Ferrow E, Roots W, 1989. A preparation technique for TEM specimens, application to synthetic Mg-chlorite. Eur. J. Mineral. 1: 815–819.

21. Pusch R, Karnland O, 1986. Aspects of the physical state of smectite-adsorbed water. SKB Technical Report TR 86-25, SKB Stockholm.

22. Pusch R, 1999. Experience from preparation and investigation of clay microstructure. Eng. Geology, Vol.54 (pp.187–194).

23. Windisch O, 1937. Die Neue Fotoschule. Heering-Verlag, Harzburg. (p.123).

24. Pusch R, Karnland O, Hökmark H, 1990. GMM – A general microstructural model for qualitative and quantitative studies of smectite clays. SKB Technical Report TR 90-43, SKB Stockholm.

25. Pusch R, 1973. Influence of organic matter on the geotechnical properties of clays. Doc. D11:1973. Nat. Swed. Build. Res. Counc., Stockholm.

26. Söderblom R, 1966. Chemical aspects of quick-clay formation. Eng. Geol.. Vol.1 (pp.415–431).

27. Bors J, Gorny A, Dultz S, 1994. Some factors affecting the interactions of organophilic clay minerals with radioiodine. Radiochim. Acta, Vol.66/67 (ppm.139–143).

5 Correlation of microstructural constitution and bulk physical properties of MX-80 buffer

5.1 General

The hydraulic conductivity and swelling pressure are particularly important practical properties of the buffer and they are believed to depend very much on the microstructural constitution. Gas conductivity and ion diffusion transport are also thought to be controlled by the microstructure and all these issues will be in focus of this report. A major feature of importance in this context is the variation in density on the microstructural scale.

5.2 Hydraulic conductivity

5.2.1 General

The variation in density and geometry of the components that make up the microstructure has a very significant impact on the hydraulic conductivity. The most important features are the presence and interconnectivity of open paths of capillary dimensions. They are extremely small and with limited continuity in very smectite-rich clay like MX-80 of high density but constitute channels with considerable water transport capacity when the bulk density is low, particularly when the clay is in Ca-state. The geometrical features can be evaluated from ultrathin sections of suitably prepared clay samples as outlined in Chapter 4 [1]. In principle, one can distinguish quantitatively between denser and softer parts of the clay matrix by analyzing digital micrographs and ascribe to them characteristic average hydraulic conductivities by which the net average conductivity of a clay element can be calculated (Figure 5-1). Such analyses have yielded good agreement between microstructural parameters and the conductivity of bulk clay as will be shown and discussed in this chapter.
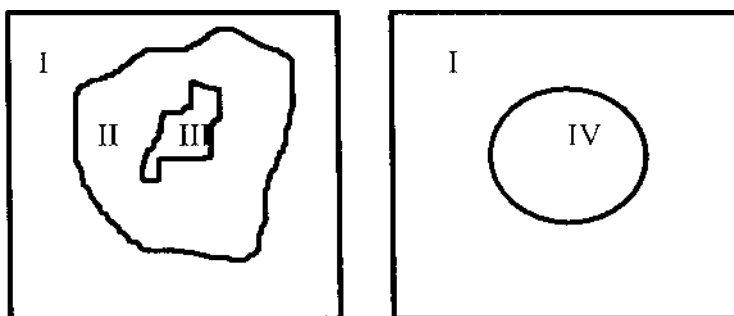

Figure 5-1. *Schematic micrographs. Left: Typical picture of ultrathin section with varying density in soft matrix region (I to III). Right: normalized picture with defined channel cross section and density of the clay gel in the channel (IV) and of the clay matrix (I).*

Typical relationships between the bulk density and gel density are shown in Table 5-1 for MX-80.

Table 5-1. Bulk and gel densities for MX-80 [1].

Bulk density, kg/m^3	Gel density, kg/m^3
2130	2000
1850	1650
1570	1150

There is close similarity of the bulk and gel densities when the firstmentioned exceeds 1800–1900 kg/m^3, which is explained by compression of softer paths causing a high degree of microstructural homogeneity, while densities lower than 1500–1600 kg/m^3 imply considerable density variations on the microstructural level and the significant difference between bulk and gel densities as indicated by Table 5.1. This means that pervious channels filled with soft clay gels are abundant and since these gels collapse on percolation with salt solutions, forming isolated coagulated aggregates and leaving larger voids unfilled, the hydraulic conductivity will be significantly increased.

5.2.2   Conductivity of hydraulically heterogeneous material

A simple check of the relevance of the presently derived way of quantifying microstructure is to compare experimental bulk hydraulic conductivity data for Na and Ca smectite clay with calculations based on F_2 and ρ_{gel}. For the calculation one can apply basic flow theory taking the microstrucure to consist of a system of elements with different hydraulic conducitivities (Figure 5-2).
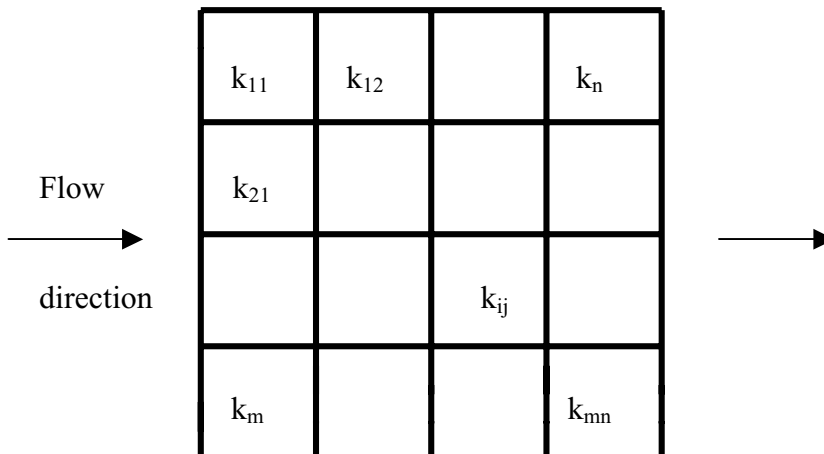

Figure 5-2. *System of elements with different hydraulic conductivity permeated in one direction.*

Theoretically, the hydraulic conductivity K of soil with elements of different conductivity can be expressed in the following way [2]:

$$K = 1/m[\sum_{i=1}^{m} n\{\sum_{j=1}^{n} 1/kij\}^{-1}$$ (5.1)

where: K = average hydraulic conductivity
          n = number of elements normal to flow direction
          m = number of elements in flow direction
          kij = hydraulic conductivity of respective element

The fraction F_2 of a section that is permeable is listed in Table 5-2 as a function of the bulk density. Taking the conductivity of this fraction, i.e. the clay gels, to be the experimentally determined conductivity of clay with this bulk density, the net average conductivity can be calculated by applying Eq.(5.1). Such data are given in the table for three typical bulk densities and one realizes that the agreement between the model-derived data for untreated MX-80 in Na form and actually determined ones is very good.

Table 5-2. Microstructural data and conductivities for MX-80 in Na form. Percolation with distilled water.

Bulk density kg/m^3	F_2	Gel density kg/m^3	Gel conductivity m/s	Calculated bulk cond. m/s	Experimental bulk cond. m/s
2130 Na	0.17	2000	7E-14	E-14	2E-14
1850 Na	0.24	1650	2E-12	4E-13	3E-13
1570 Na	0.80	1150	E-10	8E-11	8E-11

5.2.3   Difference between Na- and Ca-states

Assuming the same F_2 values and gel densities as for MX-80 in Na form but applying typical hydraulic conductivities of MX-80 in Ca-state, one gets the data in Table 5-3, which shows very good agreement between calculated and true conductivity data for bulk densities down to about 1800 kg/m^3. The reason for the very obvious theoretical overrating of the conductivity of MX-80 in Ca form with a bulk density of 1570 kg/m^3 is the poor degree of homogeneity of the clay gel in external voids. The lamellae make up thicker and denser stacks than in the Na case and large voids are hence formed in the heterogeneous Ca gels. MX-80 in Ca form is therefore not mechanically stable at lower densities than about 1600–1800 kg/m^3, which is easily demonstrated by conducting simple sedimentation tests in the laboratory. The Ca gels consist of poorly connected, large aggregates that are moved by flowing water in percolation tests of the common type that imply a hydraulic gradient of 30–50. The aggregates tend to clog voids and form plugs by prolonged percolation thereby causing substantial reduction of the conductivity as manifested by the conductivity data.

Table 5-3. Microstructural data and conductivities for MX-80 in Ca form. Percolation with strongly brackish Ca-dominated water.

Bulk density kg/m^3		F_2	Gel density kg/m^3	Gel con-ductivity m/s	Calculated bulk cond. m/s	Experimental bulk cond. m/s
2130	Ca	0.17	2000	2E-13	3E-14	5E-14
1850	Ca	0.24	1650	8E-11	2E-12	2E-12
1570	Ca	0.80	1150	7E-5	6E-05	2E-09

5.2.4 Influence of porewater chemistry

The electrolyte concentration of the porewater is known to affect the hydraulic conductivity substantially at low and medium bulk densities. This is because coagulation of the clay gels produces denser aggregates with larger void space and higher conductivity than when the percolated water is salt. Using the density and F_2-values in Table 5-3 and taking the conductivity of the permeable fraction, i.e. the clay gels, to be the experimentally determined conductivity of clay with this bulk density, the calculated net average bulk conductivity turns out to be practically the same for sea water percolate as for distilled water for the clay with a bulk conductivity of 2130 kg/m^3. The experimentally determined conductivity of this clay using sea water and distilled water also yield practically the same value, i.e. 2E-14 m/s.

For the bulk density 1850 kg/m^3 the calculated and experimentally found conductivities at percolation with sea water are both about 2E-11 m/s, which is about the same as for percolation with distilled water, while for 1570 kg/m^3 the theoretical conductivity is 8E-8 m/s while experimental data are in the range of E-10 to E-9 m/s. The latter deviation is explained as for clay in Ca-state state, i.e. by clogging of voids through flow-generated particle migration.

5.2.5 Channel flow modelling

The size and frequency of the channels containing clay gels can be estimated on the following grounds:

- The channels have a circular cross section.

- The diameter of the widest channel is 50 μm in MX-80 clay with a bulk density 1570 kg/m^3, 20 μm in clay with 1850 kg/m3 density, and 5 μm in clay with 2130 kg/m^3 density, as concluded from transmission electron microscopy. Gel-filled voids with a diameter less than μm are of no importance to the bulk conductivity

- The size of the channels have normal statistical distribution (Figure 5-3).
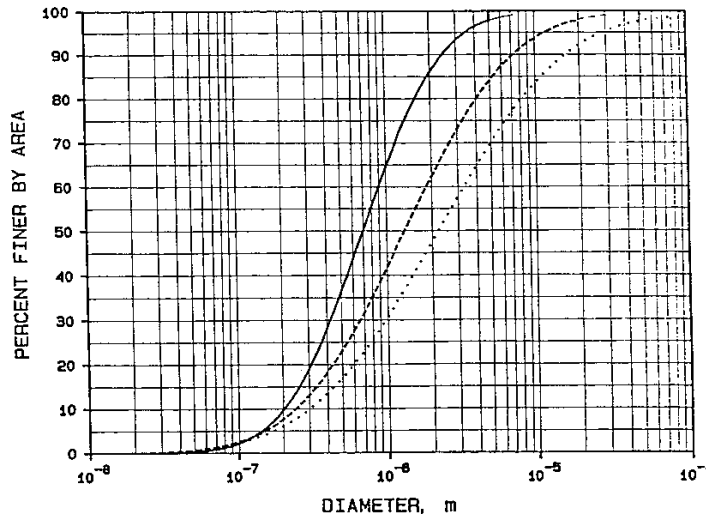
Figure 5-3. *Assumed size distribution of pore size in clays A (full line), B (broken line), and C (dotted line).*

Using these criteria one gets the size distributions in Table 5-4.

Table 5-4. Number of differently sized channels per 250x250 μm^2 cross section area [3].

Bulk density, kg/m^3	Number of 20–50 µm channels	Number of 5–20 µm channels	Number of 1–5 µm channels
2130	0	0	135
1850	0	10	385
1570	2	85	950

Practically all water flow takes place within the three-dimensional network of gel-filled channels with stochastic properties (Figure 5-4). The channels, which represent the pervious paths in the clay are characterised by their lengths, widths, apertures and transmissivities. The rest of the clay matrix is assumed to be porous but impermeable. The basis of the development of the present model is the code 3Dchan [4].
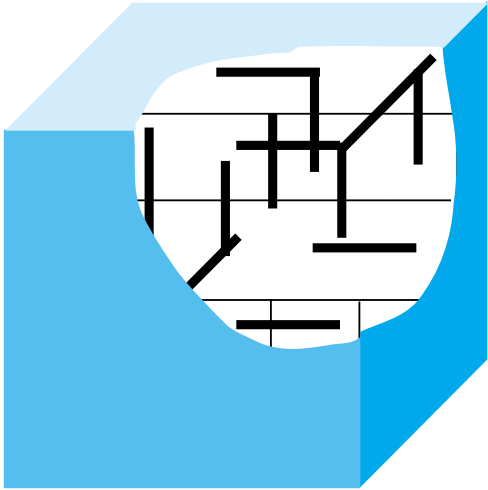
Figure 5-4. *Schematic view of the 3D model concept.*

Calculation of the bulk hydraulic conductivity can be made by assuming that a certain number (commonly 6) of channels intersect at each node of the orthogonal network and that each channel in the network consists of a bundle of N capillaries with circular cross section. Figure 5-5 shows a small part of the channel network and illustrates that the channels have different diameters.
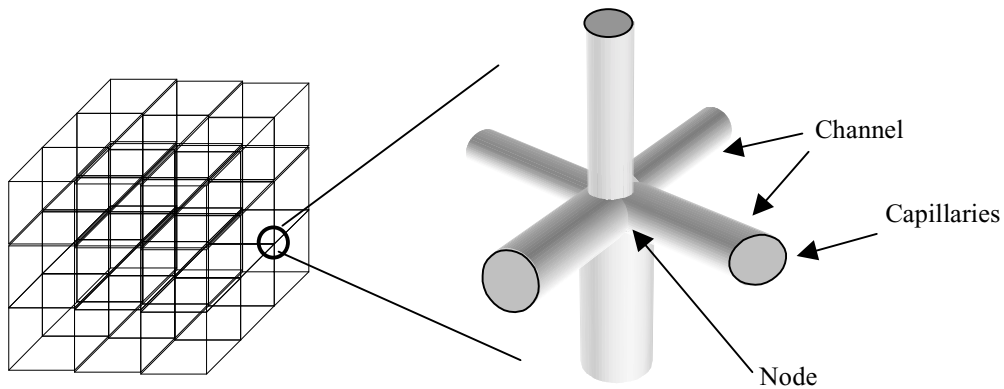
Figure 5-5. *Channel network mapped as a cubic grid with gel-filled channels intersecting at a node in the grid.*

The number of channels, which are assumed to have the length L, contain bundles of N capillaries with a diameter (d) that is proportional to the channel width is chosen to match the total porosity of the clay. After complete grain expansion the voids filled with homogeneous clay gels are assumed to have a normal size distribution with the same intervals as in the 2D model, i.e. 1–5 μm for the clay with 2130 kg/m^3 density, 1–20 μm for the clay with 1850 kg/m^3 density, and 1–50 μm for the clay with 1570 kg/m^3 density. The code generates a certain number of channels for a given volume [4]. Using the Hagen-Poiseuille law the flow rate through the channel network is calculated for given boundary conditions assuming a pressure difference on the opposite sides of the cubic grid and no flow across the other four sides. Table 5-5 specifies the density, total porosity n, and resulting bulk hydraulic conductivity of the considered clay types.

Table 5-5. Hydraulic conductivity (K) of three clay types prepared by compacting MX-80 powder and saturating them with electrolyte-poor water. n is the porosity.

Bulk density of air-dry powder kg/m^3	Dry density kg/m^3	Density at water saturation kg m^{-3}	n	Calculated K, m/s	Experi-mental K, m/s
2000	1800	2130	0.13	3E-12	2E-14
1500	1350	1850	0.20	1.3E-11	3E-12
1000	900	1570	0.47	2.4E-10	8E-11

One finds that the calculated bulk conductivity of MX-80 clay with the density 1570 kg/m^3 at saturation is on the same order of magnitude as typical experimental data, while the model significantly overrates the conductivity of the denser clays. The major reason for this discrepancy is that the model does not account for variations in cross section of the channels, which becomes increasingly important when the density rises. Thus, the most narrow parts control the percolation and since the conductivity of a capillary is an exponential function of the diameter the net effect of constrictions is more obvious for dense than for soft clays.

Following an earlier attempt to model microstructural constrictions [3], one can assume that 10 % of the length of all channel capillaries have a radius that is 2/3 of the diameter of the longer parts. The impact of such constrictions on the conductivity can be calculated by applying a theory proposed by Dullien [5] for capillaries with two dimensions. Taking the large diameter as d_1, the small one as d_2, $d_1=4d_2$ and the length of the small diameter as L_2, and also $L_2=0.1(L_1+L_2)$ one gets the equivalent diameter as $d_2/(L_2)^{1/4}$, which gives a reduction of the K-values according to Table 5-6. One finds that the corrected theoretical conductivity values agree well with the experimental data except for the densest clay for which some further reduction in capillary diameter is justified.

Table 5-6. Comparison of corrected theoretical hydraulic conductivity and experimental values.

Density at water saturation, kg m^{-3}	Corrected theoretical K, m/s	Experimental K, m/s
2130	E-13	2E-14
1850	5E-12	3E-12
1570	6E-11	8E-11

In conclusion, one can consider the concept with channels filled with gels containing numerous capillaries as a reasonably relevant theoretical model although the true void arrangement in the gels naturally has a stochastic nature with large variations in particle spacing and interaction that are not included in the channel model. In this respect the MMM model, which averages the geometrical and density properties of the microstructure, is superior to the GMM model.

5.3　　Swelling pressure

The swelling pressure is expected to be proportional to the product of the true swelling pressure of the pressure-controlling component a and the volume ratio $(a^3-b^3)/a^3$. This ratio is $(1-F_3,)$, which represents the volume fraction of this component. For the bulk density 2130 kg/m^3 ρ_a is 2000 kg/m^3 and the theoretical swelling pressure of this component about 11 MPa as calculated by use of colloid-chemical theories [6, 7]. $(1-F_3)$ is 0.93 and the product consequently about 10 MPa, which is practically the same as the experimentally determined value. For the bulk density 1570 kg/m^3 ρ_a is 1750 kg/m^3 and the true swelling pressure about 0.3 MPa. $(1-F_3)$ is 0.75 and the product hence about 0.2 MPa. This value is also in good agreement with experimental data as illustrated by Table 5-7.

Table 5-7. Calculated and experimentally determined swelling pressures (p$_s$) of MX-80 saturated with distilled water [1].

Bulk density kg/m^3		$1-F_3$	Density of massive part, kg/m^3	p_s of massive part, MPa	Calculated bulk p_s MPa	Experimental bulk p_s MPa
2130	Na	0.93	2150	15.0	14.0	14.0
1850	Na	0.80	1900	1.5	1.2	1.0
1570	Na	0.75	1750	0.5	0.4	0.3

Applying the same principle as for the hydraulic conductivity, i.e. assuming that the major microstructural features expressed in terms of F_3, are the same as for saturation with distilled water, one gets for MX-80 in Ca form the same theoretical swelling pressure as for MX-80 saturated with distilled water when the bulk density is 1850 and 2130 kg/m^3, respectively. These pressure values agree well with experimental ones. For 1570 kg/m^3 on the other hand, the theoretical value is 0.3 MPa while a typical experimental value is about 0.02 MPa. The discrepancy is due to insufficient sensitivity of the model for densities representing conditions close to complete expansion of the densest part of the clay matrix (*a*).

The influence of increased Na concentration in the porewater is similar to the corresponding impact on the hydraulic conductivity. Thus, when exposing MX-80 clay with a bulk density 2130 kg/m^3 to sea water, the swelling pressure is not changed at all, while for 1850 kg/m^3 the theoretical value is around 1.0 MPa while a typical experimental value is on the order of 0.5 MPa. For the lowest bulk density 1570 kg/m^3 the theoretical swelling pressure is about 0.15 MPa, while recorded swelling pressures are only a few tens of kPa. Again, the sensitivity of the MMM model is not sufficient to account for conditions close to complete expansion of the stacks of lamellae.

5.4   Ion diffusion

5.4.1   Porewater chemistry

The porewater chemistry of smectite-rich clay results from complex interactions between the solution and the smectite minerals in which the accessory minerals also take part [1]. Equilibrium modelling can explain the basic chemical reactions like dissolution, precipitation and ion exchange as exemplified in Chapter 6, which deals with microstructural changes.

The small space between mineral surfaces in dense smectite clay means that the ion distribution and mobility adjacent to these surfaces play a major role in modelling ion diffusion. MGC (modified Gouy-Chapman) theory and the conventional GC theory can be used for calculating the negative potential and the interaction of electrical double-layers but it is clear from i.a. analysis of dielectric permittivity profiles that the potential can only be defined for the midpoint between clay platelets. The major flaw of the GC theory is that it implies unreasonably high cation concentrations close to the mineral surfaces. The MGC is therefore a preferable scientific tool [1].

5.4.2   Ion migration and sorption in porous medium with narrow channels

The basic expression for ion diffusion flux J has the following form:

$$J=nD_p(dc/dx) \tag{5.2}$$

where: n = Porosity
           D_p = Diffusion constant in water
           dc/dx = Concentration gradient

Since smectites have a sorption potential that affects the diffusion rate, the diffuison flux one defines the so-called apparent diffusivity D_a:

$$D_a = n\, D_p/(n + K_d \rho_d) \tag{5.3}$$

where: K_d = Distribution factor
            ρ_d = Dry density

For the specific purpose of modelling ion diffusion through narrow channels one can express the ion diffusion flux J by the expression in Eq.5.4 [1]:

$$J = \phi \tau^{-2} D[\eta^{-1}(1+\gamma)]\Gamma \tag{5.4}$$

where: ϕ = Surface potential
            τ = Tortuosity factor
            D = Diffusion coefficient
            η = Measure of viscosity of surface-near shear zone
            Γ = Surface-excess charge at distance γ from the surface

In this model K_d appears in the following form:

$$K_d = \phi\Gamma/(1-\phi)\rho_d \tag{5.5}$$

Defined in this way K_d accounts for negative adsorption, i.e. repulsion and exclusion of ions. This effect has been substantiated by a study performed by Jarmo Lehikoinen [1]. He assumed the clay microstructure to consist of an array of parallel capillaries with periodic stepwise changes in diameter as in Figure 5-6 and the channel dimensions according to Table 5-8 and found the relative amounts of monovalent anion concentration in percent in a REV for different concentrations as shown in Figure 5-8. The latter picture illustrates that Donnan exclusion is valid not only for the interlamellar space but also between aggregates and stacks if the distance between mineral surfaces is sufficiently small.

Table 5-8. Channel dimensions [1].

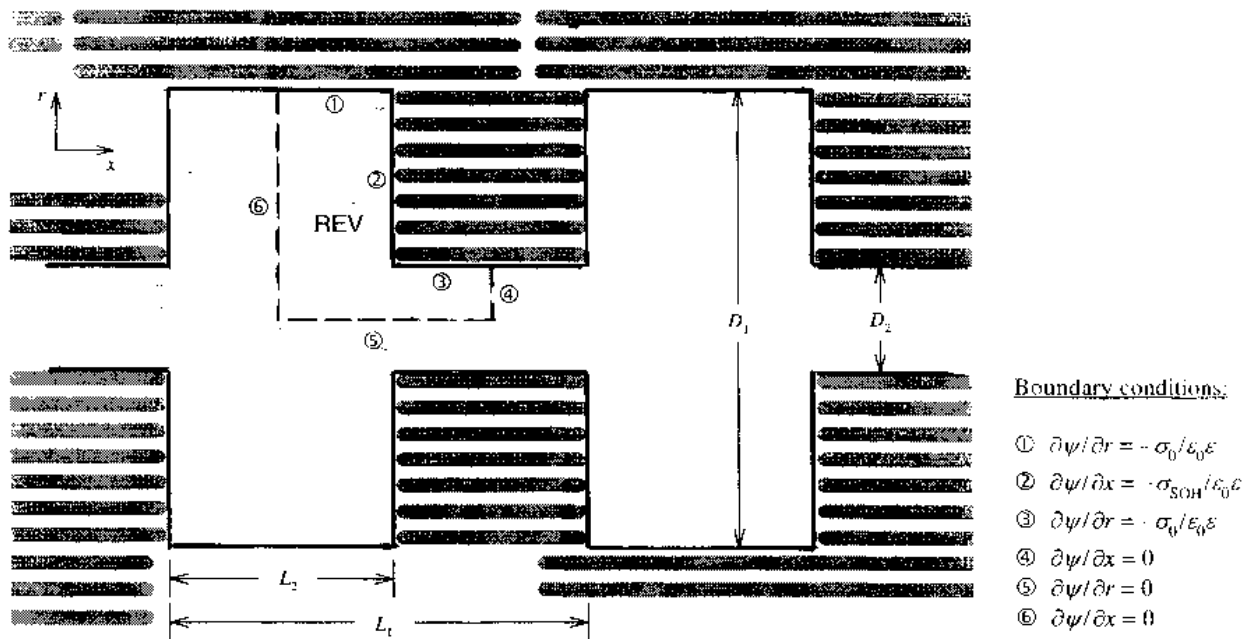| Bulk density at water saturation, kg/m³	D_1, Å	D_2, Å	L_1, Å	L_2, Å
2130	50	10	100	50
1850	100	20	200	100
1570	500	30	1000	500

Figure 5-6. *Channel geometry. The grey horizontal bars represent smectite lamellae grouped in stacks. The area within the broken lines makes up the Representative Element (REV) [1].*
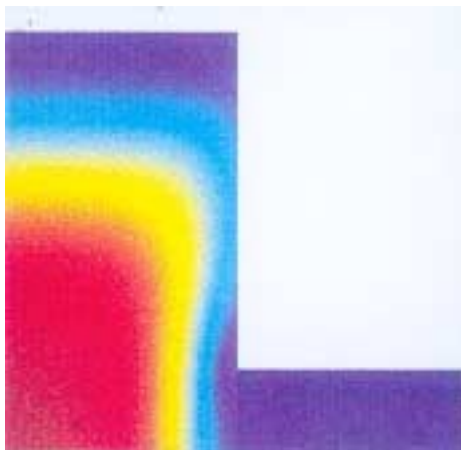

Figure 5-7. *Relative monovalent anion concentration (%) in a REV for equilibrating 0.1 M monovalent electrolyte in MX-80 clay with the density 2130 kg/m³. The picture shows that anions (red and yellow) are confined in the center of the wide part of the widest channels (50 μm) and that only cations (blue) are located close to the mineral surfaces and in the channel [1].*

5.4.3 Ion flux capacity according to the present model (MMM)

Naturally, the stochastic nature of the microstructure implies that both the width and straightness of the channels vary and that the density of the gel fillings is not a constant. The channel size and gel density vary over any individual cross section in isotropic clay, still yielding approximately the same F_2-value for each of them. This parameter is hence a useful quantitative measure of the conductivity-controlling microstructural component. Since it also represents the part of the clay in which pore diffusion takes place it is a determinant of the diffusion capacity as well. Thus, the ratio of void volume available for uniaxial diffusion, and total volume, should be approximately proportional to F_2 for anions and to unity for non-reactive cations like sodium. The ratio of the ion diffusion capacity for e.g. iodine and sodium should hence be about 0.17 for a bulk density of 2000 kg/m^3, which is about 4 times higher than the experimentally determined ratio [1]. The main reason for this discrepancy is that channel tortuosity and constrictions have not been accounted for. Hence, when applying the correction of F_2 used in calculating the hydraulic conductivity caused by constrictions one arrives at a ratio for iodine and sodium diffusion capacity that is very close to the recorded value.

5.5 Gas conductivity

Gas penetrates smectite clay in a finger-like mode when the gas pressure exceeds the sum of the piezometric head and a critical (treshold) pressure, which has been experimentally validated [8, 9]. The microstructural heterogeneity explains why pressurized gas moves in local pathways. They are "paths of least resistance" represented by interconnected voids or elements with lower density than the rest of the clay matrix.

The resistance to gas-induced displacement of the clay matrix in dense MX-80 clay is logically related to its swelling pressure since gas penetration requires separation of dense matrix components ("fracturing"). Hence, according to the data in Table 5-9 the critical gas pressure should be close to the bulk swelling pressure for MX-bentonite with a density of about 2100 kg/m^3, for which there is much experimental support. For lower densities it is probable that soft clay gels will consolidate and become as dense as the massive clay matrix, which would also yield critical pressures on the same order of magnitude as the swelling pressure of this matrix. However, the possibility for gas to find its way through soft clay without displacing denser parts is believed to lead to a lower critical gas pressure, which is also supported by Table 5-9 as well as by the outcome of various other experiments [10].

Table 5-9. Experimentally determined critical gas pressure in MPa for MX-80 in Na form.

Density at saturation, kg/m^3	Experimentally deter-mined critical gas pressure	Swelling pressure of dense clay matrix in Na MX-80
2130	20.0	15.0
1850	2.0	1.5
1570	0.1	0.5

5.6 MX-80 clay interacting with organics represented by HDPy[+]

5.6.1 General

The microstructural constitution of HDPy[+]-treated MX-80 is very different from that of untreated clay as concluded from electron and light microscopy. Consequently, the physical properties of the HDPy[+]-treated material are also different from those of ordinary MX-80 clay. The microstructure and hydraulic conductivity as well as the swelling pressure will be documented in this chapter. Figure 4-18 illustrates the typical strongly aggregated nature of the clay.

5.6.2 Hydraulic conductivity

The hydraulic conductivity of the HDPy[+]-treated clay is specified in Table 5-10. For the density 1630 kg/m^3 the conductivity was found to be about 50 times higher than for untreated MX-80, while it was around twice as high for the higher density 1760 kg/m^3.

Using the same mathematical expressions for the microstructural parameter F_2 as for untreated MX-80, F_2 should be 0.38 for 1630 kg/m^3 and the gel density 1600 kg/m^3, which would yield the actually recorded bulk conductivity E-10 m/s if one takes the K-value of the HDPy[+]-treated MX-80 gel to be 2E-10 m/s. However, the heterogeneity of the HDPy[+] clay makes this sort of estimates uncertain.

Table 5-10. Bulk hydraulic conductivity (K) of untreated and HDPy[+]-treated MX-80 clay saturated and percolated with distilled water.

Density at saturation, kg/m^3	K, m/s of untreated MX-80	K, m/s of HDPy[+]-treated MX-80
1630	2E-12	E-10
1760	5E-12	E-11

5.6.3 Swelling pressure

The swelling pressure of the HDPy[+]-treated clay is specified in Table 5-11. For the density 1630 kg/m^3 the value was found to be almost twice as high as that of untreated MX-80, while it was about the same as for the untreated MX-80 for the higher density 1760 kg/m^3.

Table 5-11. Swelling pressure (p_s) of untreated and HDPy[+]-treated MX-80 clay saturated and percolated with distilled water.

Density at saturation, kg/m^3	p_s, MPa of untreated MX-80	p_s MPa of HDPy[+]-treated MX-80
1630	0.35	0.60
1760	0.60	0.70

The value 0.63 of the factor $(1-F_3)$ for the HDPy$^+$-treated MX-80 clay with a density of 1760 kg/m^3 is somewhat lower than that of untreated MX-80 clay with the same density (0.75–0.80 MPa) but the density of the massive part (red and black parts of the digitalized pictures) is somewhat higher, i.e. about 1800 kg/m^3. Hence, the theoretical bulk swelling pressure being the product of $(1-F_3)$ and the estimated swelling pressure 1 MPa of the massive part, should logically be on the same order of magnitude as the actually recorded pressure.

The nature of the swelling pressure of HDPy$^+$-treated MX-80 clay is not fully understood. It can be assumed, however, that it is at least partly due to hydration as indicated by the diagram in Figure 5-8, which suggests the same diffusion-controlled uptake of water and development of the swelling pressure as in ordinary MX-80 clay. This suggests that water molecules populate part of the interlamellar space in addition to HDPy$^+$-ions.
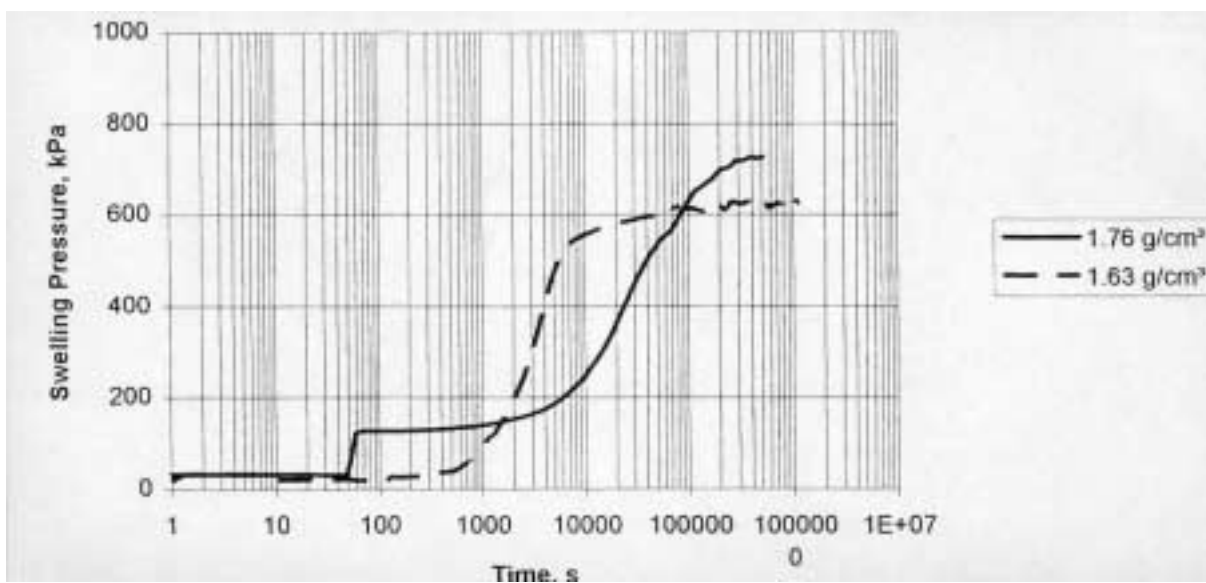

Figure 5-8. *Development of swelling pressure in HDPy$^+$-treated MX-80 clay.*

5.7 Tentative conclusions from comparison of theoretically predicted and recorded physical properties

The following major conclusions can be drawn:

- The conceptual structural model of clay formed by compacting MX-80 grains with subsequent hydration implies that the clay does not become homogeneous but contains interconnected voids filled with clay gels of lower density than the rest of the clay matrix. Taking micrograph-derived structural parameter data as a basis and applying flow theory for heterogeneous media the calculated bulk hydraulic conductivity is about the same as the experimental. The recently developed 3D capillary-filled channel-type model with theoretically derived water flux partly overrates the conductivity, suggesting that the channels have a varying cross section with the most narrow parts controlling the net conductivity.

- The derived microstructural models for compacted and hydrated MX-80 clay buffer yield data on the hydraulic and gas conductivities and also the swelling pressure that agree well with experimentally determined bulk data both for untreated and HDPy$^+$-treated MX-80 over a large bulk density span. Microstructural parameters can be evaluated from micrographs for both clay types.

- The microstructural models do not have sufficient resolution power to describe the most detailed features. However, since the structural variations on the gel scale are stochastic, statistically based models like the presently proposed MMM, which agrees on the whole with the earlier GMM model, may be applicable for developing theoretical models of greater detail.

- MX-80 saturated with organic material like HDPy$^+$ has a much more heterogeneous microstructural constitution than untreated MX-80 and its gel-forming potential is significantly lower. The HDPy cation is adsorbed in the interlamellar space in a "pillared" fashion, which allows interlamellar hydration. The stacks of lamellae are rigid and require much higher compaction pressure than 100 MPa to yield bulk densities exceeding about 1800 kg/m^3 after water saturation.

5.8 References

1. Pusch R, Muurinen A, Lehikoinen J, Bors J, Eriksen T, 1999. Microstructural and chemical parameters of bentonite as determinants of waste isolation efficiency. European Commission Final Report Contr. No. F14W-CT95-0012.

2. Börgesson L, Pusch R, Fredriksson A, Hökmark H, Karnland O, Sanden T, 1992. Identification of zones disturbed by blasting and stress release. Final Report of the Rock Sealing Project. Stripa Project Technical Report TR 92-08, SKB Stockholm.

3. Pusch R, Karnland O, Hökmark H, 1990. GMM – A general microstructural model for qualitative and quantitative studies of smectite clays. SKB Technical Report TR 90-43, SKB Stockholm.

4. Neretnieks I, Moreno L., 1993. Fluid flow and solute transport in a network of channels. Journal of Contaminant Hydrology, 14, (pp 163–192).

5. Moreno L, 2000. Personal communication.

6. Yong R N, Warkentin B, 1975. Soil Properties and Behaviour. Elesevier Publ. Co., Amsterdam.

7. Pusch R, 1978. Engineering aspects of clay-weathered Blekinge gneiss. Geologiska Föreningens i Stockholm Förhandlingar, Vol.101 (pp. 27–31).

8. Horseman S T, Harrington J F, 1997. Study of gas generation in MX-80 buffer bentonite. British Geological Survey, WE197/7.

9. Pusch R, Hökmark H, Börgesson L, 1987. Outline of models of water and gas flow through smectite clay buffers. SKB Technical Report TR 87-10, SKB, Stockholm.

10. Pusch R, 1997. Transport phenomena in smectite clay explained by considering microstructural features. Proc. MRS Scientific Basis for Nuclear Waste Management XXI, Vol. 506, Ed. McKinley/McCombie. Materials Research Soc., Warrendale, Pennsylvania, USA.

6 Microstructural stability

6.1 General

We will consider here three major processes that can alter the microstructure of a fully water saturated buffer clay:

- Physically induced effects primarily by changes in density through compression or expansion, shearing, high hydraulic gradients, and gas percolation.

- Physico/chemically induced effects by changes in porewater chemistry.

- Chemically induced effects by dissolution and precipitation.

6.2 Physically induced effects

6.2.1 Compression

Compression of water saturated buffer clay can be caused by:

- Canister load.

- Contraction of the deposition holes by rock creep or failure.

Compression of the buffer naturally increases the density by which the hydraulic conducitivity is reduced and the swelling pressure increased as shown in Chapter 5. These changes have different explanations. Thus, the drop in conductivity when consolidation takes place under a successively increased efferctive pressure is believed to be due to the effect illustrated in Figure 6-1, implying that the largest voids and softest parts are compressed first. The continuity of the channels is thereby reduced and frequent constrictions are formed. The increase in swelling pressure, on the other hand, is probably caused by an increased number and size of the contacts between denser aggregates.
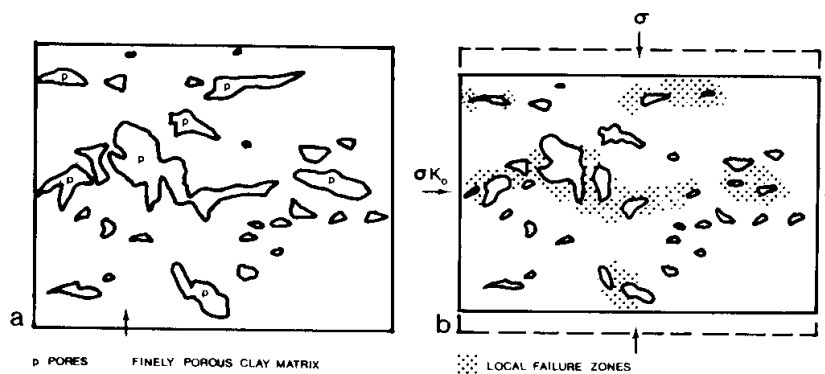

Figure 6-1. Consolidation of the clay microstructure under an increased load means that the largest voids and soft parts are compressed first, reducing the interconnectivity of permeable paths and creating more contacts between dense particle aggregates [1].

6.2.2   Expansion

Expansion of the buffer can and will take place in conjunction with the displacement of the overlying backfill that has a much lower swelling pressure than the buffer. The drop in density of the clay will naturally cause an increased hydraulic conductivity and a drop in swelling pressure. As for compression, the detailed mechanisms are different. The densest microstructural units expand most, leaving the softer parts largely unchanged, which means that the bulk hydraulic conductivity is not increased very much if the expansion is moderate. The swelling pressure, on the other hand, is assumed to drop significantly even for a rather small expansion.

6.2.3   Shearing

Shearing causes breakage and orientation of clay particles as demonstrated by earlier microstructural investigations [2, 3, 4]. The mechanism is illustrated in Figure 6-2, implying that dense aggregates remain fairly unaffected at the moderate strain that is associated with the maturation of the buffer clay including the expansion of the uppermost part in deposition holes, while softer parts undergo shearing. Hence, the characteristic variation in microstructural density is assumed to be preserved in principle. However, very large shear strain induced by tectonic movement of nearfield rock blocks is expected to cause strong alignment and breakdown of dense aggregates, yielding a laminated and hence very anisotropic constitution (micrograph in Figure 6-2).
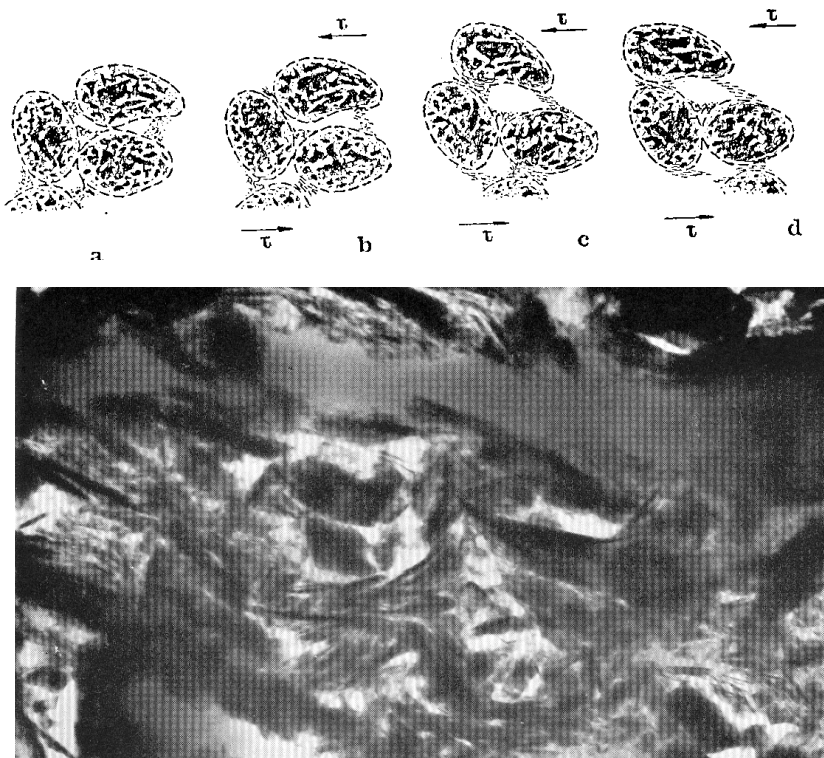

Figure 6-2. *Microstructural alteration by shearing. Upper: Minor microstructural strain; Lower: Significant microstructural changes by large shear strain (Height of micrograph is 9 μm) [3, 4].*

6.2.4   Water and gas penetration

High hydraulic gradients may arise in the water saturation phase and in the subsequent saturated state, causing quick penetration of water into the buffer in the form of a hydraulic wedge as illustrated by Figure 6-3 in soft parts of the buffer. This causes displacement of such parts of the clay and may result in channels that may not self-seal.
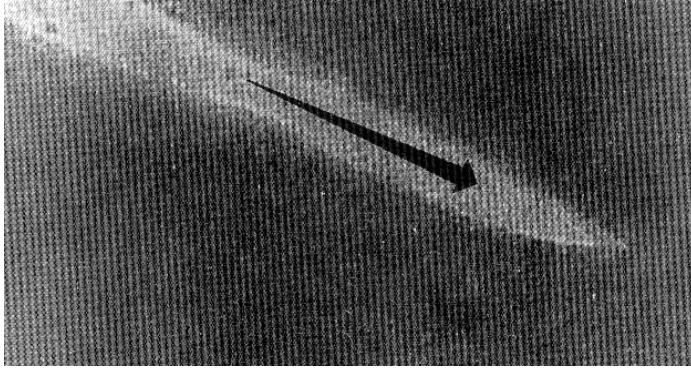

Figure 6-3. *Piping in the form of a hydraulic wedge penetrating into a soft clay gel [5].*

Gas percolation is believed to have a similar effect as concluded from microstructural investigations. Thus, micrographs of gas-percolated MX-80 clay have given evidence of gas channels in the clay matrix as demonstrated by Figure 6-4 [6].
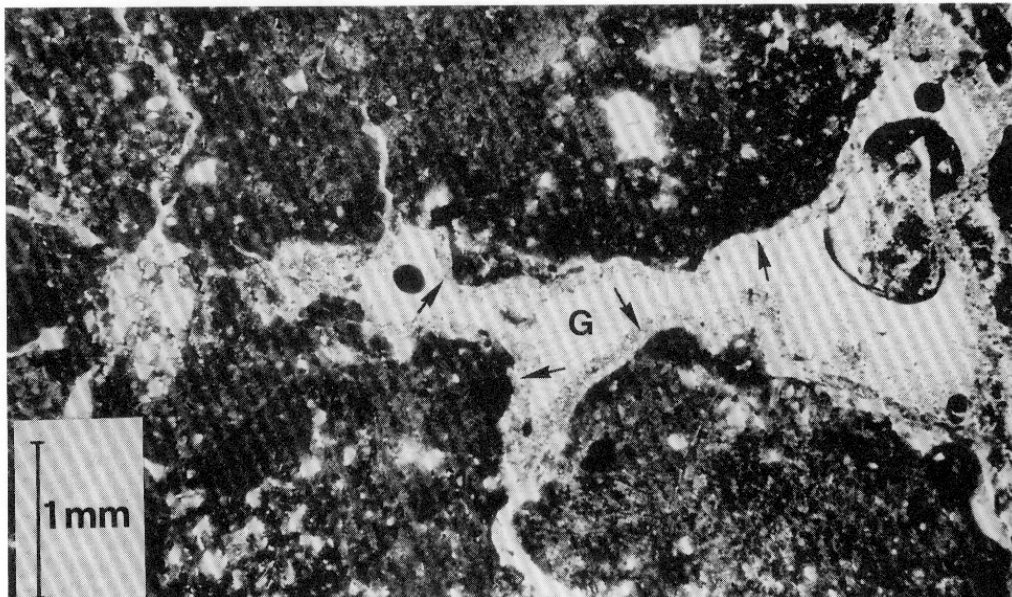

Figure 6-4. *Channels formed by gas penetration [6]. Micrograph of large gas path through MX-bentonite with a density of 1630 kg/m3 at saturation. G represents gas channel and arrows point at sheared clay along the channel (polarized light, 30 μm thin section).*

Figure 6-4 demonstrates that particle orientation and consolidation of the clay gel takes place adjacent to gas channels, which suggests that the clay/water system has a potential to self-seal by expansion and re-establishment of clay gels rather soon after termination of the gas percolation. Such sealing has been recorded in numerous gas percolation tests, which have all shown that the gas pressure required to cause penetration of gas in cyclic pressurization tests with intermittent pressure drops is approximately the same as in the preceding pulse [7].

6.3 Physico/chemically induced effects

6.3.1 Changes in porewater chemistry

The microstructural differences between smectite clays formed by saturation with fresh and salt water has been described in Chapters 3 and 4 and the related differences in physical properties in Chapter 5. Figure 6-5 illustrates the earlier mentioned more homogeneous nature of the firstmentioned clays and the larger and denser particle aggregates in clays formed and matured under saltwater conditions and a question of great practical importance is if a clay of either type can be transformed to the other by replacement of the porewater through percolation or diffusion. Theoretically, the least dense parts of low-electrolyte Na clay matrix should coagulate and yield continuous passages by percolation with salt solutions, particularly if they are rich in calcium, since this will reduce the interlamellar space. An additional effect should be that coagulation reduces the continuity of the clay gels and causes separation and release of particle aggregates, which may move with flowing water and cause clogging and redcuction of the hydraulic conductivity.
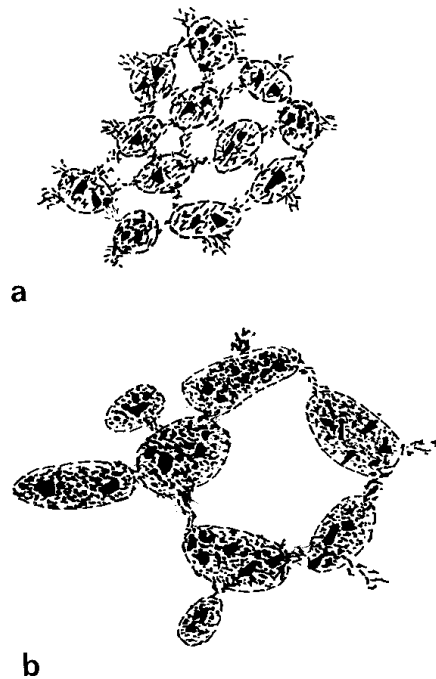

a

b

Figure 6-5. Schematic illustration of the impact of porewater salinity on clay microstructure. a) Clay deposited in fresh-water. b) Marine clay [3].

Experiments with determination of the hydraulic conductivity have shed light on the influence of changes in porewater chemistry on the hydraulic conductivity and swelling pressure. No systematic investigation of such changes have been made on MX-80 clay but a preliminary study shows a very moderate increase in hydraulic conductivity and drop in swelling pressure on increasing the salinity of percolating water from practically zero to 3.5 % $CaCl_2$ solution for a density at saturation of 1900 kg/m^3. This is in line with the outcome of systematic tests on a clay with about 50 % expandables [8], which also showed rather small changes even at very large variation in salinity as summarized below [9]. Changes from an initial state of smectite clay with Na as dominant adsorbed cation and a low electrolyte content to salt Ca-porewater are due to coagulation and exchange of adsorbed cation, the latter effect being important only for bulk densities at water saturation of less than 1700–1800 kg/m^3.

The experiments illustrated in Figures 6-6 to 6-10, were made on Friedland Ton, a clay of Tertiary age containing around 25 % montmorillonite in Na form and 25 % mixed layer smectite/illite. Compaction of air-dry clay powder to a dry density of 1430 kg/m^3 was made for reaching a bulk density of 1900 kg/m^3 at complete water saturation. The sample was first percolated with 20 % $CaCl_2$ solution, recording the swelling pressure and hydraulic conductivity, after which it was percolated with distilled water, and then, in series, with 10 % $CaCl_2$ solution, distilled water, and finally 3.5 % $CaCl_2$ solution.
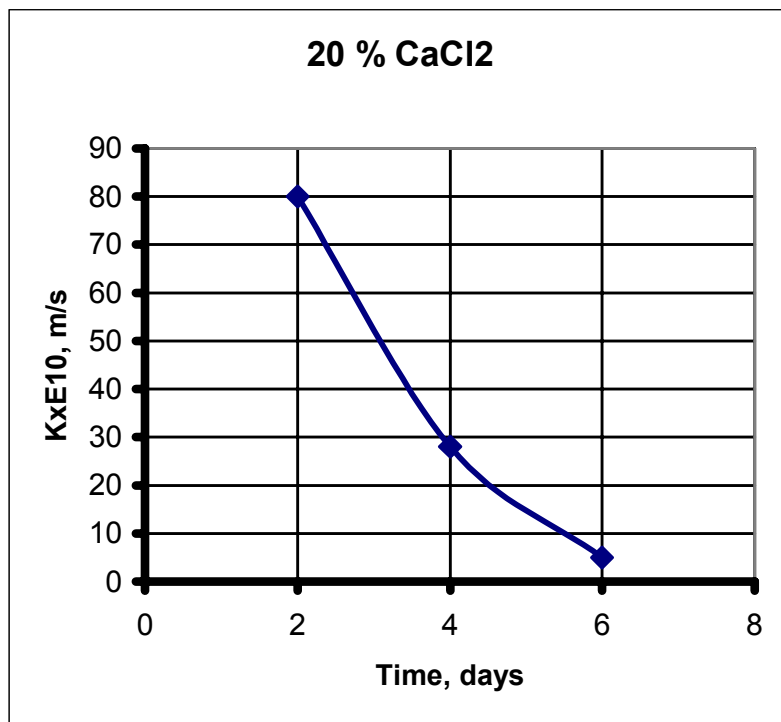

Figure 6-6. *Recorded hydraulic conductivity for percolation with 20 % CaCl$_2$ solution. The initial hydraulic conductivity was 8E-9 m/s but dropped to about 5E-10 m/s after 6 days. The estimated microstructural response is concluded to be confined to coagulation of softer parts of the particle network and to migration of aggregates that are set freeand clog channels where they have constrictions.*
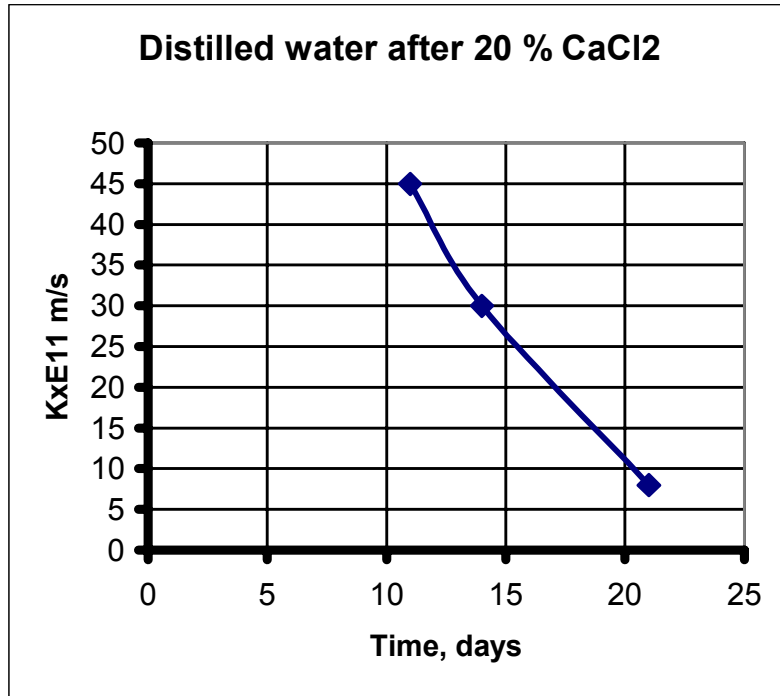
Figure 6-7. Recorded hydraulic conductivity for percolation with distilled water after the 20 % CaCl₂ solution treatment. The conductivity dropped to 8E-11 m/s after 3 weeks. The microstructural response is dispersion of aggregates and formation of sealing clay gels.

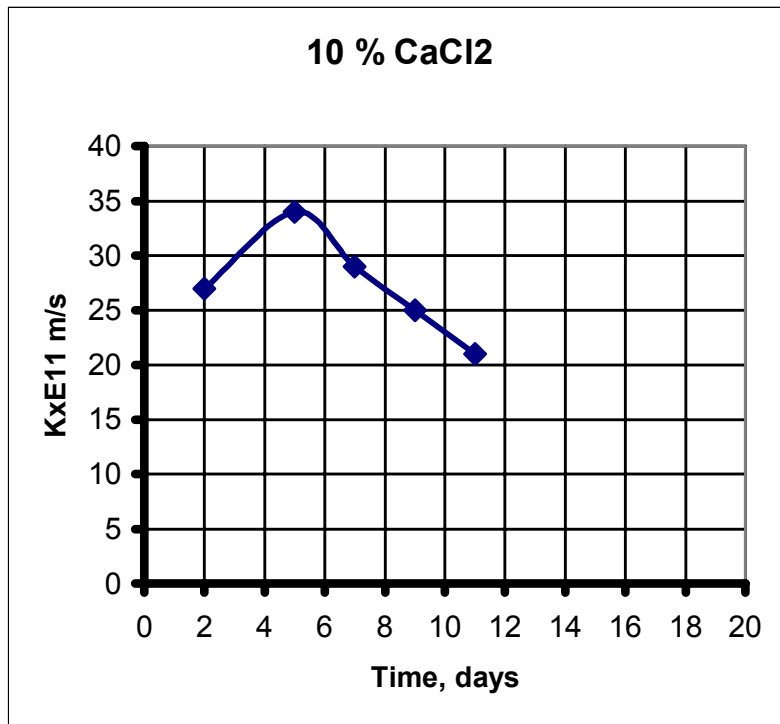*Figure 6-8. Recorded hydraulic conductivity for percolation with 10 % CaCl₂ solution after the test with distilled water.The flow through the clay sample rose slightly in the first five days and then dropped to yield a hydraulic conductivity of about 2E-10 m/s after about 11 days. This drop is believed to be due to migration of small particle aggregates causing clogging of channels.*
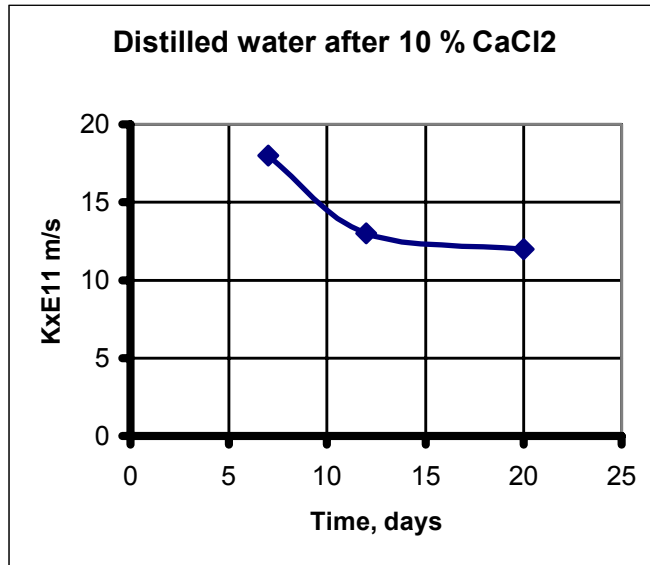
Distilled water after 10 % CaCl2

Figure 6-9. Recorded hydraulic conductivity for percolation with distilled water following the test with 10 % CaCl$_2$. The hydraulic conductivity remained constant at about 1.9E-10 m/s in the preceding test with 10 % CaCl$_2$ for about a week and then dropped to 1.2E-10 m/s in the following two weeks, indicating some dispersion and reduction in size of open or gel-filled voids.
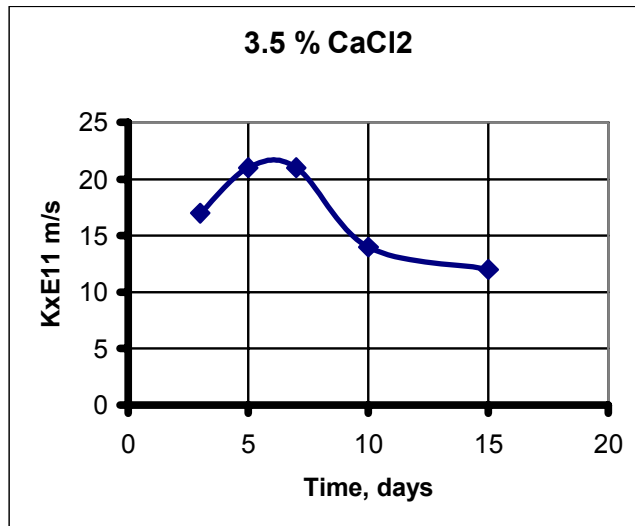
3.5 % CaCl2

Figure 6-10. Recorded hydraulic conductivity for percolation with 3.5 % CaCl$_2$ following the test with distilled water. The hydraulic conductivity increased from the value 1.2E-10 m/s in the preceding test with distilled water to 2.2E-10 m/s in three days and then dropped back to about 1.2E-10 m/s in the following ten days. This indicates that clogging of voids by particle aggregates transported by flowing water compensated for the increase in conductivity caused by salt-induced coagulation of clay particle network.

The experiments referred to validate the proposed colloid-chemical model of coagulation of clay by saturation or percolation with salt water. However, exchange of the initial porewater of dense smectite clay by a solution with significantly different electrolyte content causes a relatively moderate change in conductivity, which suggests that only a small fraction of the clay matrix is sufficiently soft to undergo substantial structural reorganization. They also show that aggregates formed in clays with salt porewater are mobile and can be transported by flowing porewater to constrictions where they cause clogging and reduction of the hydraulic conductivity. The observations are in line with the idea of the microstructure of dense smectite clay consisting of dense aggregates separated by less dense parts.

6.3.2 Ion exchange

Cation exchange

The lattice charge deficit and exposure of structural elements like hydroxyls gives the smectites an ability to adsorb and exchange ions and charged inorganic and organic molecules. This is manifested by several investigations of the cation exchange capacity, which have shown that many cations are not equally replaceable and do not have the same replacing power. The extent to which ion exchange will take place is primarily a matter of the ion exchange capacity but the available space for interlamellar cation exchange may be a limiting factor at very high densities. In principle, the following law of replacement potential applies:

$$Li^+ < Na^+ < K^+ < Ca^{2+} < Mg^{2+} < NH_4^+,$$
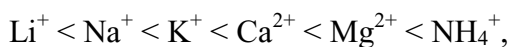
which means that, in general, Ca^{2+} will more easily replace Na^+ than Na^+ will replace Ca^{2+}.

However, there is no single universal replaceability series. It varies depending on a number of conditions, among which the ion concentration is most important. Na^+ vs. Ca^{2+} represents a particularly important case of competition. Thus, as the amount of exchangeable calcium on the clay mineral drops, it becomes more and more difficult to release. Sodium, on the other hand, tends to become easier to release as the degree of saturation with sodium ions becomes less.

Furthermore, cation exchange depends on the nature of the anions in replacing solutions as illustrated by the ease in replacement of Na^+ by Ca^{2+} when calcium hydroxide is present as compared with calcium sulphate. This is related to complexation through formation of salts with the clay and a soluble anion, which may make montmorillonite undergo structural alteration in conjunction with the formation of new compounds.

The explanation for the different cation replacement potential is the impact of size and valence. The smaller the diameter and the higher the valence, the higher the replacing potential, with the exception of hydrogen, which behaves like a divalent or trivalent ion. In general, it is the size of the hydrated ion, rather than the size of the unhydrated ion, that controls the replaceability. Thus, it appears that for ions of equal valence, those which are least hydrated have the greatest energy of replacement and are the most difficult to displace when present upon the clay. Li^+, although being a very small ion, is considered to be strongly hydrated and, therefore, to have a very large hydrated size. The low replacing potential of Li^+ and the fact that it is easily replaced are thought to be a consequence of the large hydrated size but there are indications that Li^+ and Na^+ are in fact only weakly hydrated in interlamellar positions, which offers a more reasonable explanation of their strong ability to be replaced [10].

Potassium is special since its ionic diameter 2.66 Å is about the same as the diameter of the cavity in the oxygen layer, so that this cation can fit into one of these cavities. As a consequence, the potassium ion is rather difficult to replace.

Montmorillonite typically has a cation exchange capacity of 80–150 meq/100 g.

Anions

There are three types of anion exchange mechanisms in smectites:

1. Replacement of OH ions of clay-mineral surfaces. The extent of the reaction depends on the accessibility of the OH ions; those within the lattice are naturally not accessible.

2. Anions that fit the geometry of the clay lattice, like phosphate and arsenate, may be adsorbed by fitting onto the edges of the silica tetrahedral sheets and growing as extensions of these sheets. Other anions, such as sulphate and chloride, do not adsorb because their geometry does not fit that of the silica tetrahedral sheets.

3. Local charge deficiencies may form anion-exchange spots on basal plane surfaces.

The lastmentioned mechanism is considered to give a small contribution to the net anion exchange capacity. The other two may be important in clay minerals like kaolinite but they are assumed to be rather unimportant in montmorillonite, which commonly has an anion exchange capacity of 5–10 meq/100 g.

Organic matter

Organic ions and molecules can enter the interlamellar space or be adsorbed on the edges and basal surfaces through hydrophilic groups or hydrogen bonds. It appears from various investigations that the CEC determined with certain organic cations is the same as when e.g. Ca^{2+} is adsorbed. This means that these organic cations can completely replace the alkaline-earth cation. $HDPy^+$ is an organic cation that has been extensively tested as reported in Chapter 4 and 5.

6.3.3   Cementation

Hydrothermal, fluid-saturated conditions

The hydrothermal conditions in KBS3 deposition holes are believed to affect the buffer clay in two ways, i.e. the earlier mentioned compression of stacks under the prevailing effective stress, and dissolution/precipitation processes. Precipitation of released silica may weld the lamellae together and reduce the expandability of the clay [11]. This may lead to the structural constitution in Figure 6-11, which is supported by a number of rheological tests that showed a considerable increase in strength already at 90°C as illustrated by Figure 6-12 and 6-13, and Table 6-1.
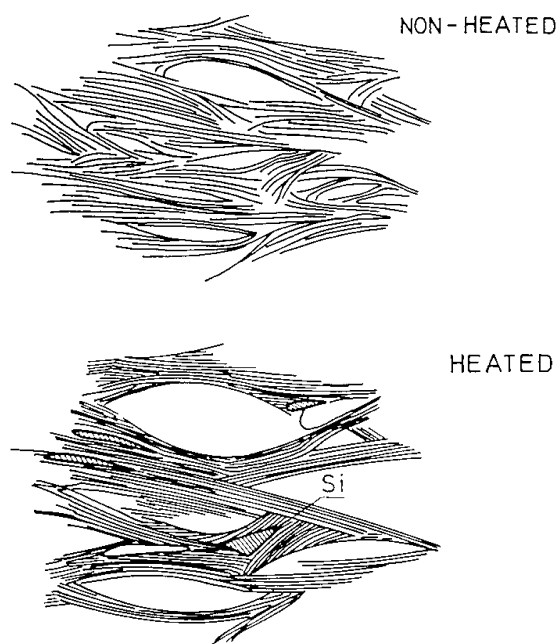

Figure 6-11. *Schematic illustration of heat-induced microstructural changes. Cementation may be particularly important at cooling after heating [12].*
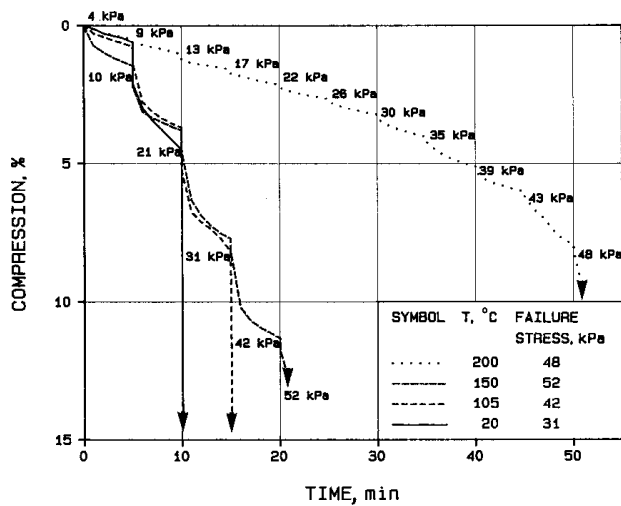
Figure 6-12. Axial compression versus time at unconfined compression of Na montmorillonite clay with a density of 1300 kg/m³, hydrothermally treated for 0.5 to 1.0 years. Arrows indicate failure. The figure 21 kPa for the untreated sample corresponds to a shear strength of 10.5 kPa, while 52 kPa for the 150°C sample represents a shear strength of 26 kPa [12].
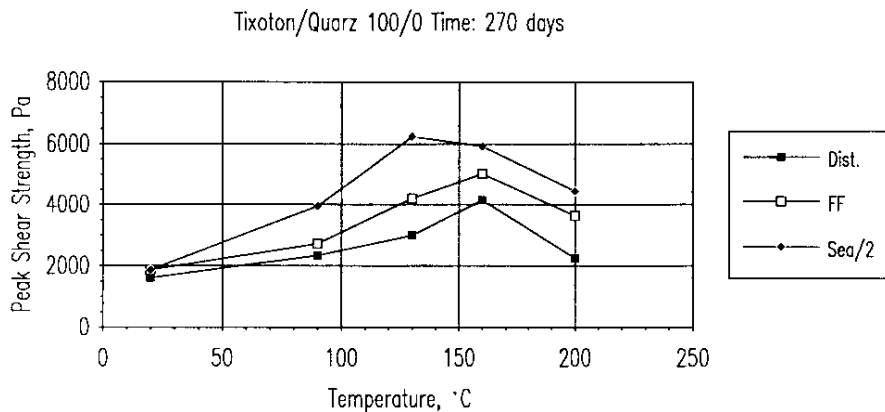
Figure 6-13. Shear strength of a bentonite (GEKO/QI) with about 90 % smectite in Na form (converted from the original Ca-state). The clay had a density at water saturation of 1080 kg/m³ and was exposed to different temperatures in hydrothermal cells for 270 days [12].

The test results in Figure 6-13 and Table 6-1 were obtained from hydrothermal tests in which small samples were kept in large pressure vessels with distilled water, Ca-rich strongly brackish water (FF), and seawater with 50 % concentration of that of the oceans (Sea/2). The density was 1080 kg/m³ in all the tests and the temperature ranged from 20 to 200°C. The shear strength was determined by laboratory vane boring.

91

Table 6-1. Shear strength in Pa of bentonite grout exposed to heating for different periods of time. The measurements were made after cooling [12].

Temperature °C	Distilled water	1 % CaCl$_2$ solution	Seawater with 50 % concentration	Time of treatment, days
20	1200	2050	2050	10
90	2200	2250	3300	10
130	3000	3900	4100	10
160	2400	4500	5900	10
200	2500	4800	4800	10
20	1200	1900	2000	90
90	2800	2400	3600	90
130	3200	3300	5000	90
160	3500	4600	4600	90
200	2800	3800	4000	90
20	1500	1800	1900	270
90	2400	2700	4000	270
130	3000	4300	6400	270
160	4200	5000	6000	270
200	2300	3500	4500	270

The major conclusions from this study were:

- Heating of clay with low-electrolyte pore water up to 160°C gave an increase in strength that was approximately proportional to the duration of the hydrothermal treatment. Since the swelling pressure of the very soft clay can not have caused compression of the stacks, resulting in a stronger particle network, chemical changes in the form of precipitation of silicious matter are believed to be the reason for the strengthening. Heating to 270°C gave a slight drop in strength, which is logically explained by loss in mass.

- Heating of the clay with ocean-type (50 % concentration) and Ca-dominated salt water gave a strength increase up to about 130°C to 160°C, while heating to 270°C gave a significant drop in strength, except for the shortest test period. The lack of strength reduction in most of the 10 day tests points to chemical effects rather than heat-induced rearrangement of the particles as major strengthening factor.

- It is probable that most of the recorded strength increase was caused after cooling by precipitation of cementing compounds released in the hydrothermal treatment.

The slightly increased hydraulic conductivity and loss in swelling pressure of denser clay on heating to 100–150°C are believed to be caused by compression of stacks of lamellae facilitated by partial interlamellar dehydration and growth of the voids in the fashion indicated in Figure 6-11. The compression of network branches that made them denser should be associated with particle alignment, which is in fact also indicated by the growth of the 17 Å peak at X-ray diffraction analysis of samples treated with ethylene glycole (Figure 6-14).
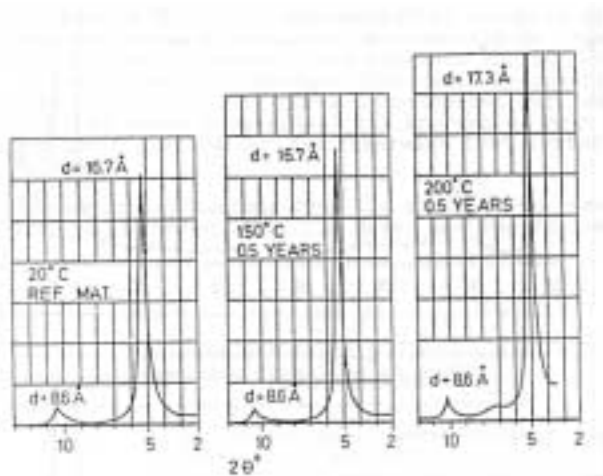
Figure 6-14. *XRD patterns for EG-treated MX-80 saturated with KCl after hydrothermal treatment. The sharp high peaks obtained for 150 and 200°C indicated improved orientation of the network of particles. A very slight illite peak is seen in the 200°C record.*

<u>Hydrothermal, vapor-related effects</u>

A special effect is due to the thermal gradient that prevails in the buffer for a few thousand years. The gradient across the buffer will be on the order of 0.1 to 0.5 °C per cm for some tens of years and 0.01 to 0.1 °C per cm for hundreds of years and it can maintain dissolution of minerals in the hottest part and precipitation where the temperature is lower [11]. A special case of this kind is vapor attack on the smectite minerals and their arrangement in the unsaturated phase [13]. It may cause permanent changes in microstructure and bulk properties as summarized below.

The conditions in the deposition holes of a KBS3 repository imply that steam will be produced in the buffer clay near the hot canisters. When the joints between the large buffer blocks become tight by absorption of water supplied by the surrounding rock, a closed system of interconnected voids is formed around the canisters (Figure 6-15). This space is filled with air and water vapor and the relative humidity will be 100 % when the wetting front of the water moving in from the rock is close to the hot canister surface. These conditions are similar to the hydrothermal conditions that prevail in the final phase of orogenetic processes, in which precipitation of cementing compounds take place.
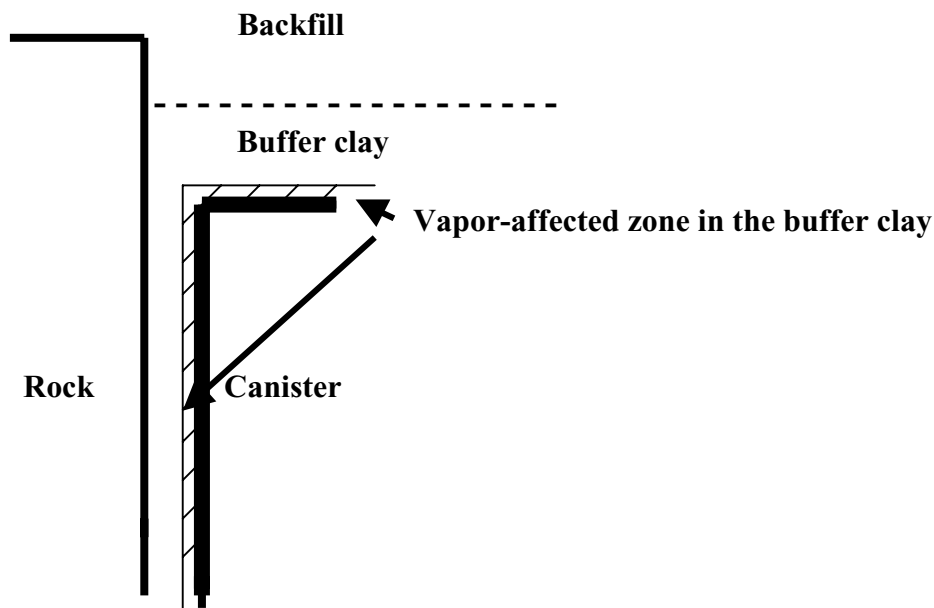
Figure 6-15. *Vapor-filled zone in the buffer clay close to canisters [13].*

The vapor conditions were simulated in autoclave tests after which the clay was saturated with distilled water and the swelling pressure and hydraulic conductivity determined. For clay exposed to 110°C and having a density of 1750 to 1850 kg/m^3 at complete water saturation the recorded pressure was practically the same as that of untreated clay. However, the vapor-treated samples had a hydraulic conductivity that was 50 to 100 times higher than that of unheated clay with corresponding densities. The reason for the higher conductivity of the vapor-treated samples can be explained be a reduced gel-producing potential caused by cementation.

Scanning electron microscopy using EDX element analysis showed that vapor treatment at 110°C produced large and dense aggregates and precipitation of silica (Figure 6-16). Transmission electron microscopy of acrylate-treated specimens demonstrated that the voids were somewhat larger and the particle aggregates somewhat denser in hydrothermally treated vapor-affected MX-80 clay than in untreated clay, Figure 6-17 [13]. The microstructural changes in MX-80 clay exposed to vapor at 110°C appear to be similar but somewhat more obvious than those taking place in fully water-saturated clay at temperatures of 150–200°C (cf. Figure 6-18).
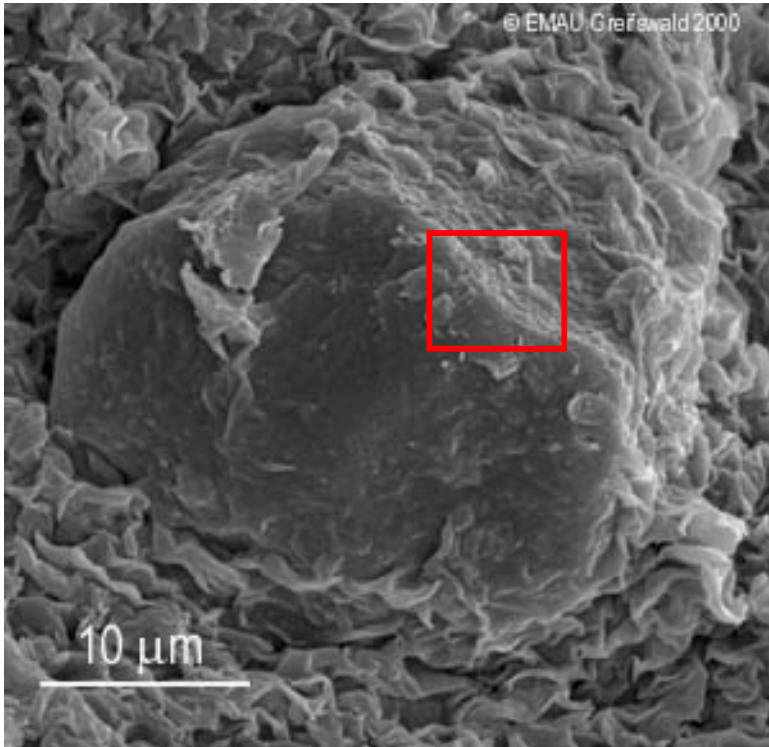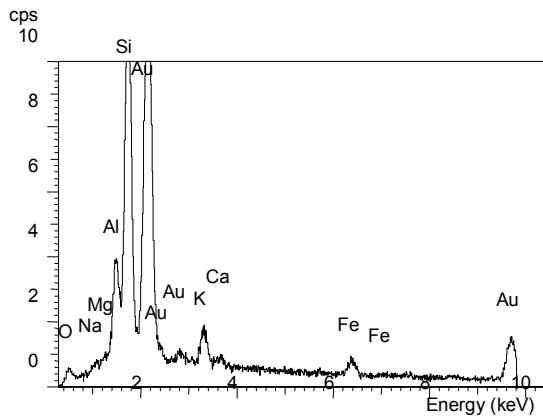
Figure 6-16. *Micrograph of aggregate in MX-80 clay exposed to 110°C vapor. The aggregate, which is surrounded by a typical wavy matrix of clay particles, is made up of equally oriented densely arranged groups of montmorillonite lamellae. The element analyses of the edge of the aggregate shows some excess Si that may represent silica precipitates [13].*
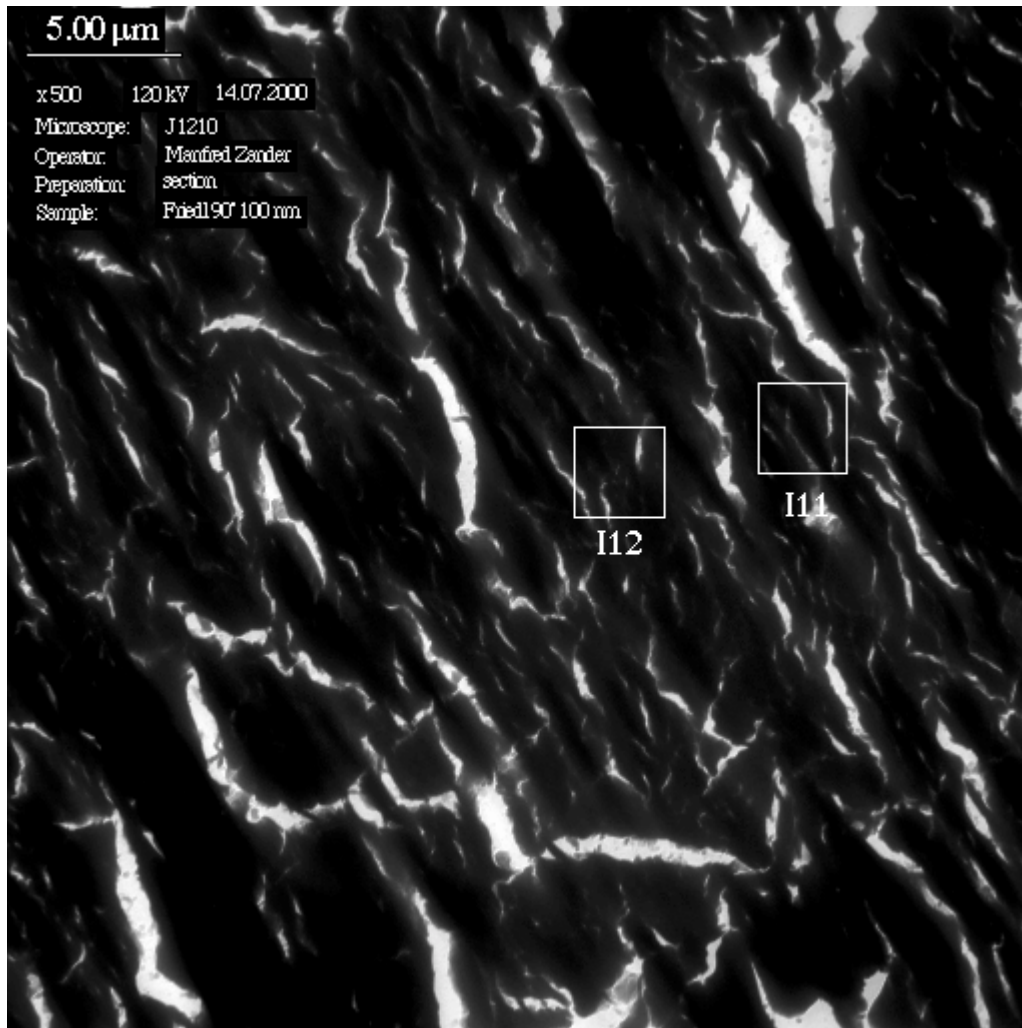
Figure 6-17. *TEM micrograph with 500 x magnification of 0.1 µm thick section of MX-80 clay exposed to 110°C vapor and then hydrated and homogenized in an oedometer to a density of 1750 kg/m³. Open and gel-filled voids are seen, three with a long diameter of 5–20 µm and about sixty with a long diameter of 1–5 µm. The total cross section area is about 1000 µm² [13].*

The evaluation of micrographs with 0.1 µm thickness gave the same conclusions as of those of 1 µm thickness, which indicates that many of the voids are disc-shaped with similar diameter in all directions. However, in accordance with theory the number of voids of all sizes is higher in the thinner section. Thus, certain cross sections representing areas on the order of 1000 µm² showed larger numbers of 5–20 µm voids as illustrated by Figure 6-17, in which one can identify half a dozen voids of this size. Since such a high frequency was not seen in the 1 µm thick sections indicating that some voids of this size may be very flat and enclosed in 1 µm thick clay matrix.

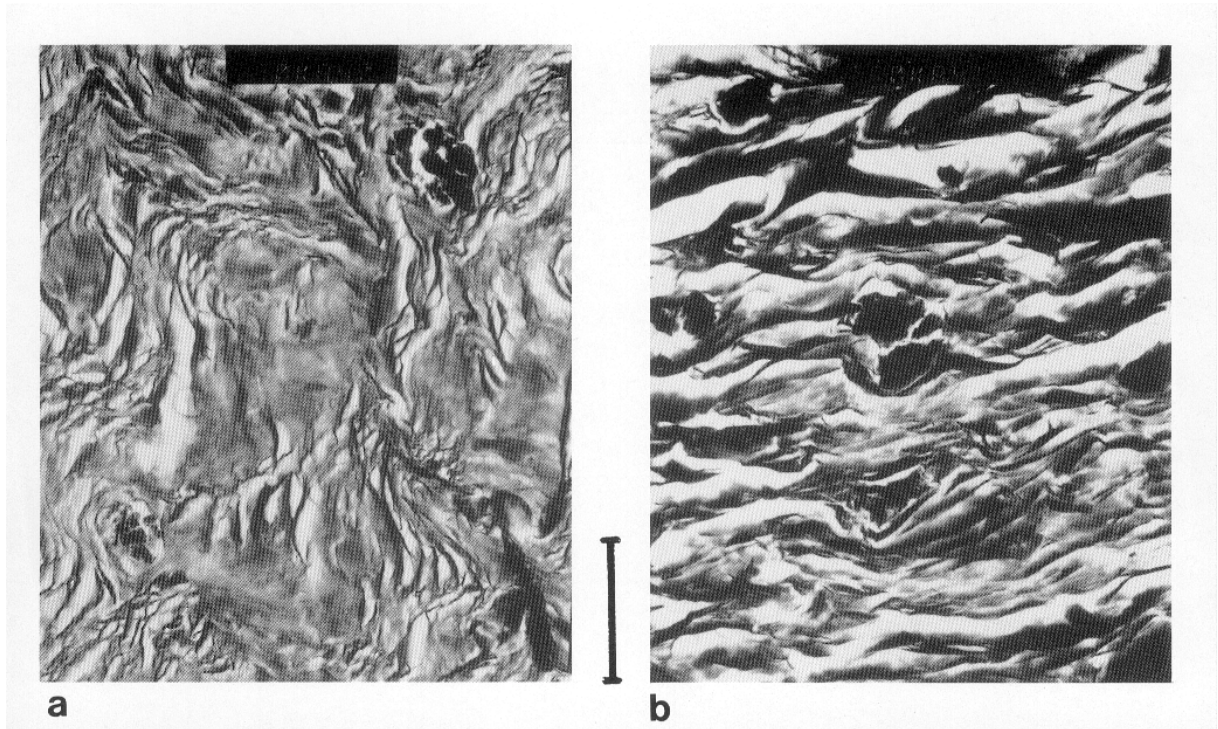*Figure 6-18.* *Typical transmission electron micrograph of MX-80 with 2000 kg/m3 density. Left: Untreated. Right: Autoclaved at 150ºC for 1 year. The microstructure of the hydrothermally treated clay is characterized by the obvious features: 1) The voids between the aggregates are less completely filled with soft gels than in the untreated clay, and 2) The particle aggregates are denser than in the untreated clay [14]. Bar is 10 μm.*

6.4 Mineral alteration

6.4.1 General

The issue of conversion of smectite to non-expandable minerals is considered to be the major threat to effective canister isolation in a long perspective [15, 16, 17]. The matter of conversion of smectite (S) to illite (I) under hydrothermal conditions has been investigated for decades because of its importance in oil prospection. Much of the international research work has therefore been focused on deep sediments, primarily on the ones of the Mexican Gulf, from which the basic conversion model of S to I via mixed-layer I/S mixed-layer models stem. In the 10 year period from early 1980 more refined XRD and TEM analyses have shown that conversion of S to I and chlorite takes place through dissolution and precipitation and it is presently believed that neoformation of illite as a separate phase in S-to-I conversion may be the dominant alteration mechanism [15].

A classical study by Janet Hoffman and John Hower in 1979, discussed and referred to in [15], showed that the entire illitic shale mineralogy of the disturbed belt in Montana of Mesozoic age (>65 M years) resulted from heating of bentonite to 100–200°C, implying that temperatures lower than 60°C gave no change of smectite at all. The main reaction was concluded to be the following:

$$S + F_k (+Mi) = I + Q + Chl \qquad (6.1)$$

where: S = Smectite
F_k = K-feldspar
Mi = Mica
Q = Quartz
Chl = Chlorite

Quartz was assumed to be formed by decomposed feldspars and from silica in montmorillonite tetrahedrons being replaced by aluminum. Potassium required for the conversion stemmed from the decomposed feldspars and the mica. Chlorite would be formed by integration of brucite layers in smectite crystals.

Comprehensive analyses show that reactions according to Eq.6.1 led to a very obvious drop in S content in Gulf sediments down to 5 km depth where the temperature is about 200°C. Hoffman and Hower described the conversion of S as a successive transformation to I via mixed-layer I/S with random ordering for temperatures below 100°C and certain regular orderings for the temperature interval 100 to 200°C. Recent investigations tend to show that there is a wide range of expandable layers at any temperature and that the fraction of expandable layers in I/S mixed layers can be anything from 20 to 90 % at 100°C.

6.4.2   Mechanisms

Further investigation of S-to-I conversion has improved the understanding of the involved processes. A main finding was that there are at least two high-temperature smectite phases, giving off different amounts of H_2SiO_4 when altering pH and pMg in the porewater [15]. It was confirmed that conversion of Na smectite to illite requires access to potassium and aluminum according to the reaction in Eq.(6.2):

$$\text{Smectite} + K^+ + \text{Na-smectite} = \text{Illite} + Si^4 + Na^+ + H_2O \qquad (6.2)$$
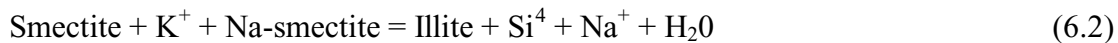
The following major conclusions were drawn from this investigation [15]:

- Prerequisites for conversion of Na smectite to illite are an increase in lattice charge, interlamellar cation exchange of sodium by potassium, and compression to squeeze out interlamellar water. The meaning of this is that interlamellar potassium uptake requires excess potassium ions in the solution, forming K-smectite, while collapse to yield illite requires an increase in effective pressure. Illitization may therefore not be observed in laboratory experiments except if a sufficiently high effective pressure is applied or the clay is dried. This is supported by the investigation reported in Chapter 2.5.

- There is a successive increase in spin-spin coherence time T_2 when the water content increases, which would demonstrate long-range influence on the organization of water or as large numbers of interlamellar hydrates. This has been shown to be incorrect by separating the proton relaxation times of interlamellar and extralamellar water, which led to an explanation of the temperature-dependent structure of the interlamellar water [15].

- Potassium-bearing minerals like K-feldspar and mica are probably not the major potassium origin. Instead, potassium dissolved in the porewater or in the groundwater of the nearfield rock may be the most important potassium source.

A different approach, equally or even more probable and of profound microstructural importance has been made by investigators like Pollastro, Bain and Nadeau [15, 16, 17], implying that two separate phases grow on the expense of the original smectite, i.e. *I/S* mixed layer minerals in lath-form, and illite hexagons. Compositional variations in clastic reservoirs offshore Norway indicate that illite and chlorite were continuously recrystallized at depths where the temperature has been in the interval 100–160°C.

Reconsideration of the illitization of the Gulf smectite sediments has indicated that the kinetics may be controlled by microstructural features. Thus, migration of necessary reactants, primarily potassium, may depend on the various initial and successively formed paths, which become wider in the illitization process because illite has a lower density than smectite (2650 and 2750 kg/m^3, respectively). There is evidence that smectite domains dominate initially and that illite aggregates grow within a shrinking matrix of smectite, i.e. on the expense of parent smectite as indicated in Figure 6-19. At complete conversion, corresponding to an illite content of 70–80 %, illite aggregates are assumed to make up a coherent particle network with smectite residue and open voids distributed in it. This would imply a significant increase in hydraulic conductivity and drop in swelling pressure.
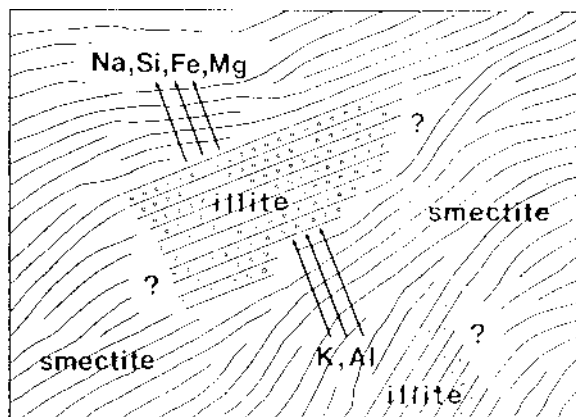

Figure 6-19. *Schematic picture of early local formation of illite in smectite matrix [18].*

6.4.3   Rate of conversion

Temperature is the driving force of chemically induced changes of smectite meaning that the conversion is basically of thermodynamic origin. However, a number of factors control the rate in practice, like the access to potassium and rate of migration of this element into the altering clay. Still, a simple basic approach is to model the rate of conversion by assuming that reorganization of the crystal lattice or, alternatively dissolution/neoformation, is an Arrhenius-type process. Such models have first been proposed by Bethke/Altaner [19] and Pytte [20], the firstmentioned being purely theoretical and based on the assumption that different groupings of smectite and illite lamellae are generated, and the latter being semi-empirical. For these models, of which Pytte's has formed a basis for predicting the long-term performance of the KBS3 buffer, major parameters are the activation energy for crystal breakdown and the K/Na ratio.

In the form used today Pytte's model expresses the conversion rate as follows:

$$-dS/dt = [Ae^{-U/RT(t)}]\ [(K^+/Na^+)mS^n]$$
(6.3)

where: S = Molar fraction of smectite in the reaction product I/S
R = Gas constant
T = Absolute temperature
t = Time
m, n = Coefficients depending on K/Na ratio and K concentration

The model has been used in various contexts applying different activation energies, which vary between a few kcal/mole to 29 kcal/mole according to literature data. The major problem is to apply a representative activation energy, which is concluded to be 25 to 27 kcal/mole for a natural analogy of major importance, i.e. the Kinnekulle case [21]. Examples of smectite-to-illite conversion illustrating the importance of temperature for a potassium content relevant to the KBS3 case is given in Figure 6-20. It represents the two activation energies 25 and 27 kcal/mole and shows that only 40 % of the smectite content would remain after 10 years at 200°C if the lower activation energy applies, while the higher energy value would imply that 90 % would remain intact. For the KBS3 case with an average temperature of 90°C for about 1000 years the final smectite content would be more than 95 % even for the lower activation energy.

Geochemical modelling using the codes DISSOL, THERMAL, KINDIS and CISSFIT have been used by Fritz and others for predicting changes recorded in laboratory experiments [22]. The experiments, which were made with the clay samples saturated with distilled water and strongly brackish water with Ca or Na as dominant cation, gave the alterations listed in Table 6-2. The calculations agreed in principle with the experiments, which showed no loss in smectite, quick dissolution of quartz and feldspars, but late recrystallization of quartz. The lastmentioned process is of great importance since it verifies that hydrothermally induced cementation actually takes place. All the analyses were made after cooling, meaning that some or all of the precipitation occurred when the temperature had been lowered.

Table 6-2. Mineral composition in hydrothermal experiments with MX-80 at 200°C over different periods of time. S=Smectite, Q=Quartz, F=Feldspars, Calcite=C. Very dominant=*, Abundant=**, Small amount=* [12].**

Mineral	Original	10 days, 200°C	90 days, 200°C	270 days, 200°C
S	***	***	***	***
Q	*	None for dist. w. * for brack. w.	None for dist. w. * for brack. w.	*
F	*	None	None	None
C	*	Almost none	Almost none	None

smectite fraction at start	SO		0	1
time	t	s		0
frequence factor	A	1/s		80800
activation energy	Ea	cal/mol		25000
gas constant	R	cal/(deg*mol)		1,987
temperature	T	K		323
K+ concentration	(K+)	mole/l		0,01
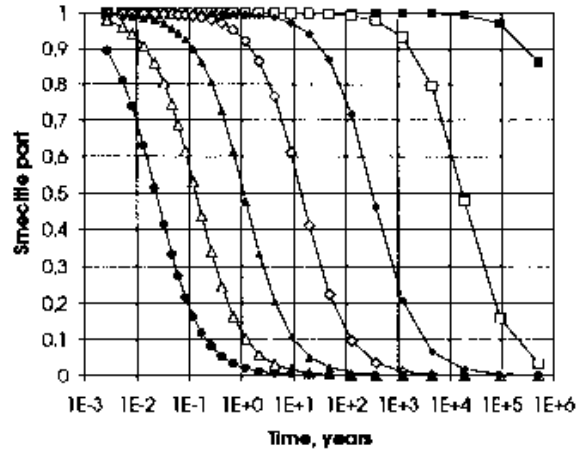
smectite fraction at start	SO		0	1
time	t	s		0
frequence factor	A	1/s		80800
activation energy	Ea	cal/mol		27000
gas constant	R	cal/(deg*mol)		1,987
temperature	T	K		323
K+ concentration	(K+)	mole/l		0,01
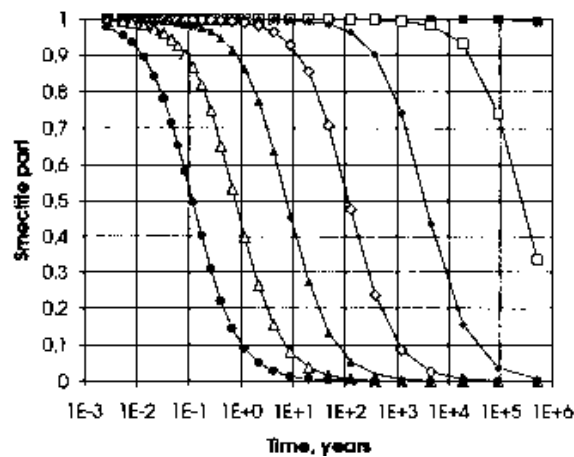
Figur 6-20. *Rate of conversion of smectite at a K^+ concentration of 0.01 moles/liter in the porewater according to Pytte's model for various temperatures. Scale: Vertical = proportion of smectite (1=100 %), Horizontal = log time from E-3 to E6 years. Upper diagram is for the activation energy 25 kcal/mole and the lower for 27 kcal/mole [21].*

6.4.4   Geological evidence

Clay materials

A number of natural pre-Quaternary clays originating from bentonites as concluded from geological examinations have been investigated with respect to the mineralogical composition and physical properties as well as to the microstructural constitution [23]. The clays, from which undisturbed samples were extracted for laboratory testing of the hydraulic conductivity, swelling pressure, and for microstructural characterization, are listed in Table 6-3 with respect to the hydrothermal history, smectite content, and density. The data in the table indicate that the smectite content is related to the temperature history, hence supporting the validity of the conversion model described in this chapter. However, there are a number of uncertainties, like lack of information on the initial mineral composition of the sediments, and at present it is necessary to confine oneself to consider the differences in physical properties that are associated with the presently found mineral compositions. The fact that all of the clays, except the Cretaceous Fish Clay, have approximately the same high density makes comparison of the hydraulic conductivity relevant.

Table 6-3. Pre-Quaternary clays investigated [23]. Dominant clay mineral S=Smectite, I=Illite.

Clay	History	Smectite content, %	Density, kg/m^3
No I. (MX-80) *S*	–	65	1900–2100
No II (Gotland) *I*	120–150°C for 10 M years	0	2110–2200
No III (Kinnekulle) *I/S*	100–150°C for 1000 years	25	2050–2150
No IV (Kinnekulle) *I/S*	100–150°C for 1000 years	15	2100
No V (Boom) *I/S*	<100°C	10	2050
No VI (Forsmark) *I/S*	<200°C	3	2050–2300
No VII (Ignaberga) *I/S*	No heating	5	2000–2100
No VIII (Fish) *I/S*	No heating	30	1830–1850

Relation between smectite content and physical properties

There is a fairly obvious relationship between the smectite content and the hydraulic conductivity of the clays, which have nearly the same density, i.e. around 2100 kg/m^3 except for the Fish Clay. This is obvious from Figure 6-21, in which all plottings are within a rather narrow band except for the softer Fish clay. Plotting of the total clay content versus the hydraulic conductivity gave a less obvious relationship, which demonstrates that the smectite is a more effective sealant than other minerals belonging to the clay fraction.

In principle, the hydraulic conductivity appears to be increased by about one order of magnitude when the smectite content of smectitic clay with a density of 2000 to 2100 kg/m^3 goes down from 65 to 25 % and by another order of magnitude, i.e. to E-12 to E-11 m/s, when it drops from 25 to 15 %.
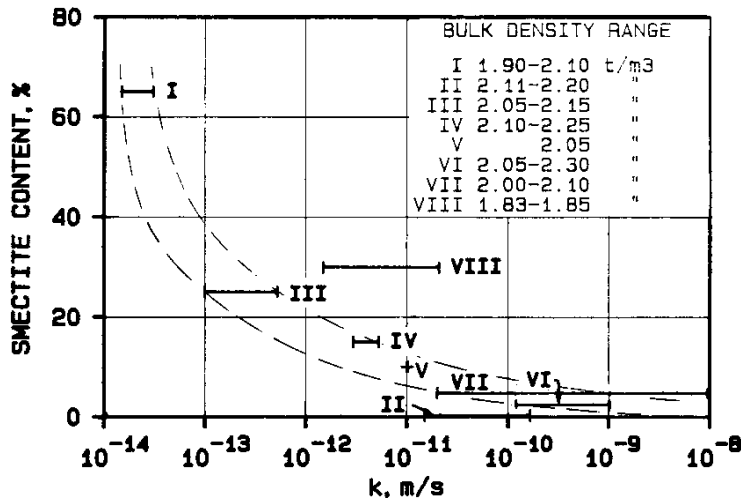
Figure 6-21. *Hydraulic conductivity versus smectite content of eight pre-Quaternary clays. The smectite content is expressed in weight percent of the total mineral mass [23].*

<u>Microstructural constitution</u>

Some of the pre-Quaternary clays were investigated with respect to their microstructural constitution expressed in terms of the F_2 parameter and the average size of open voids a_p as shown in Table 6-4. The obvious outcome of this comparison is that the almost pure illite (No II) has the highest F_2 value and the widest open voids, which explains why it has the highest hydraulic conductivity. The general microstructure is shown in Figures 6-22 and 6-23. For the smectitic clays one finds that MX-80 has higher F_2- and a_p-values than the less smectite-holding *I/S* clay (No III) despite its lower hydraulic conductivity. This is explained by the lower conductivity of the denser, major part of the clay matrix in MX-80 than of the corresponding part of the *I/S* clay. This is even more obvious for the illite clay, which makes it clear that water flow through smectite-rich clay like MX-80 takes place only in the narrow, gel-filled channels, while smectite-poor clays are permeated much more uniformly, i.e. also aggregates of densely grouped particles let water through. This difference is fundamental and explained by the different ratios of interlamellar and extralamellar water.

Table 6-4. Microstructural parameters of pre-Quaternary clays.

Clay	F_2	Average diameter of open voids, a_p μm	Hydraulic conductivity, m/s
No I. (MX-80) *S*	0.17	0.20	5E-14
No II (Gotland) *I**	0.37	0.20	E-11 to E-10
No III (Kinnekulle) *I/S*	0.07	0.12	E-13 to E-12

* The Gotland illite is believed to represent totally illite-converted bentonite
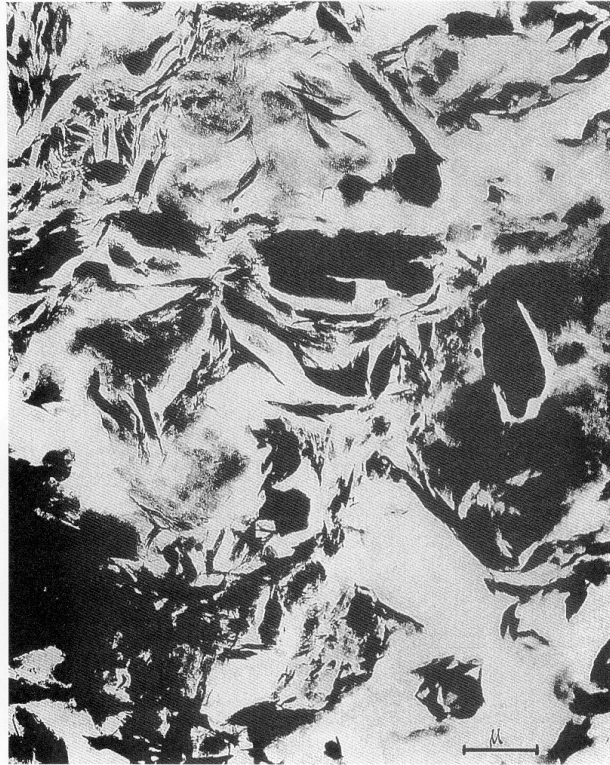
104

Figure 6-22. Micrograph of Gotland illite (No II) showing frequent dense aggregates and numerous open voids in the clay matrix.

Figure 6-23. Micrograph of the Ordovician Kinnekulle I/S clay (No III) showing large dense aggregates and large, partly gel-filled voids. The width of the micrograph is 8 μm, i.e. approximately the same as of the illite clay in Figure 6-22.

6.5 Tentative conclusions from examination of physical and chemical processes that can affect the microstructure

The following aspects and conclusions are significant:

- Physically induced changes in density through compression or expansion, shearing, high hydraulic gradients, and gas percolation may take place but the basic pattern of clay aggregates separated by softer parts of the clay matrix is maintained. For densities of the order of magnitude intended for the KBS3 buffer, self-sealing will restore the microstructure when the conditions are changed back to the original ones.

- Physico/chemically induced effects by changes in porewater chemistry has a minor impact on MX-80 clay with higher density than about 1800 kg/m^3, firstly because the denser parts of the clay matrix will undergo only insignificant changes in interlamellar spacing and secondly because of geometrical restraint to large changes in particle arrangement and orientation. The changes in bulk physical properties will be much smaller than is found for clay sedimented in water with different chemical constitution.

- Chemically induced effects will take place in MX-80 buffer by dissolution, precipitation, and conversion of smectite to illite. Temperature alone has little effect on the microstructure when the bulk density is low while it yields compression of stacks of lamellae and of aggregates of stacks at higher density due to the swelling pressure. The most obvious effect of temperature is dissolution of the minerals by which silica and aluminum are set free and can cause cementation and neoformation of illite as well as *I/S* mixed layer formation. A typical microstructural feature of smectite clay that has been exposed to high temperature and pressure is large, dense aggregates, which are believed to have been formed by partial interlamellar dehydration during heating and prevented from expansion at cooling by precipitated silicious matter.

- Two of the pre-Quaternary clays that have been investigated and characterized with respect to the microstructure are of particular interest since they are concluded to represent two stages in long term alteration of the KBS3 buffer clay. One of them, the Kinnekulle clay, is of Ordovician age and has been exposed to pressure and heat conditions that are similar to those that will prevail in a repository. It has a smectite content of up to 25 % and is ductile and not much more permeable than MX-80 clay. The other is older, i.e. of Silurian age, and is assumed to have been converted from smectite-rich bentonite to illite by being exposed to similar temperature conditions for a much longer time. Both materials represent clays with a sufficiently low hydraulic conductivity to be acceptable as buffer clay. The different hydraulic properties are explained by the different microstructural constitutions.

6.6   References

1. Pusch R, Influence of organic matter on the geotechnical properties of clays. Document D11:1973, Nat. Swed. Build. Res. Council, Stockholm.

2. Pusch R, 1970. Microstructural changes in soft quick clay at failure. Canadian Geotechnical Journal, Vol.7, No.1 (pp. 1–7).

3. Pusch R, 1970. Clay Microstructure. Document D:8:1970. Nat. Swed. Build. Res. Council, Stockholm.

4. Pusch R, Feltham P, 1980. A stochastic model of the creep of soils. Geotechnique, Vol.30, No.4 (pp.497–506).

5. Pusch R, Erlström M, Börgesson L, 1987. Piping and erosion phenomena in soft clay gels. SKB Technical Report TR 87-09, SKB, Stockholm.

6. Pusch R, Ranhagen L, Nilsson K, 1985. Gas migration through MX-80 Bentonite. NAGRA Technical Report 85-36.

7. Horseman S T, Harrington J F, Sellin P, 1999. Gas migration in clay barriers. Eng. Geol. Vol.54, Nos.1–2 (pp. 139–149).

8. Pusch R, Schomburg J, 1999. Impact of microstructure on the hydraulic conductivity of undisturbed and artificially prepared smectitic clay. Eng. Geol. Vol.54, Nos.1–2, (pp. 167–172).

9. Pusch R, 2000. Experimental study of the effect of high porewater salinity on the physical properties of a natural smectitic clay. (In press).

10. Forslind E, Jacobsson A, 1972. Clay-water systems. Water, a Cemprehensive Treatise (Ed. Franks), Plenum, New York.

11. Pusch R, Takase H, 1998. Chemical processes causing cementation in heat-affected smectite – the Kinnekulle bentonite. SKB Technical Report TR-98-25, SKB, Stockholm.

12. Pusch R, Karnland O, Hökmark H, Sanden T, Börgesson L, 1991. Final report of the Rock Sealing Project – Sealing properties and longevity of smectite clay grouts. Stripa Project Technical Report 91-30, SKB Stockholm.

13. Pusch R, 2000. On the effects of hot water vapor on MX-80 clay. SKB Technical Report TR-00-16, SKB, Stockholm.

14. Pusch R, Karnland O, 1988. Hydrothermal effects on montmorillonite, A preliminary study. SKB Technical Report TR 88-15, SKB, Stockholm.

15. Pusch R, 1993. Evolution of models for conversion of smectite to non-expandable minerals. SKB Technical Report TR 93-33, SKB Stockholm.

16. Nadeau P H, Bain D C, 1986. Composition of some smectites and diagenetic illitic clays and implications for their origin. Clays and Clay Minerals, Vol.34 (pp.455–464).

17. Pollastro R M, 1985. Mineralogical and morphological evidence for the formation of illite at the expence of illite/smectite. Clays and Clay Minerals, Vol.33 (pp.265–274).

18. Ahn J H, Peacor D R, 1989. Transmisson and analytical electron microscopy of the smectite-to-illite transition. Clays and Clay Minerals, Vol.34 (p.165).

19. Bethke C M, Vergo N, Altaner S P, 1986. Pathways of smectite illitization. Clays and Clay Minerals, Vol.34 (p.125).

20. Pytte A M, 1982. The kinetics of the smectite to illite reaction in contact metamorphic shales. Thesis M.A. Dartmouth College, N.H.

21. Pusch R, Madsen F T, 1995. Aspects on the illitization of the Kinnekulle bentonites. Clays and Clay Minerals, Vol.43 (pp.261–270).

22. Fritz B, DelNero M, 1994. Smectite to illite reactions. Comparison between modelling and experimental results. Centre de Geochimie de la surface/CNRS, University of Strasbourg, France.

23. Pusch R, Börgesson L, Erlström M, 1987. Alteration of isolating properties of dense smectite clay in repository environment as exemplified by seven pre-Quaternary clays. SKB Technical Report TR 87-29, SKB, Stockholm.

7 Discussion and conclusions

7.1 General

Engineered clay barriers are being proposed for the conceptual design of radioactive waste repositories in many countries since most clay types, especially smectites, have a very low hydraulic conductivity and exhibit excellent retardation capabilities for both cationic and anionic radionuclides. The present document describes the evolution and function of the microstructure of MX-80 clay with special respect to the physical properties of buffer clay in bulk.

The basic part of the work comprised derivation of conceptual and numerical models for the evolution of the microstructure of smectite clay resulting from compaction of air-dry grains of MX-80 clay powder with subsequent exposure of the blocks to water for saturation under confined conditions. Changes induced by mechanical and chemical processes were considered, like the influence of thermal gradients in the saturation process of the "buffer clay" as well as gas percolation, compression, expansion and shearing, including also chemical changes induced by temperature, dissolution and precipitation.

7.2 Microstructural model

The model of microstructural evolution represents the basic case of air-dry MX-80 grains being compressed under 100 MPa pressure and then water saturated under confined conditions. This case is valid only for the central part of the canister-embedding buffer of the KBS3 concept and does not reflect the complex scenario with initial expansion and subsequent consolidation of the shallow buffer close to the rock in the deposition holes. Nor does it describe the microstructural evolution close to the hot canister, where fracturing due to dessication takes place initially and where hydration and expansion then lead to closure of the cracks and subsequently to a more homogeneous state. Modeling of these two parts of the buffer requires development of conceptual models based on systematic laboratory experiments before mathematical modeling is worth while.

Quantification of the microstructure requires digitalized micrographs taken by transmission electron microscopy using suitably impregnated specimens. The problem with identifying and applying a preparation technique that preserves the microstructure sufficiently well appears to have been solved. Furthermore, the basis for selecting a suitable specimen thickness for microscopy has been worked out.

Practically useful microstructural parameters refer to the fraction of a thin section that represents dense and soft parts of the clay matrix. Variations in density on the microstructural level are the most obvious features of clays prepared by compacting clay powder, which means that complete homogenization of such clays will not occur despite the wellknown macroscopic self-healing ability. Still, the degree of homogeneity may improve in a long-term perspective due to creep on the microscale.

The proposed way of analyzing micrographs for deriving microstructural parameters has limitations because of the scale dependence, meaning that investigated micrographs need to have a minimum size. Optical microscopy may be a valuable complement to transmission electron microscopy when investigating clays with relatively wide voids.

7.3 Correlation of microstructure and bulk physical properties

7.3.1 General

The derived microstructural parameters are directly coupled to the most important bulk physical properties, i.e. the hydraulic conductivity, gas penetrability, swelling pressure and cation/anion diffusion capacities.

7.3.2 Importance of the microstructural constitution for water and gas transport through the buffer

Artificially prepared buffer clays inherit their basic structure from the powder grains from which compacted blocks are prepared. Despite considerable homogenization through hydration and expansion of the grains under confined conditions, density variations persist and the study has shown that even at very high densities, softer and more pervious zones are formed by partly or wholly interconnected "external" voids filled with more or less dense clay gels. At bulk densities exceeding 2000 kg/m^3 after water saturation and maturation, the gel density is not significantly lower than that of the densest parts. However, when the bulk density is less than about 1800 kg/m^3 after saturation the fraction of a cross section through the clay matrix that represents the softer parts increases and the density of their gel fillings drops, by which the hydraulic conductivity increases. For low bulk densities the density of the gel fillings may be so much reduced that they do not remain stable at high electrolyte content of the porewater. This is particularly obvious when calcium is the major cation in the porewater.

As to gas penetration the microstructural models suggest that the critical pressure is related to the swelling pressure. The fact that the density variations are small for high bulk densities means that the separation of matrix components ("fracturing") that is required for letting gas through is on the same order of magnitude as the bulk swelling pressure. For lower bulk densities, displacement or consolidation of the clay gels in "external" voids is concluded to take place in conjunction with gas penetration.

7.3.3 Importance of the microstructural constitution for the swelling pressure of the buffer

The density variations that persist in fully hydrated and matured MX-80 clay buffer have an impact on the swelling pressure. At bulk densities exceeding 2000 kg/m^3 after water saturation and maturation, the gel density in "external" voids is not significantly lower than that of the densest parts, which form the major part of the clay matrix and determine the bulk pressure. As for the hydraulic conductivity the conditions are different for bulk densities lower than about 1800 kg/m^3 after saturation since the fraction of a cross section that

represents the softer parts dominates. For low bulk densities neither the gels that make up the soft parts nor the network of dense aggregates are continuous, at least not when the clay is in Ca-state, which means that the swelling pressure is very low.

7.3.4 Importance of the microstructural constitution for ion transport through the buffer

The size and connectivity of the channel-forming "external" voids filled with soft gels vary in matured clay. They control the conductivity and also represent the part of the clay in which pore diffusion of cations and anions takes place. At high densities the limited degree of continuity and constrictions of the channels leading to anion-excluding charge conditions mean that the anion diffusion capacity is very low, while cation diffusion may be extensive because it takes place not only through channels but also through the interlamellar space and along the surfaces of stacks of lamellae, i.e. by surface diffusion.

7.4 Major outcome of the study

The derived relationships between the microstructure and practical bulk clay properties – referring in particular to the MMM model – are believed to be of assistance in interpreting bulk laboratory and field data from experiments on MX-80 clay and similar buffer materials. Also, selection of a suitable repository design with respect to geometry and density of the buffer blocks can be aided by applying the models. The most important value of the work performed is that parameter variation can be made for optimizing the sealing ability of buffer clays.

The work led to a strongly improved understanding of the evolution of the microstrcuture of buffers and to definition of microstructural parameters and data that can be used for characterizing smectite clay and for predicting water and gas permeation and diffusive transport of ionic species.

The key factor is the density of the buffer material since it determines the microstructural constitution, the most important feature being the variation in density since it determines the size and interconnectivity of voids and soft gel components.